HAL open science

Large thrusting and late faulting shape the Aiguilles Rouges crystalline massif (Western Alps), structural implications

Antoine Mercier, P.H. Leloup, Gabriel Courrioux, Séverine Caritg, Simon Lopez, P. Grandjean, S. Passot, A. Kalifi

To cite this version:

Antoine Mercier, P.H. Leloup, Gabriel Courrioux, Séverine Caritg, Simon Lopez, et al.. Large thrusting and late faulting shape the Aiguilles Rouges crystalline massif (Western Alps), structural implications. Tectonophysics, 2022, pp.229691. 10.1016/j.tecto.2022.229691 . hal-03918662

HAL Id: hal-03918662

https://hal.science/hal-03918662v1

Submitted on 3 Jan 2023

HAL is a multi-disciplinary open access archive for the deposit and dissemination of scientific research documents, whether they are published or not. The documents may come from teaching and research institutions in France or abroad, or from public or private research centers.

L'archive ouverte pluridisciplinaire **HAL**, est destinée au dépôt et à la diffusion de documents scientifiques de niveau recherche, publiés ou non, émanant des établissements d'enseignement et de recherche français ou étrangers, des laboratoires publics ou privés.

Distributed under a Creative Commons Attribution - NonCommercial 4.0 International License

This manuscript version is made available under the CC-BY-NC-ND 4.0 license
https://creativecommons.org/licenses/by-nc-nd/4.0/

Large thrusting and late faulting shape the Aiguilles Rouges crystalline massif (Western Alps), structural implications.

A. Mercier[a], P. H. Leloup[a], G. Courrioux[b], S. Caritg[b] S. Lopez[b],
P. Grandjean[a], S. Passot[a], A. Kalifi[a]

[a]Univ Lyon, Université Claude Bernard Lyon 1, ENSL, UJM, CNRS, Laboratoire de Géologie de Lyon: Terre, Planètes et Environnement, 2 rue Raphaël Dubois, F-69622, Villeurbanne, France.
[b]Bureau de Recherches Géologiques et Minières, Direction des Géoressources, 3 av. Claude-Guillemin, BP 36009 45060 Orléans Cedex 2, France.

Corresponding author: Antoine Mercier (antoine.mercier@univ-lyon1.fr , antoine.mercier@gmx.com)

Keywords:

- Alpine geology
- Microtectonics
- Orogenesis
- 3D geological modeling
- Helvetic Basal Thrust
- Crystalline External Massifs

Abstract

Although the Helvetic nappes of the Western Alps have been widely studied, their style, amount, and timing of deformation during the Alpine orogeny remain a subject of controversy. The discussion partly arises from various interpretations of the external crystalline massifs geometry and of the cover/basement relationships. Here, we apply structural analysis based on new field data, microtectonics, and 3D geological modeling on the Aiguilles Rouges and Mont-Blanc massifs, to better quantify their tectonic evolution and their relationship with the nappe stacking. Our results show large thrusting of the Helvetic Mesozoic sedimentary cover above the Aiguilles Rouges basement towards the WNW. The basal contact of the Helvetic nappes, which we call the Helvetic Basal thrust (HBT), often corresponds to a décollement level localized above the Triassic unconformity, but that locally also affects the basement. We suggest that most of the subalpine ranges are klippes above the HBT, and estimate the shortening of the thrust from previously published cross-sections to be between 13 and 32 km. According to published ages, we argue that the HBT was active in the Oligo-Miocene, between ~30 and ~14 Ma. After ~14 Ma and until ~6 Ma, the HBT is offset by late steep out-of-sequence faults, including back-thrusts and the Mont-Blanc shear zone that was previously a ramp of the HBT. The transition of the major thrust system from the HBT rooting above (east) of the Mont-Blanc to the Alpine sole thrust rooting below (west) of the Aiguilles Rouges occurred between 18 and 14 Ma.

1 Introduction

For two centuries the European Alps are a natural laboratory to study continental lithosphere deformation during mountain building. Since the early studies, a constant question has been to evaluate the importance of vertical versus horizontal displacements in the building of reliefs. Although the occurrence of large thrust sheets, as initially proposed from field observations (e.g., Bertrand, 1881; Argand, 1916), are now well explained in the frame of plate tectonics, controversies still arise on the precise geometry, amount, and timing of major thrusting during the orogeny.

Two completely different views are proposed in the external domain of the belt's western part. For most authors, the present-day geometry, results from the intense folding of the Mesozoic sedimentary cover, originally deposited in half grabens, together with the basement in a ductile basement fold nappe (e.g., Escher et al., 1993). In such a case the geometry of the half grabens guides later deformation(s), and the cover is considered para-autochthonous because horizontal displacements are moderate (e.g., Escher et al., 1993; Burkhard & Sommaruga, 1998; Bellahsen et al., 2014). Alternatively, it is proposed that the Mesozoic cover is significantly displaced to the west above a thrust: the Helvetic Basal Thrust (HBT) (e.g., Leloup et al., 2005; Pfiffner, 2014).

The existence and kinematics of such thrust are important not only for the understanding of the regional geology but also have implications on a) the estimate of total shortening in the external Alps; b) the timing and mechanism of uplift of the external ranges; c) the timing and mechanism of folding within the subalpine belts; d) the way shortening is absorbed in a layered media with

contrasting rheology (sedimentary cover vs. basement); e) the influence of the initial geometry (paleo-topography: horst and grabens) on the deformation style.

Here, we present a detailed 3D structural study of the cover/basement relationships in the Chamonix synclinorium between the Mont-Blanc and Aiguilles Rouges ranges. These field observations are key to characterize the deformation within the orogenic wedge, and thus to discuss the outcome of rheological models (e.g. Spitz et al., 2020; Bauville et Schmalholz, 2015).

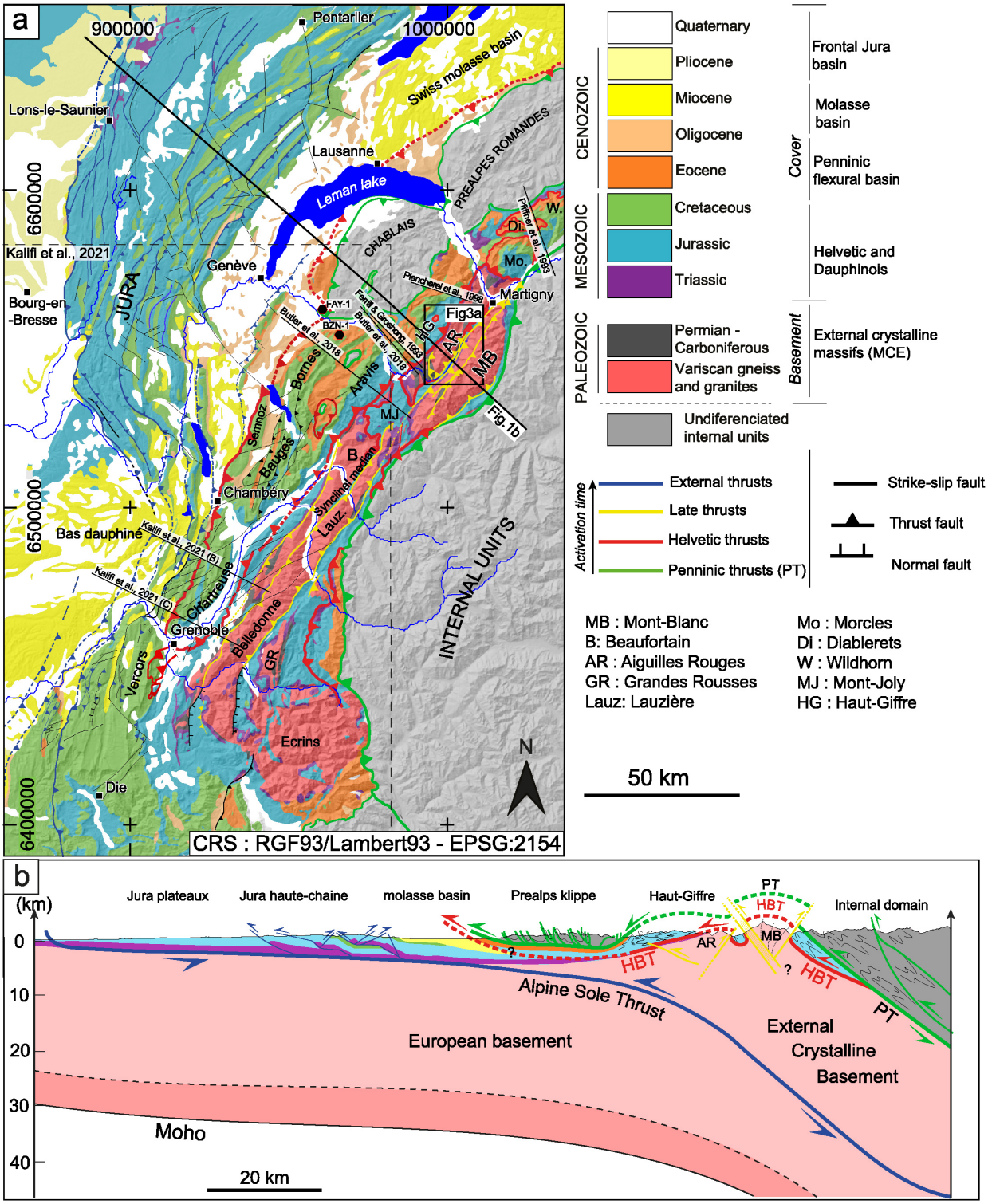

Fig. 1. Structural frame of the western Alps. **a)** Structural map with the main thrust systems: Penninic thrust, Helvetic thrust, Alpine Sole Thrust, and late thrusts. The black frame corresponds to the location of Fig. 3a. Location of cross-sections that are discussed in the text is indicated with the reference therein (Pancherel et al., 1998; Ferril and Groschong, 1993; Butler et al., 2018; Kalifi et al., 2021). **b)** Synthetic cross-section of the western Alps. The crustal structure is from Lacassin et al., (1990) and Pfiffner et al. (1997), the Jura deformation from Affolter (2004,

2008), the structure of the Prealps klippe is from Mosar (1989), the structure of the Aiguilles Rouges and Mont-Blanc area is from this study, and Leloup et al. (2005); the structure in the internal domain is from Ceriani et al. (2001). Cross section trace is located in the map (a).

2 Geological setting

The western Alps are an accretionary wedge resulting from the Cenozoic convergence between Europe and Apulia continental margins. The anterior subduction of the ocean started during the mid-Cretaceous and led to the collision in the Paleogene. The wedge is split into two parts: the internal domain containing ophiolites and rocks that have been deformed at high temperature and/or deeply subducted during the Alpine orogeny, and the external domain where Alpine metamorphism is limited to green-schist facies (e.g., Bousquet et al., 2004). The internal domain is thrust above the external one along the west verging Penninic thrust, with the Prealps being interpreted as a klippe of the internal domain (e.g., Mosar, 1989) (Fig. 1). Such interpretation implies at least 95 km of thrusting to the NW above the Penninic thrust, which has been later folded upward to expose a window of the external domain in the Mont-Blanc/Aiguilles Rouges area (Fig. 1). Motion on the Penninic thrust was coeval with the sedimentation of flysch deposits in a flexural basin during the Upper Eocene/Lower Oligocene (e.g., Homewood, 1983; Ruffini et al., 1997) and ended at ~30 Ma (e.g., Pfiffner et al., 2002).

The external domain exposes both basement ridges, the external crystalline massifs, and their folded sedimentary cover (Fig. 1). The basement consists of Variscan (≥ 300Ma) metamorphic gneisses, granites, and Carboniferous/Permian sedimentary rocks. The overlying sedimentary cover span in age from Triassic to Miocene. The external crystalline massifs straddle for 330 km along the belt from Aar to Ecrins and form slivers separated by sedimentary rocks (Fig. 1) that have been interpreted either as paleo-horsts inherited from Mesozoic rifting (e.g., Lemoine & Tricart, 1986), crustal culminations above thrust ramps (e.g., Lacassin et al., 1990; Pfiffner et al., 1997; Menard & Thouvenot, 1987), anticline cores (e.g., Escher et al., 1993), or a combination of those. The sedimentary cover is folded and locally forms the Helvetic nappes whose extent, geometry, and timing are still discussed.

The Mont-Blanc and Aiguilles Rouges ranges are two NE-SW trending external crystalline massifs separated by a narrow structure filled with Mesozoïc sediments: the so-called Chamonix synclinorium, trending N030°(Fig. 1). From the early 1920s, it has been suggested that the Chamonix synclinorium corresponds to the root of the Morcles Nappe, the lowest of the Helvetic nappes (Collet & Paréjas, 1920; Paréjas, 1922; Eltchaninoff, 1982; Butler, 1985). However, thrusting at the bottom of the Morcles Nappe has been minimized or even denied. For example, Ayrton (1980) proposes that the synclinorium is the contact zone between the autochthonous sedimentary cover of the Mont-Blanc and that of the Aiguilles Rouges. Several authors propose that the Morcles nappe is para-autochthonous, being the reverse limb of a buckle anticline, whose core consists of the folded basement (so-called external Mont-Blanc) and the periphery of cover rocks expulsed from a Mesozoic Half-graben (Ramsay, 1981; Epard, 1986; Escher et al., 1993; Burkhard & Sommaruga, 1998; Egli & Mancktelow, 2013; Bellahsen et al., 2014) (Fig. 2a).
Alternatively, it has been proposed a two phases scenario, with first, thrusting toward the NW of most of the cover and part of the basement; and second exhumation of the Mont-Blanc along the steep reverse Mont-blanc shear zone and doming of the Aiguilles Rouges above a deeper thrust (Leloup et al., 2005) (Fig. 2b).

Yet others consider that the linear shape of the Chamonix Synclinorium, and of the Mont-Blanc range, partly results from right-lateral strike-slip faulting along the Simplon Rhône fault system (Gourlay & Ricou, 1983; Hubbard & Mancktelow, 1992; Seward & Mancktelow, 1994) connected to the Simplon low - angle detachment fault that was active between ~18.5 and 4 Ma (Campani et al., 2010).

In the northwestern Alps, the instrumental earthquakes are best explained by a strike-slip state of stress with σ1 trending WNW-ESE (Fréchet et al., 2011). The most significant instrumental earthquake in the Aiguilles Rouges area was the M_w 4.5 Vallorcine earthquake (8th September 2005) that activated the N060° trending right-lateral Gros-Nol Fault (Fréchet et al., 2011B) (Fig. 3a). That fault is oblique to the Chamonix synclinorium that trends ~N030°.

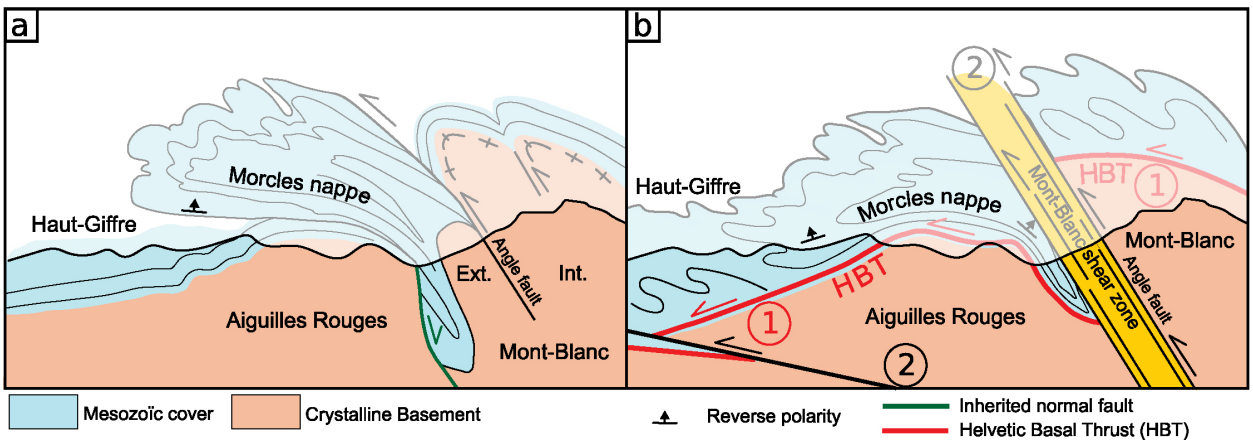

Fig. 2. Contrasting models for Alpine deformation of the external crystalline massifs and their cover, as exemplified in the Aiguilles Rouges and Mont-Blanc massifs. a) One-stage folding of a thick sedimentary series located within half grabens, resulting in parautochtonous folds (basement fold nappe). The external Mont-Blanc basement is tightly folded and the normal limb of the cover roots in the Angle Fault (e.g., Escher et al., 1988, 1993). b) Two stages of deformation model. 1st stage: Thrusting (mostly décollement of the cover with respect to the basement) towards the west. 2nd stage: offset of the thrust level by a reverse shear zone (Mont-Blanc shear zone) and updoming of the Aiguilles Rouges (e.g., Leloup et al., 2005).

3 Data and Methods

3.1 Structural analysis

At the regional scale, the structural study is mainly based on published geological maps at the 1:50 0000 scale in France (Corbin & Oulianoff, 1928; Ayrton et al., 1987; J. L. Pairis et al., 1992) and 1:25 000 in Switzerland (Collet et al., 1952), that we completed and updated with field observations, measurements, and mapping. At the outcrop scale, we characterize the style, intensity, and geometry of the deformation by qualitative observation and precise measurements of the orientation of the structural features (stratigraphy, cleavage, shear planes, lineations, etc.). We meticulously select oriented samples and produce oriented thin sections to characterize the deformation at a microscopic scale. The main shear criteria used are the relationship between cleavage and shear planes (Berthé et al., 1979), asymmetrical boudinage (Lacassin, 1988), delta

and sigma porphyroclasts (Hanmer & Passchier, 1991), and lattice preferred orientation in quartz (Gapais & Barbarin, 1986; Passchier & Trouw, 2005).

Field data (observations, measurements, samples, photos, etc.) are managed in a relational database, *DataGeol*, that we specifically designed for the processing of structural geology field data. *DataGeol* efficiently organizes, stores, and archives the data into different tables that are standardized with vocabularies, structured with constraints (primary keys), and linked together with foreign keys. The database is coded with the Structured Query Language (SQL) through the open-source system PostgreSQL with PGadmin graphical interface, which is a powerful programming language for object-relational databases. The use of a database and the SQL language allows interrogations and queries of the data for different applications purpose either for mapping in a GIS, structural analysis, 3D modeling, or any other export tables. Note that DataGeol is fully compatible with the vocabularies of the Open Geospatial Consortium (OGC) and the data model standard of the Darwin Core.

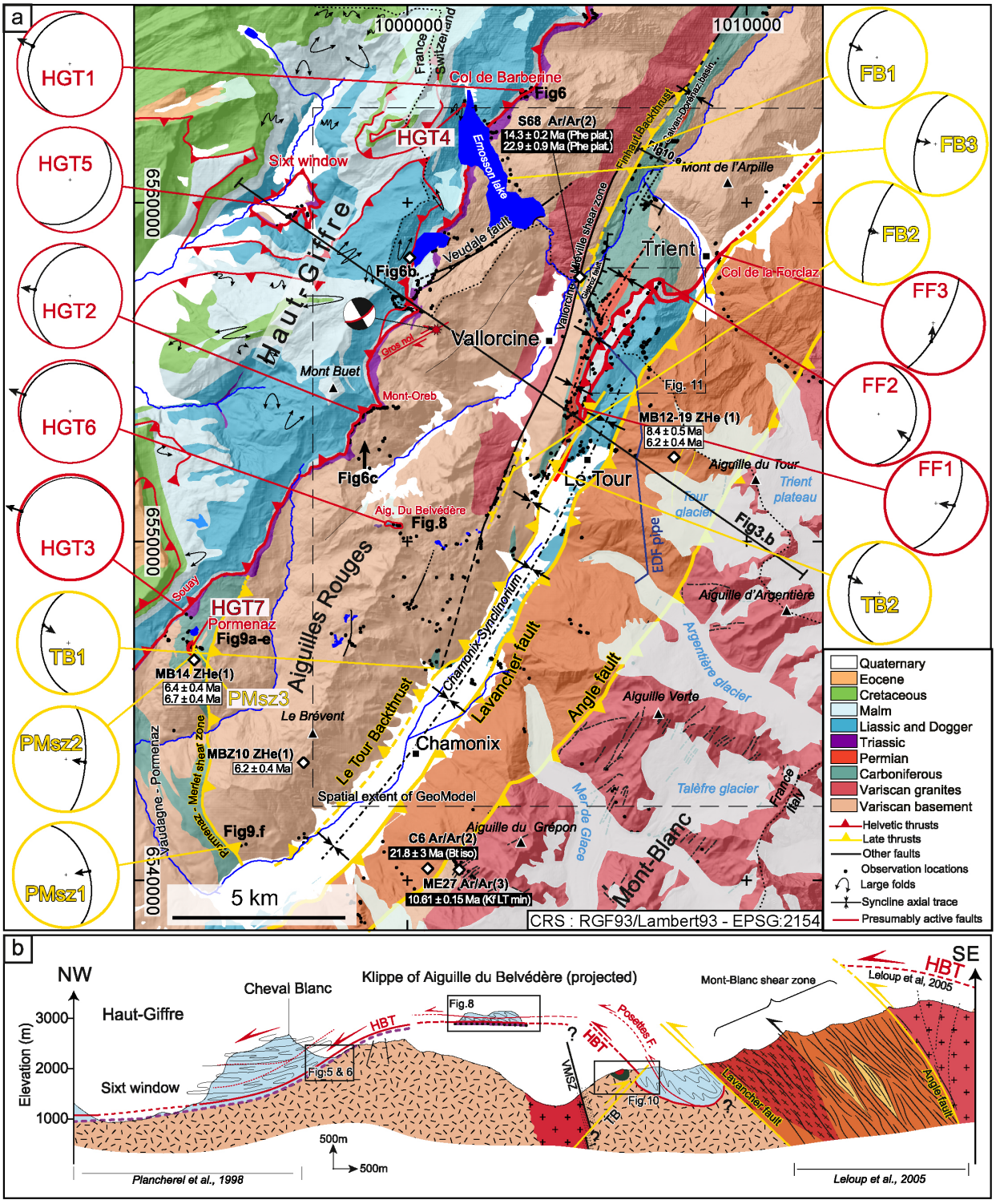
a
HGT1
HGT5
HGT2
HGT6
HGT3
HGT7
TB1
PMsz2
PMsz1
FB1
FB3
FB2
FF3
FF2
FF1
TB2
1000000
1010000
6650000
6640000
France
Switzerland
Col de Barberine
Fig6
HGT4
S68 Ar/Ar(2)
14.3 ± 0.2 Ma (Phe plat.)
22.9 ± 0.9 Ma (Phe plat.)
Emosson lake
Finhaut Backthrust
Salvan-Dorénaz basin
Mont de l'Arpille
Sixt window
Haut Giffre
Veudale fault
Fig6b
Trient
Col de la Forclaz
Méville shear zone
Vallorcine
Gletz fault
Gros rol
Mont Buet
Mont-Oreb
Fig. 11
MB12-19 ZHe (1)
8.4 ± 0.5 Ma
6.2 ± 0.4 Ma
Aiguille du Tour
Trient plateau
Tour glacier
Fig6c
Le Tour
Aig. Du Belvédère
Fig.8
Fig3.b
EDF pipe
Aiguilles Rouges
Souay
Aiguille d'Argentière
Pormenaz
Fig9a-e
Chamonix Synclinorium
Lavancher fault
Angle fault
Argentière glacier
MB14 ZHe(1)
6.4 ± 0.4 Ma
6.7 ± 0.4 Ma
PMsz3
Aiguille Verte
Le Brévent
Le Tour Backthrust
Chamonix
MBZ10 ZHe(1)
6.2 ± 0.4 Ma
Merlet shear zone
Vaudagne - Pormenaz
Spatial extent of GeoModel
Talèfre glacier
Mer de Glace
Fig9.f
Aiguille du Grépon
C6 Ar/Ar(2)
21.8 ± 3 Ma (Bt iso)
ME27 Ar/Ar(3)
10.61 ± 0.15 Ma (Kf LT min)
Mont-Blanc
France
Italy
5 km
CRS : RGF93/Lambert93 - EPSG:2154
Quaternary
Eocene
Cretaceous
Malm
Liassic and Dogger
Triassic
Permian
Carboniferous
Variscan granites
Variscan basement
Helvetic thrusts
Late thrusts
Other faults
Observation locations
Large folds
Syncline axial trace
Presumably active faults
b
NW
SE
Elevation (m)
3000
2000
1000
Haut-Giffre
Cheval Blanc
Klippe of Aiguille du Belvédère (projected)
Mont-Blanc shear zone
Leloup et al, 2005
HBT
Fig.8
Fig.5 & 6
Sixt window
Poselles F.
VMSZ
TB
Fig.10
Lavancher fault
Angle fault
500m
500m
Plancherel et al., 1998
Leloup et al., 2005

Fig. 3. Structure of the Chamonix Synclinorium. a) Structural map. Location in Fig. 1a. Structure of the Haut-Giffre cover is from Pfiffner et al., (2010). HGTx, TBx, PMszx, FFx, FBx are acronyms for sites corresponding to several locations (HBT: Haut-Giffre Décollement, TB: Le Tour back thrust, PMsz: Pormenaz-Merlet shear zone, FF: Forclaz fault, FB: Finhaut back thrust). Samples and datations references are (1: Boutoux et al., 2016; 2: Rolland et al., 2008 and 3: Leloup et al., 2005). ZHe : U/Th/He technique on Zircons; Ar/Ar: $^{40}Ar/^{39}Ar$ method. Bt.: Biotite; Kf.: Potassium-rich feldspar; Phe.: Phengite; Min.: Minimum age; Plat.: Plateau age; Iso.: Inverse isochrone age. The map without stereo plots and surcharge is available as Fig. S1. Stereo plots show mean fault or shear plane kinematics in each site (lower hemisphere equal-area projection, arrows showing upper bloc motion). Precise locations and sites are given in Table S1. Mean shear or fault plane measures reported in the stereo-plots are available in Table S2. Stereoplots with all the data from each site are available in Fig. S2. Dashed black frames correspond to the spatial extent of the GeoModel (Fig. 4) and the zoom in the Posettes area (Fig. 11) Cross-section. Location and legend on (a). All structural data, locations, sites, samples, and 3D GeoModels are provided in a repository, see Data Availability statement.

3.2 3D Geological Modeling

Classically, the geometry of the geological structure deduced from observations at the surface and at depth is depicted through surface mapping and vertical cross-sections. When numerous cross-sections are performed, a relatively precise idea of the 3D geometry can be given. However, the cross-sections are only 2D projected representations of the surrounding data, and the original 3D data position, orientation, and uncertainty are lost.

The 3D geological approach of GeoModeller implements numerically geological concepts to build an implicit 3D model based on geological rules (Calcagno et al., 2008). The interface between two geological formations corresponds to an isopotential surface described by a potential field. That potential field is interpolated from the measured orientation data (stratification, cleavage, or foliation) using the geostatistical method developed by Lajaunie et al. (1997). The method uses the structural orientation data, that locally defines the gradient of the potential field. The interface is the isopotential surface passing through the contact point(s) observed in the field. Formations with interfaces that are sub-parallel to each other and thus share the same potential field are grouped into a series. Defining a series interface necessitates at least one structural measurement (orientation) within the series and one contact point (location). This is well adapted to model sedimentary series but can also be used in magmatic and metamorphic rocks when their internal structures are parallel to their interface (Calcagno et al., 2008). A relative chronology must be defined for the formations within the series to satisfy the geological concept of superposition. Further, a relationship between the series that are not parallel to each other, must be defined: erode if the series crosscuts the oldest ones and onlap if it does not (Calcagno et al., 2008). Faults are discontinuities that offset the potential fields, their relative timing must be defined to respect the cross-cutting relationships.

The 3D geological model encompasses a 14.3 x 20.3 km zone (Fig. s 3 and 4) and is based on new structural measurements at 432 locations at the surface. Some structural measurements are taken from published geological maps, (Corbin & Oulianoff, 1928; Amberger, 1959; Ayrton et al., 1987; J. L. Pairis et al., 1992). Other subsurface observations are taken along water penstock pipes provided by Emosson SA company (Fig. 3a). The resulting model has been built by distinguishing eight geological formations (Fig. 4) with their structural relationships defined according to the geology observed in the field and described in the bibliography. Model views are shown in Fig. s 4, 11, and 14. To better characterize the precise geometry of the synclinorium in its central part, we performed a smaller geomodel that allows a more detailled visualization of the synclinorium,

distinguishing four formations within the Mesozoic series (Fig. s 3a, 11 and 12)). The 3D GeoModels and their associated data are provided in the repository.

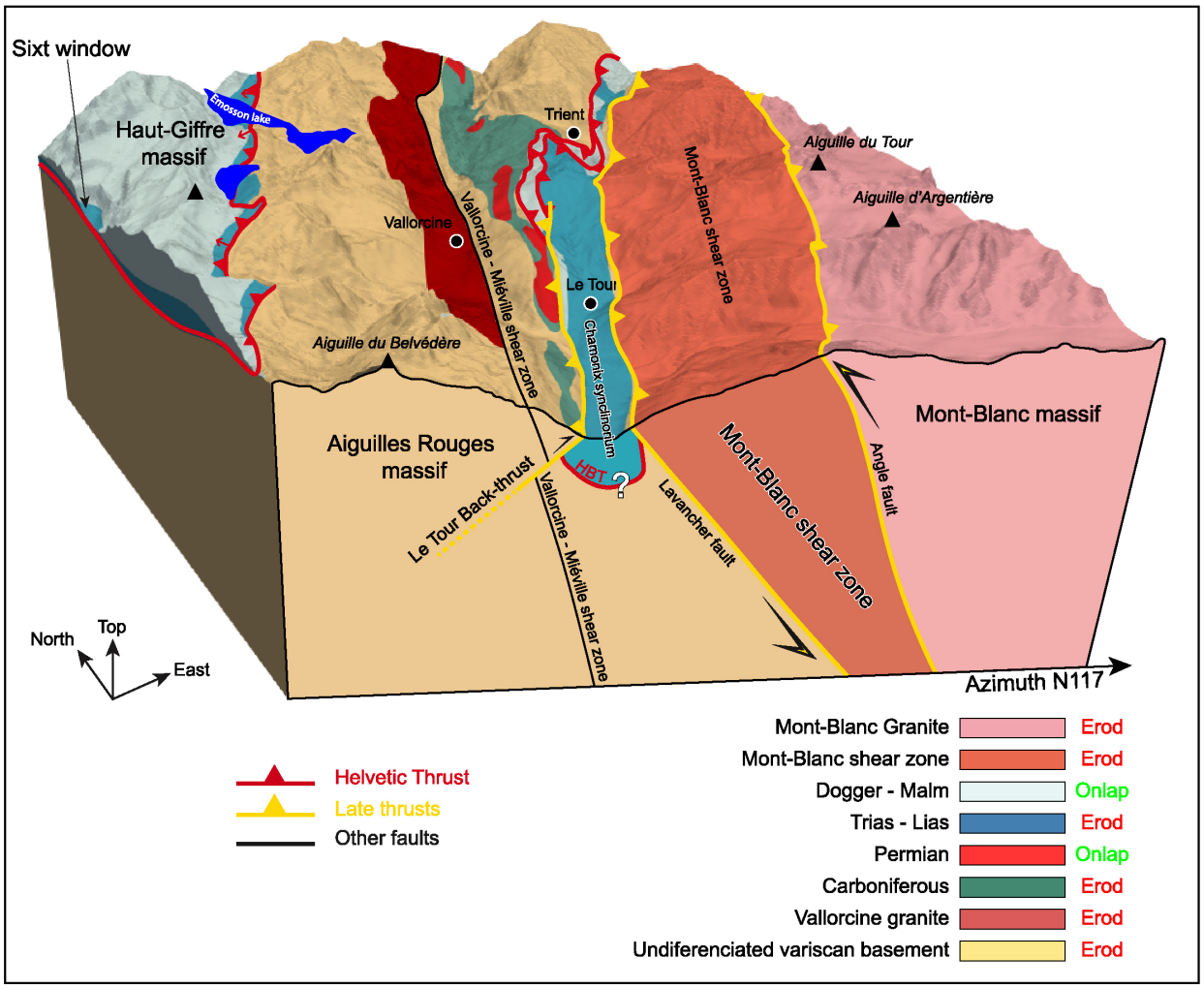

Fig. 4. View of the 3D GeoModel. The model is cross-cut perpendicularly to the structures across the Chamonix Synclinorium south of Le Tour village. See the associated stratigraphic pile and their relation that were used in the modeling.

4 Structures and cover/basement relationships in the Mont-Blanc/Aiguilles Rouges area

4.1 Geological background

4.1.1 Basement of the Aiguilles Rouges and Mont-Blanc ranges.

Within the Aiguilles Rouges, the basement corresponds to gneiss and granites with a polymetamorphic Variscan history and overlain by Carboniferous/Permian sediments (e.g., Von Raumer & Bussy, 2004). During the Variscan history, the Aiguilles Rouges followed a clockwise P-T path with the formation of eclogites at maximum metamorphic conditions of ≥60 km depth and 700±75°C (Vanardois et al., 2022) possibly at ~395 Ma. High-K calc-alkaline granite emplacement occurred at 332±2 Ma in the south of the massif (Bussy et al., 2000), with peak temperature, probably reached at 327±2 Ma (Bussy et al., 2000) during crustal thickening.

Migmatitisation occurred at 320±1 Ma during decompression in part within the transpressive NE-SW right-lateral Berard-Emosson shear zone (Bussy et al., 2000; Genier et al., 2008; Simonetti et al., 2020). The long and narrow Vallorcine granite intruded that shear zone at 306.5±1.5 Ma (Bussy et al., 2000). Its emplacement is interpreted to take place during NE-SW dextral strike-slip deformation (Brändlein et al., 1994). The granite is bounded in the south-east by the Vallorcine-Mieville shear zone (Fig. 3a) that is interpreted to be a late Variscan strike-slip shear zone (Reinhard & Preiswerk, 1927; Steck & Vocat, 1973) partly reactivated during the Alpine orogeny under low-grade metamorphic conditions (Kerrich et al., 1980; Steyrer & Sturm, 2002; Rolland et al., 2008). The precise history of that fault is most likely polyphase and still discussed. Post-Variscan cooling and exhumation were very fast, and sedimentation in the Salvan Dorénaz basin started at 308±3Ma (Moscovian, Carboniferous) by coarse detrital deposits and lasted until at least 295±3 Ma (Asselian, Permian) (Capuzzo & Bussy, 2000; Capuzzo et al., 2003; Capuzzo & Wetzel, 2004). The Variscan gneiss and granites are unconformably overlain by Triassic sandstones. Within the Aiguilles Rouges Alpine metamorphism and deformation are milder than in the Mont-Blanc with a maximum temperature of 320°C in the Carboniferous rock (Boutoux et al., 2016), and mostly brittle deformation (e.g., Von Raumer & Bussy, 2004).

Within the Mont-Blanc massif, the basement is very similar to the Aiguilles Rouges. The massif is mainly composed of a calc-alkaline granite intruding Variscan metamorphic gneiss. The granite has been dated by U/Pb on zircons at 304±3 Ma (Bussy and Von Raumer, 1993).

4.1.2. Cover of the Aiguilles Rouges and Mont-Blanc ranges.

On the western margin of the Aiguilles Rouges massif, the bottom of the Mesozoic sedimentary cover corresponds to a sandstone layer dipping 15° to 35° to the north-west that can be followed continuously for about 25 km (e.g., Amberger, 1959; Ayrton et al., 1987; J. L. Pairis et al., 1992) (Fig. 3a and b). The layer marks a clear stratigraphic and angular unconformity as it rests on Variscan gneiss with steep foliation (average N012, 70°E) (Fig. S3). The sandstone level is overlain conformably by red and green siltites, dolostones, and cargneule attributed to the Triassic (Collet et al., 1952; Ayrton et al., 1987; J. L. Pairis et al., 1992). The same succession is found at several localities along the unconformity and defines the Triassic autochthonous cover of the Aiguilles Rouges. Locally, white limestone is found above this series (Fig. 3a) and is attributed either to the Upper Jurassic (Collet et al., 1952, Ayrton, 1972) or the Cretaceous (Ayrton et al., 1987, B. Pairis et al., 1973, J. L. Pairis, 1992). At other locations the succession is topped by Aalenian black slates, (Ayrton et al., 1987, Collet et al., 1952, J. L. Pairis et al., 1992). That Mesozoic series has been interpreted as an incomplete stratigraphic succession resulting from condensed sedimentation atop a Mesozoic horst (e.g., Corbin & Oulianoff, 1928; Ayrton et al., 1987).

The autochthonous/allochthonous nature of the cover above the Aiguilles Rouges basement is debated since decades. On the western flank of the Aiguilles Rouges the Mesozoic series above the Triassic have been considered as the para-autochthonous cover of the Mont-Blanc, belonging to the Morcles fold-nappe with insignificant thrusting with respect to the underlying basement (e.g., Escher et al., 1988, Bellahsen et al., 2014). In the highest peak of the Aiguilles Rouges, (Fig. 3a), Collet and Paréjas, (1920) proposed that the Aalenian is thrust atop the Triassic, but the associated folds were later interpreted as local structures of minor importance (e.g., Corbin & Oulianoff, 1928; Ayrton at al., 1987). Similarly, white limestones in Pormenaz (Fig. 3a) have been considered allochthonous (Duparc et al., 1966, Dobmeier and Von Raumer, 1995) or autochthonous (J.-L. Pairis et al, 1992).

The complex geometry of the Chamonix synclinorium has led to several interpretations. Some consider that the western boundary of the Chamonix synclinorium corresponds to the Triassic basal unconformity atop the Variscan gneiss (Ayrton, 1980; Ayrton et al., 1987). In the para-autochthonous hypothesis, that boundary is a Mesozoic normal fault bounding a half-graben filled by a thick series of syn-rift sediments, while the top of the horst presents an incomplete stratigraphic succession (e.g., Bellahsen et al., 2014, Boutoux et al., 2016). However, such a normal fault has never been characterized with direct evidence. Further north, in the Morcles massif, Badoux (1972) suggests that the Chamonix synclinorium corresponds to a deep Priabonian basin with detrital deposits sourced from the Aiguilles Rouges cover. Some argue that the Mesozoic sediments are not autochthonous but are thrust above the basement (Leloup et al., 2005, Pfiffner at al., 2010). Others consider that a major thrust within the Chamonix synclinorium separates the Mont-Blanc and Aiguilles Rouges autochthonous covers (Ayrton, 1980; Ayrton et al., 1987).

For most authors, the Chamonix synclinorium corresponds to the Morcles nappe root, but the interpretation varies on the style of deformation and amount of motion at the base on the nappe. For some, the Morcles nappe is a large anticline affecting both the basement and the cover (ductile basement fold nappe), the eastern boundary of the Chamonix synclinorium corresponding to the reverse limb of the fold, the external Mont-Blanc being the core of the fold and the normal limb rooting in the Angle fault (e.g., Epard, 1990, Esher et al., 1988, 1993) (Fig. 2a). However, no clear evidence of the folding of the Mont-Blanc basement has ever been published. Others propose that the external Mont-Blanc is not folded but corresponds to an Alpine reverse shear zone that brings the basement on top of the synclinorium (e.g., Bellière, 1956; Eltchaninoff, 1982; Butler, 1985; Leloup et al., 2005) (Fig. 2a). This ~3km wide deformation zone is characterized by south-east dipping greenschist foliation trending from N000° to N066° (N034°; 53°E on average). Previously interpreted as resulting from three distinct Variscan deformation events (Bellière, 1988), this deformation is rather interpreted as a network of Alpine shear zones affecting Variscan mylonites, gneisses, and granites (Leloup et al., 2005). Shear criteria in the Alpine mylonites indicate top to the northwest thrusting (Leloup et al., 2005). As the mineral and stretching lineation have pitches between 90° to 60° E (Average azimuth N100°), this corresponds to a thrust with a minor dextral component. The upper part of the Mont-Blanc shear zone corresponds to the Angle fault (e.g., Corbin & Oulianoff, 1928), and the lower one to the Lavancher fault (Fig. 3). The Mont-Blanc shear zone dies out southwest and northeast of the Mont-Blanc with a maximum offset between Chamonix and l'Argentière (Leloup et al., 2005). In that interpretation, the overturned stratigraphic sequence along the eastern boundary of the Chamonix synclinorium is a drag fold below the reverse fault. A variation of the basement fold nappe model is that the Mont-Blanc massif is part of a large anticline with the Mont-Blanc shear zone constituting the western reverse limb of that fold (e.g., Egli et al., 2017). Yet others consider that the linear shape of the Chamonix Synclinorium, and of the Mont-Blanc range, partly results from right-lateral strike-slip faulting along the Simplon Rhône - Belledonne fault system (Gourlay & Ricou, 1983; Hubbard & Mancktelow, 1992; Seward & Mancktelow, 1994).

4.2. Thrusting evidences in the Aiguilles Rouges

4.2.1 *Thrusting along the western margin of the Aiguilles Rouges.*

In the north of the Aiguilles Rouges, next to the Col de Barberine (site HGT1, Fig. 3a), the autochthonous Triassic is folded, brecciated, and overlain by a sliver of Variscan migmatitic gneiss itself overlain by Triassic quartzite (Fig. 5a). While the sliver of gneiss does not appear to have

been deformed at low temperatures the upper part of the Triassic level is strongly deformed, affected by recumbent folds (Fig. 5b), and strongly brecciated at the contact (Fig. 5a). The Triassic is overlain by a slice of limestone attributed to the Eocene, directly overlain by the limestones attributed to the Upper Jurassic (Collet, 1952) (Fig. 5a). The stratigraphic series is isoclinaly folded and foliated with S/C relationships suggesting a top to N285° shearing (Fig. 5c). These observations imply both the duplication of the Triassic/basement contact and intense top to the northwest shearing of a reverse stratigraphic series.

Further south, in the Mont-Oreb area (site HGT2, Fig. 3a), above the Triassic, white limestones attributed to the Upper Jurassic are strongly deformed. The limestones are metamorphosed to marbles and a strong west-dipping schistosity affects both the limestone and calcite veins (Fig. 6a). The cleavage bears a stretching lineation trending N280° (Fig. S4a) and asymmetry of the folds suggests a top to the west shear sense. intensively sheared within a major decollement (Fig. 6c). At nearby location AR0184 (Fig. 6c), the underlying Triassic sandstones are also strongly deformed, affected by an isoclinal fold with the axial plane and axis parallel to the cleavage and stretching lineation respectively (Fig. S4b). The limestones are overlain by strongly foliated and folded black slates attributed to the Aalenian, implying decoupling between the two units and thus another fault at the top of the limestones (Fig. 6c). The same fault is visible atop the white limestones at several locations, for example near the Vieux Emosson lake (Fig. 3, Fig. 6b). Further south along the Souay river, (site HGT3, Fig. 3a), above the Carboniferous sediments of the Pormenaz basin, Triassic brecciated cargneules are overlain by white limestones that are metamorphosed to marbles and mylonitized (Fig. S5a). The marbles bear a well-visible stretching lineation, trending N288° and are also asymmetrically folded with an axis trending N032° (Fig. S5b). The lineation, shear plane, and asymmetry of the fold suggest a direction of shear towards the WNW.

Above the white limestone, the Aalenian black slates are affected by numerous spectacular isoclinal folds. The folds do not show a systematic vergence (Fig. 7a, b) and are even sometimes closed (Fig. 7d). Given the steepness of the topographic slopes, few measurements of these folds have been performed, but north of the Emosson lake (Site HGT4, Fig. 3a) stratification and cleavage measurements indicate two families of fold axis trending N209° and N280° and sharing an almost horizontal axial plane (Fig. 7c). Such folds are widespread in the Haut-Giffre Mesozoic cover (Fig. 3a).

We interpret all these field observations as reflecting a major ~500 m thick shear zone affecting the Mesozoic cover above the Aiguilles Rouges basement. We term the base of that shear zone the Haut-Giffre Thrust (HGT). The direction of shearing is given by the orientation of the stretching lineation and the shear sense is top to the WNW motion (Fig. 3a). Within the shear zone, several folds are sheath folds that have highly curvilinear axes, with some axis parallel to the direction of transport. Such folds occur in shear zones with a high simple shear strain ($\gamma \geq 10$) (Cobbold and Quinquis, 1980; Quinquis et al., 1978, Lacassin & Mattaeuer, 1985).

The present-day dip of the HGT with its top to the WNW motion would correspond to a normal fault configuration (Fig. 6c). But local basement duplication implies that the fault is an additive as it duplicates formations and is thus more probably a tilted thrust. Slices of relatively young formations (Upper Jurassic in the south, Eocene in the north) near the base of the shear zone

suggest that it is a sheared reverse limb, equivalent to the reverse limb of the Morcles nappe outcropping less than 15 km to the northeast (e.g., Escher et al., 1993).

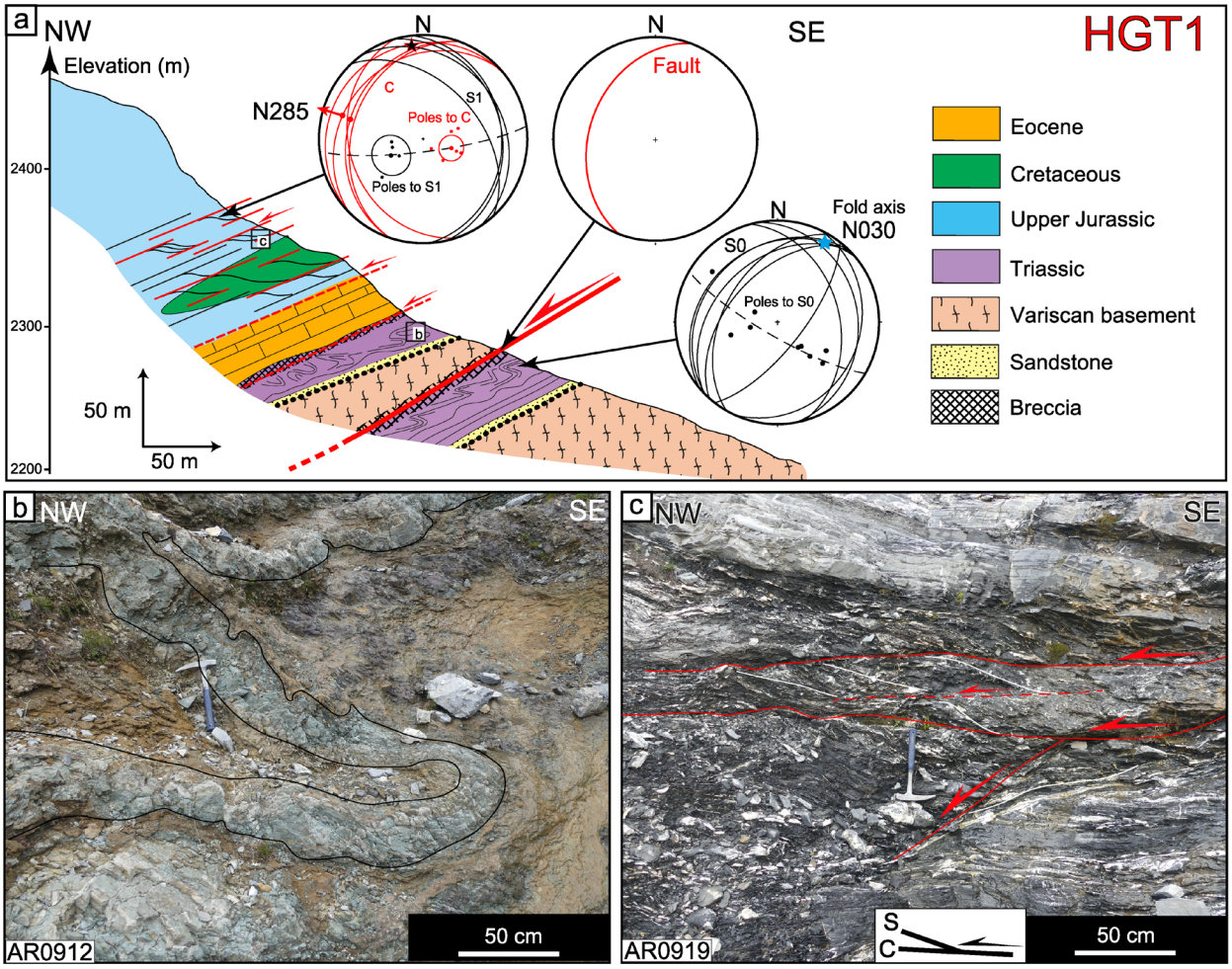

Fig. 5. Cover/basement relationships at the col de Barberine (Aiguilles Rouges, site HGT1). a) Field cross-section along a talweg 300 m west of the Barberine pass. Stratigraphic ages from Collet et al. (1952). Stereo plots (equal-area, lower hemisphere projection) show the geometry of structures in b and c. b) Recumbent fold in red and green Triassic siltites at location AR0912. The fold axis trends N030°. b) Strongly sheared black shales at location AR0919. S/C relationships indicate top to the N285° shearing.

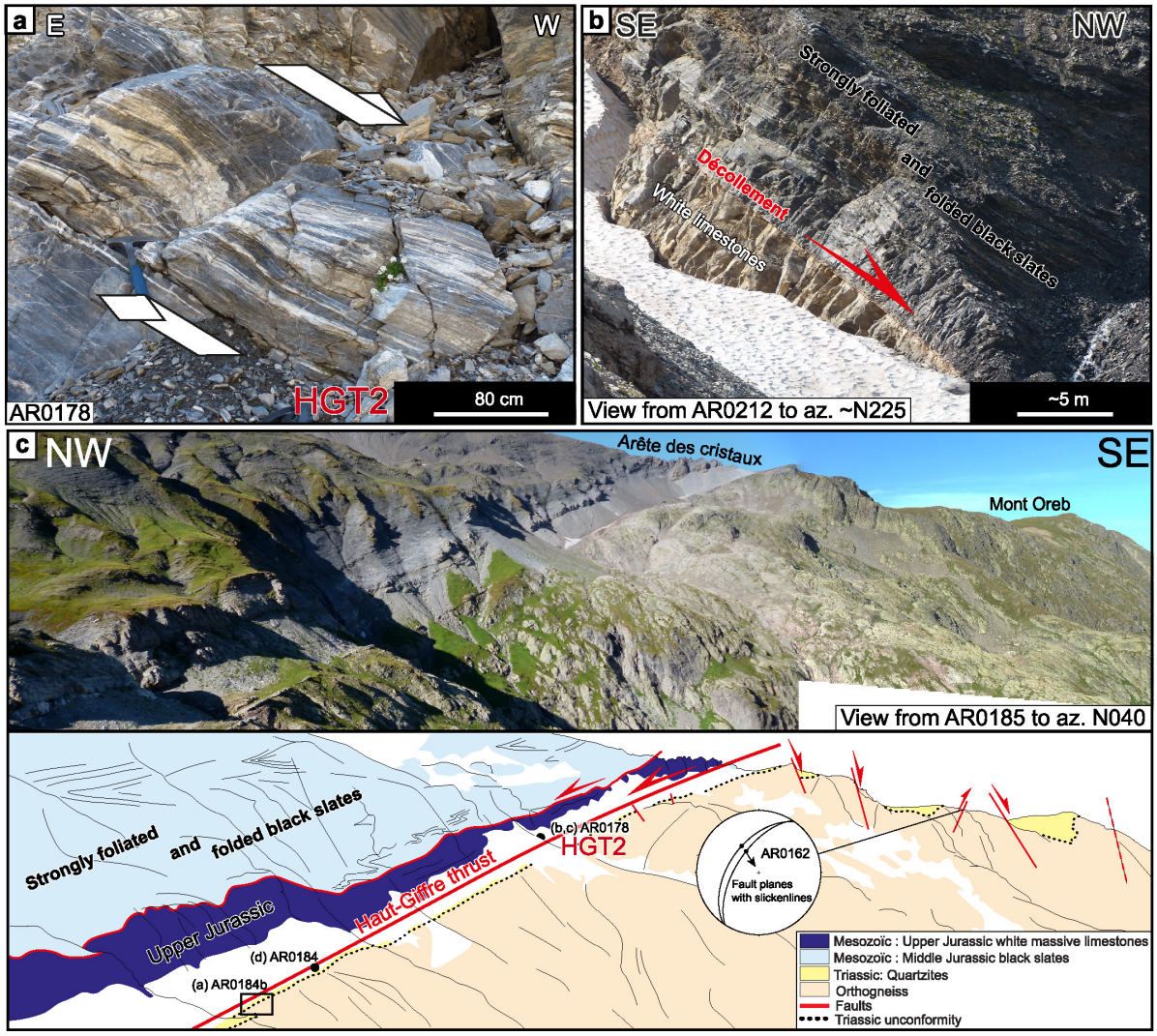

Fig. 6. Cover/basement relationships in the western side of Aiguilles Rouges. a) Shear zone at the base of the Mesozoic sedimentary cover, above the Triassic unconformity at site HGT2; b) Localized decollement above white limestones. The decollement is associated with a shear zone in the Aalenian slates; c) Picture at the top and interpreted panoramic view at the bottom of the Haut-Giffre thrust (view from location AR0185, towards ~N040°). The Upper Jurassic white limestones are visible as well as intense folding within the lower Mesozoic slates above.

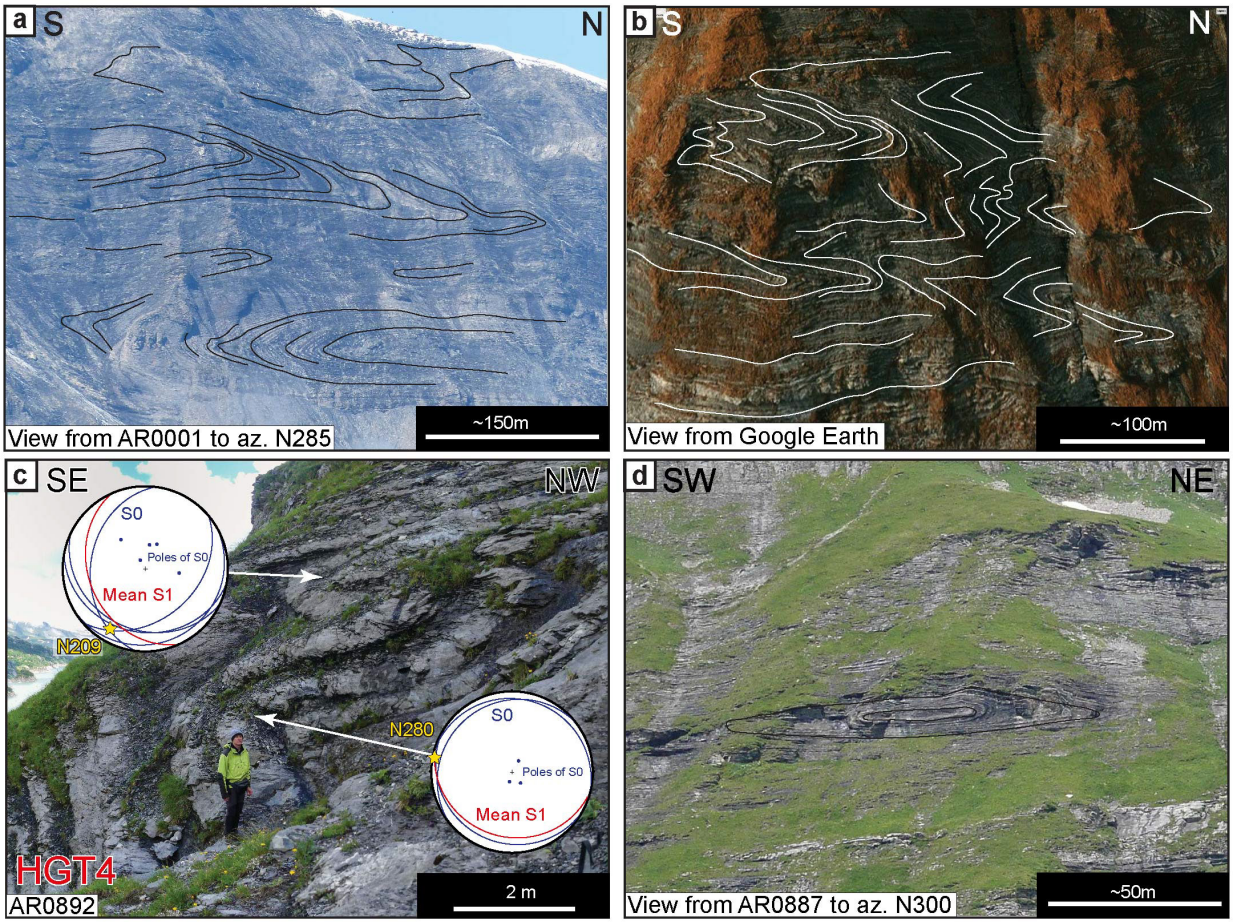

Fig. 7. Folding of the Mesozoic cover on the western flank of the Aiguilles Rouges. Locations in Fig. 3a. a) Large isoclinal folds on the Haut-Giffre massif seen from the Montagne des Posettes. Some stratifications are highlighted in black. b) Google Earth™ view of the slope above the Emosson lake. Some stratifications are highlighted in white; c) Two different types of folds affecting the Mesozoic cover above the Emosson lake (site HGT4): stereo plots (equal-area, lower hemisphere projection) show the bedding and cleavage of the folds: one with N280 trending axis, and the other with N209 trending axis.; d) Entirely closed sheath fold above Emosson lake (view from location AR0887, towards azimuth ~N300°).

West of the Aiguilles Rouges, the Giffre river has dug a deep valley in the Mesozoic sediments. In this valley, 4 km northeast of Sixt-Fer-a-Cheval village, there is a small outcrop of the basement (Site HGT5, Fig. 3a). There, the Variscan basement corresponds to chlorite bearing schist with a nearly horizontal foliation and is topped unconformably by Triassic sandstones (Fig. S6a). Above, the Triassic succession (sandstone, dolostone, green and red siltites) is nearly horizontal, itself overlain by intensively folded and sheared black slates with shear planes trending N038°; 32 SE (Fig. S6b). This outcrop is therefore a window through the Haut Giffre thrust. That window is an important constraint for the geometry of the 3D GeoModel (Fig. 3b, Fig. 4).

4.2.2 *Thrusting atop the Aiguilles Rouges.*

Atop the Aiguilles Rouges (Aiguille du Belvédère, site HGT6), outcrops Mesozoic sediments interpreted as a buttress of an autochthonous incomplete series deposited atop a Mesozoic horst (e.g., Corbin & Oulianoff, 1928; Ayrton et al., 1987). However, if the basal part of the series is the

autochthonous level of Triassic sandstone described above, the overlying dolostone layers are affected by intense northwest-verging folds with N032° trending axis and south-east dipping axial planes (Fig. 8a, b, and c), while the upper part of the summit is composed of flat-lying (sub-horizontal) black slates, with a stretching lineation striking N285° (Fig. S7a). Our interpretation is thus rather that the Mesozoic cover at this location is affected by two main top-to-the-NW flat faults (Fig. 8a), with transport direction towards ~N310° (Fig. S7b) for the bottom one and ~N285° for the top one (Fig. S7a). These faults most likely connect with the Haut-Giffre thrust located less than 2.5 km away (Fig. 3). Because the peak is in a high-mountain area, access is quite challenging. Therefore, we acquired high-resolution drone images, to build a 3D photogrammetric digital elevation model (DEM). Fig. 8a is a screenshot of the model. See data Availability for more information and links to visualize and download the model.

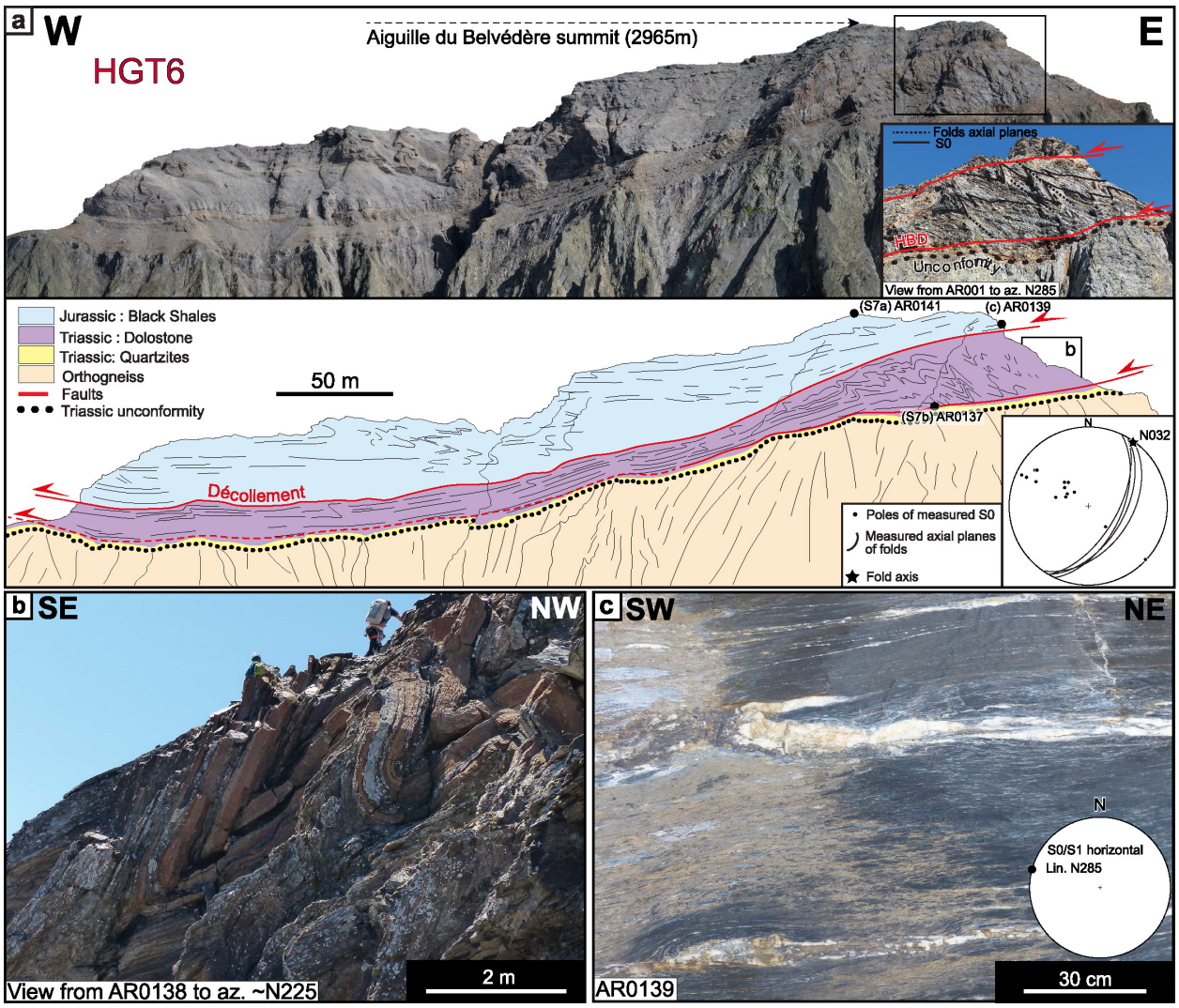

Fig. 8. Cover/basement relationships at the Aiguille du Belvédère. a) Panorama of the summit view from the south. Top: a screenshot of the 3D photogrammetric model. Bottom: geological interpretation. Insets: picture and stereo-plot (equal area, lower hemisphere projection) of northwest verging folds within the Triassic dolostones. The folds have an axis trending N032°. b) Tight northwest verging folds within the Triassic sedimentary cover (view from location AR0138, towards azimuth N225°). The folded dolostones bears a stretching lineation striking N130° (see Fig. S7b);

c) Highly deformed mesozoïc black slates with calcite isoclinal folding and boudinage (location AR0139) bearing a stretching lineation striking N285° (see Fig. S7a).

Seven kilometers southwest of the Aiguille du Belvédère, another buttress of limestones atop the basement is described at the Crête Blanche de Pormenaz (site HGT7, Fig. 3a). At this location, the Triassic sandstones rest on dark Carboniferous series and are overlain by white limestones (Fig. 9a). The Triassic sandstones are affected by a cataclastic foliation (Fig. 9b). The bottom of the limestone is also deformed and marmorized, with indications of foliation boudinage (Fig. 9c), suggesting that the basal contact of the limestones and the Triassic is tectonic rather than stratigraphic. This implies that the Mesozoic forms a small klippe. We thus interpret the basal contact as part of the Haut-Giffre décollement rather than an undeformed stratigraphic contact.

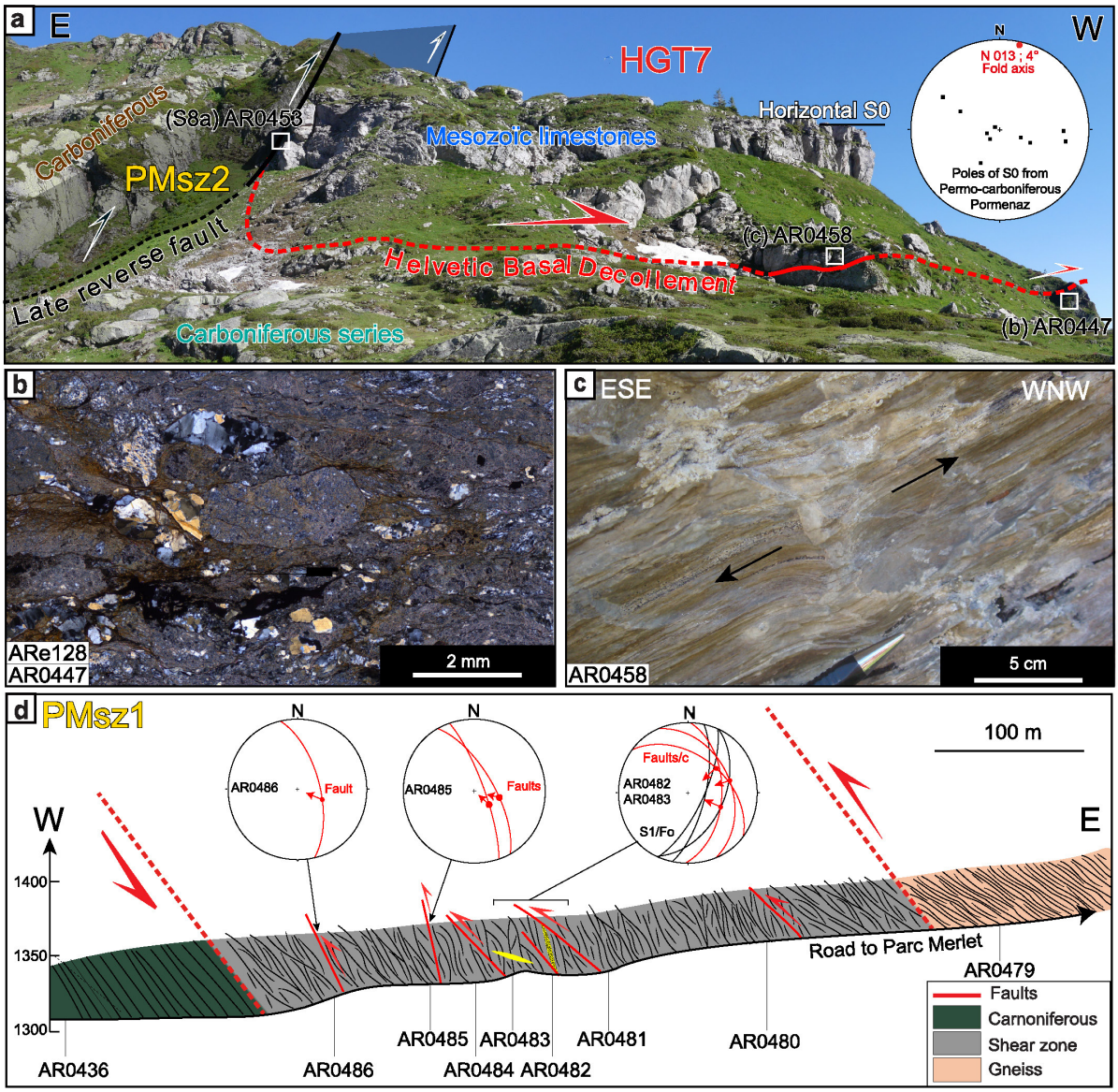

Fig. 9. Cover/basement relationships near Pormenaz (Aiguilles Rouges massif). a-c) The Crête Blanche klippe. a) General view of the klippe, the limestones are thrusted westward above a basal thurst, before being offset by a late steep thrust (See also Fig. S8a). Stereo-plot (lower hemisphere, equal area) on the right shows poles of bedding planes of the Carboniferous sediments in the Pormenaz zone: average folds axis dips ~4° to N013°. B) Foliation and

metamorphosed quartzite (location AR0447). c) Marmorized limestones showing foliation boudinage, indicating ESE-WNW-oriented stretching (location AR0458). d) Cross-section of the Merlet-Pormenaz shear zone along the road to the Merlet parc. Stereo-plots (lower hemisphere, equal area) show fault planes and shear planes along the section.

4.2.3 *Thrusting of the cover on the eastern side of the Aiguilles Rouges: The Forclaz Fault*

In the northwest of the Chamonix synclinorium, the Mesozoic sediments rest on top of the Aiguilles Rouges basement along an east-dipping contact: the Forclaz Fault (Fig. 3, and Fig. 10a). At site FF1 the Mesozoic rocks rest on top of Carboniferous sandstones and are strongly deformed with a cleavage steeply dipping to the east and a downdip lineation. A few kilometers further north at the foot of the Croix de Fer summit (site FF2, Fig. 3a), the contact cannot be observed directly but the overlying upper limestones appear much less steep and bear a well-printed stretching lineation trending N130° (Fig. 10a). The basal contact is well exposed at location AR0190 (site FF3, Fig. 3a, 10b, and 10c) along the road to the Forclaz pass, where Mesozoic sediments are separated from gneiss by a 50 cm thick quartz level (Fig. 10b). This quartz level was previously interpreted as the basal Triassic sandstone layer resting unconformably atop the Variscan gneiss (Ayrton, 1980; Ayrton et al., 1987). A thin section of the sample Are042, from that quartz layer, has been cut perpendicular to the fault contact and parallel to the lineation. At the micro-scale, the quartz grains are angular with a size below 100 µm. This suggests that the layer more likely corresponds to a deformed level separating the sedimentary rocks from the basement (Fig. 10d). Crystallographic Preferred Orientation (CPO) analysis of quartz using Electron back-scattered diffraction (EBSD) of sample ARe042 thin section has been performed (Fig. 10c) (technical information about the analysis is provided in Table S3). Data were processed with the MTex algorithm (Hielscher & Schaeben, 2008), 5788 grains were identified on 343 007 pixels, using a misorientation threshold of 15° and minimal grain size of 5 pixels. The presented stereographic plot (equal area, lower hemisphere) shows the orientations of the crystallographic axis (<a> and <c>), with color according to point density (one point per grain identified). The CPO suggests the activation of the quartz crystallographic basal plane, at about 350° − 400°C (Passchier & Trouw, 2005), with a top to the west reverse shearing along the <a1> axis trending N122° (Fig. 11c and d).

We interpret the Forclaz fault as a west verging thrust because (i) site FF3 shows a top to the northwest thrusting of the Mesozoic sediments above the Aiguilles Rouges basement (Fig. 10b and c). (ii) As already pointed out by Ayrton (1980), folds within the overlying Mesozoic have an NW vergence.

4.2.4 Thrusting within the Chamonix synclinorium: the Posettes fault.

Within the Mesozoic synclinorium, the Posettes fault dips to the southeast, runs subparallel to the Forclaz Fault, and brings Middle Jurassic black slates on top of strongly folded Upper Jurassic limestones (Fig. 10a, Fig. 3a and b). This geometry is well-constrained in the 3D models, particularly in the Montagne des Posettes zoom-in model (Fig. 11). The black slates are also strongly folded, describing a large fold with a steep axis (~ trend 70° / plunge 68°) and with a core of middle Jurassic limestones that constitute the Croix de Fer summit (Ayrton, 1980). Further east the Mesozoic series dip to the southeast and are cut by the Mont-Blanc shear zone that rises the Mont-Blanc basement (Leloup et al., 2005) (Fig. 10a).

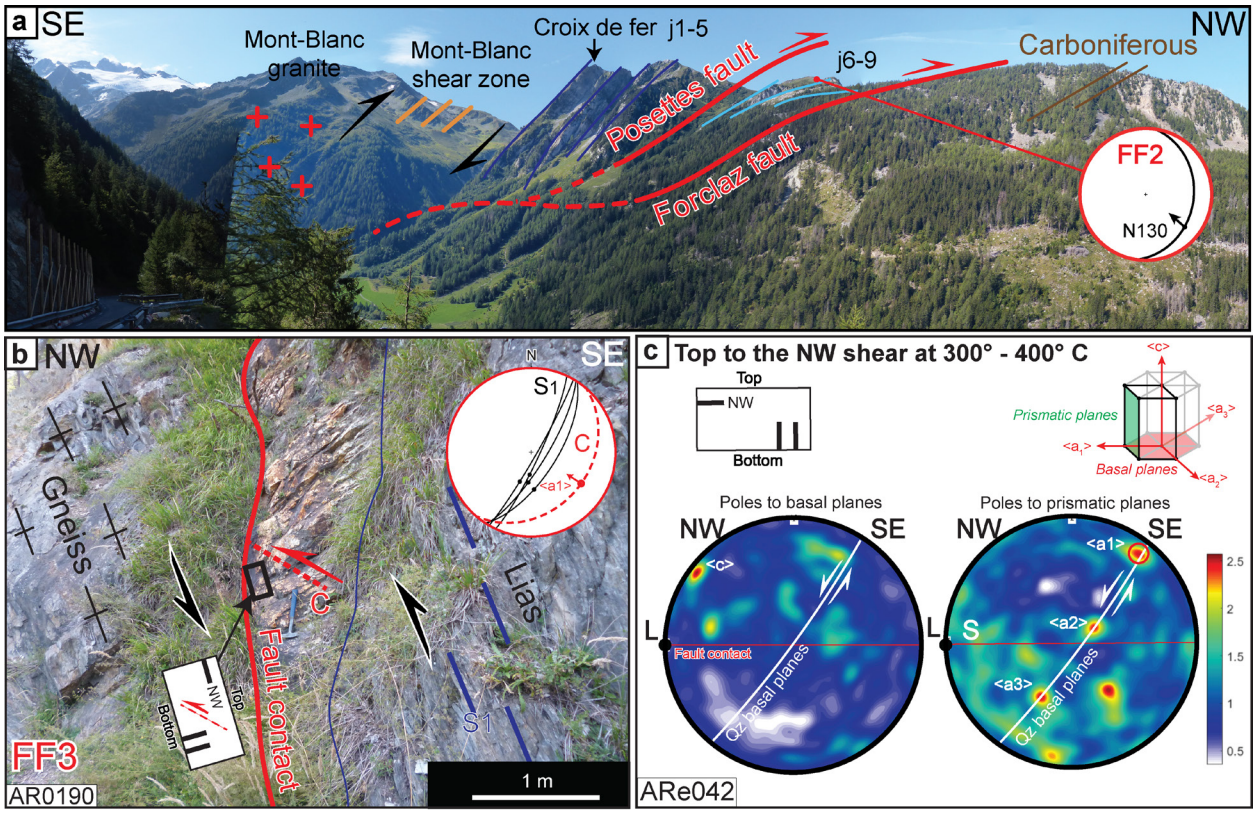

Fig. 10. Cover/basement relationships in the north of the Chamonix Synclinorium. a) The Mont-Blanc shear zone, Posettes, and Forclaz fault viewed from the north. b) Forclaz Fault quartz layer at site FF3 (location AR0190). Plotted S1 refers to the cleavage in the Liassic slates, dashed red line corresponds to the shear plane inferred from CPO analysis, plotted lineation refers to the <a1> direction; c) Crystallographic preferred orientations (CPO) of <c> and <a> axis of quartz sample ARe042 measured with EDSD technique. Equal area projection, lower hemisphere, color as a function of the measurement density, fault contact is plotted as horizontal (red line) and the lineation is in the NW-SE direction (black circle). The pattern suggests an activation of the crystallographic basal plane along the <a1> direction, compatible with a top to northwest sense of shear.

The folds with steep axis have been interpreted as reflecting strike-slip motion along the Rhône valley being part of the Simplon-Rhône dextral fault (Hubbard & Mancktelow, 1992). As Ayrton (1980) we rather interpret them as large sheath folds, like those observed in the Haut-Giffre, some of them with axis nearly parallel to that of the shearing direction within the cover décollement zone. In this interpretation, the base of the Mesozoic cover of the Chamonix synclinorium corresponds to the same Haut-Giffre Thrust.

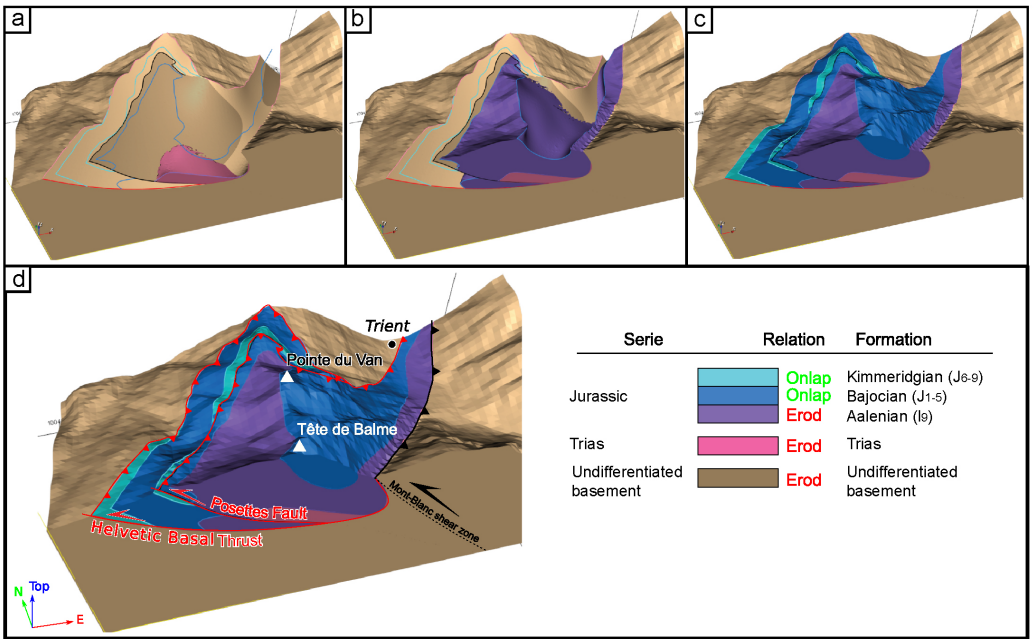

Fig. 11. Views of 3D GeoModel, from the central part of the synclinorium: the Montagne des Posettes. a) to d), views of the GeoModel with the different layers removed. The basal decollement and the Posettes thrust are highlighted in red. The Mont-Blanc shear zone is not modeled here, however, its position is shown in the Fig. . The stratigraphic pile of the model as well as the relationship between them is shown in d.

4.2.5 Synthesis on the thrusting above the Aiguilles Rouges

To sum up, the faults and shear zones found on the western limb (Haut-Giffre thrust - HGT), atop (Pormenaz and Belvédère klippes), and on the eastern limb (Forclaz fault) are segments of the same thrust at the base of the Helvetic nappes: the Helvetic basal Thrust (HBT) (Fig. 3b). Motion on the HBT is everywhere top to the WNW and its antiformal shape results from the later updoming of the Aiguilles Rouges. The HBT is nearly parallel to the cover/basement interface and is the base of a strongly sheared reverse limb of a recumbent fold. It corresponds to the base of the Morcles Nappe. It affects the Jurassic and Triassic series, and even locally the basement.

4.3. Reverse faults in the Aiguilles Rouges range and the Chamonix Synclinorium.

4.3.1 Pormenaz-Merlet shear zone.

The southwest side of the Aiguilles Rouges is characterized by the contact zone between gneiss and Carboniferous sediments (Site PMsz1, Fig. 3a). The contact corresponds to a 350m wide shear zone with foliation north-south striking and steeply dipping (~70°) to the west (Fig. 9d). Shallower shear planes trend from N156° to N182° and bear lineations trending N050° to N130°, indicating a top to the west thrusting (Fig. 9d).

Returning to the Pormenaz Crête-Blanche (Site PMsz2, Fig. 3a), the white limestones described in section 4.2.2 abut against the Carboniferous series. This contact corresponds to a steep reverse fault trending N003°;70 SE that brings the Carboniferous on top of the Mesozoïc limestones (Fig. 9a, Fig. S8a). A few decameters to the east the same shear zone brings the Variscan gneiss of the Aiguilles Rouges on top of the Carboniferous (Site PMsz3 Fig. 3a). There, flat reverse faults with

striation trending N130° affect the carboniferous, showing top-to-the-north-western shearing (Fig. S8b).

These observations lead to the interpretation of the eastern boundary of the Carboniferous sediments as a continuous reverse shear zone, as already suggested by J. L. Pairis et al. (1992) and Dobmeier and Von Raumer (1995). The fact that the shear zone bounds the Crête-Blanche klippe imply it is younger than the Haut-Giffre Thrust. The Carboniferous sediments below the shear zone are affected by folds with an axis striking N013° (Fig. 9a), suggesting an ~E-W direction of compression, compatible with the measures of the faults above.

4.3.2 Back Thrusting on the eastern side of the Aiguilles Rouges.

North of the Aiguilles Rouges, at the limit between the Salvan-Dorenaz Carboniferous – Permian basin and the Aiguilles Rouges basement (Site FB1, Fig. 3a) the Permian sediments show an ~N032° sub-vertical schistosity and west-dipping reverse shear planes trending N012° on average (Fig. 12a and b). These observations indicate that at this location the Variscan basement is thrust toward the east over the Salvan-Dorenaz basin, along a previously unreported thrust fault that we name Finhaut back thrust. According to the published geological map (Collet et al., 1952), the Finhaut back-thrust probably extends 5 km to the south (Fig. 3a). Within the basin, the sediments are strongly folded with folds axis trending ~N030° and steep axial plane schistosity trending N020° on average (Fig. 12c). Similar folds are found in the Carboniferous/Permian sediments of the Posettes area on the other side of the valley. A previously unreported ~N020° trending normal fault, the Gietroz fault, offsets the basin (Fig. 12c). A thin section of sample ARe096 (Fig. S9) indicates a normal shear sense on the fault. Both the Finhaut back thrust and the folds affecting the Salvan-Dorenaz basin could have formed coevally during an ~N110° compression phase, while the Gietroz fault is probably younger.

West-dipping reverse faults and shear zones trending ~N020°, whilst never described in the literature, are relatively common in the eastern part of the Aiguilles Rouges. Another example can be found further south (site FB2, Fig. 3a), where reverse faults trend N017;77°W with clear evidence of thrusting towards the southeast. Numerous such faults are also visible on the eastern shore of the Emosson Lake (site FB3, Fig. 3a) striking on average N015°; 59°W with striations azimuth trending ~N105°. Such a fault trending ~N033; 60°W with a striation with a pitch of 75°N is also visible at site HGT1 (location AR0162) in between possibly earlier normal faults (Fig. 6c).

The brittle regime of these faults suggests they are occurring at low pressure/temperature conditions and could be related to recent deformations. These observations suggest that back thrusting in the Aiguilles Rouges has been overlooked and may play an important role in the structuration and exhumation of the massif.

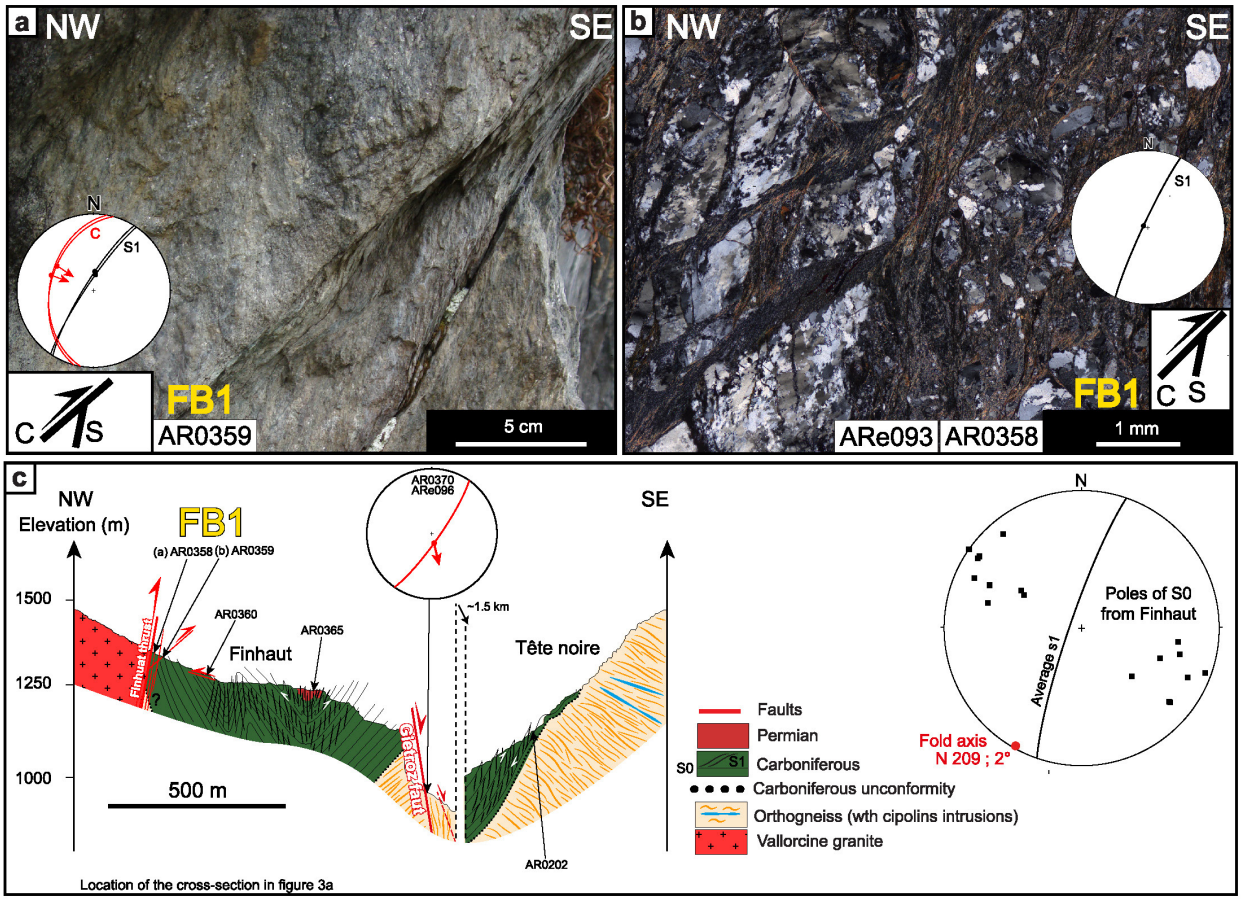

Fig. 12. The Finhaut back thrust. a) Thin section of sample ARe093 of the Finhaut thrust (site FB1, Fig. 3a). Greenschist foliation strike N025°; 85°W and S/C relationships imply a reverse motion. b) Shear planes within Carboniferous sediments in the footwall of the Finhaut back-thrust at location AR0359. Shear planes (C) strike N010°; 42°W, C/S relation implies a top to the south-east sense of shear. c) Cross-section across the Salvan-Dorénaz basin, see Fig. 3a for location. Stereo plots (equal area, lower hemisphere projection) in the Finhaut area the average folds axis dips 2° to N209°.

Further south in the Chamonix valley, most of the synclinorium western border is hidden by Quaternary deposits. However, a large outcrop of limestones attributed to the Jurassic (Ayrton et al., 1987) is visible at site TB1 (Fig. 3a). These limestones are affected by a schistosity that trends N072°;40°N and are overlain by the Aiguilles Rouges basement composed of Variscan gneiss and a Permo-Carboniferous tight syncline (Fig. 13a). Just above the contact, the Permian green siltites are foliated (N002°;44°E) and a bear mineral lineation (N126°). The thin section cut parallel to the lineation shows a clear thrust top to the southeast with S/C criteria (sample ARe033, Fig. 13c). At this location, the Aiguilles Rouges basement is therefore thrust above the cover.

Six kilometers further north near le Tour village (site TB2, Fig. 3a) Mesozoic sediments are also found below the Aiguilles Rouges basement. The Permian green siltites are foliated, with S/C criteria indicating a top to the southeast reverse shear (Fig. 13b and d). That contact continues ~2 km toward the northeast (Fig. 3a). The two faults at sites TB1 and TB2 have the same direction

and the same kinematics and are interpreted as a back-thrust fault of the Aiguille Rouges above the Chamonix synclinorium that we call the Le Tour Back thrust (Fig. 3a).

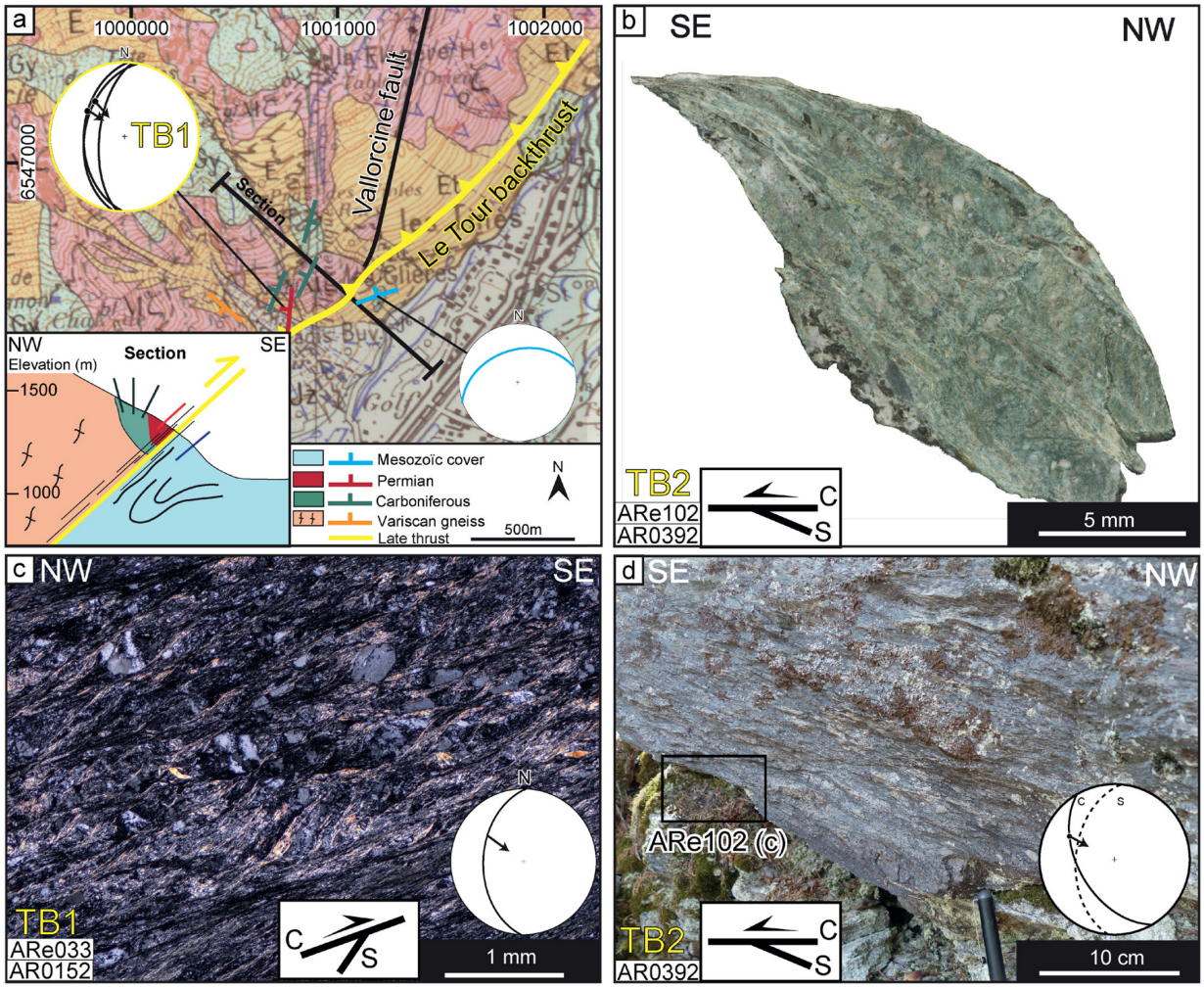

Fig. 13. Le Tour back thrust. a) Structural map and cross-section (inset). The background is the 1:50.000 geological map (Ayrton et al., 1987). Stereo-plots (lower hemisphere, equal-area projection) show the orientations of the schistosity in the Mesozoic sediments in the over-thrusting Permian schists. b) Thin section of the sample ARe102, S/C relationship suggests top to the south-east reverse sense of shear; c) Thin section of sample ARe033 cut parallel to lineation. S/C relationship suggests top to the south-east reverse sense of shear. d) Location of sample ARe102 from location AR0392, S/C relationships indicates top to the south-east sense of shear.

Further south there is no outcrop of Mesozoic sediments and the Tour back-thrust cannot be mapped. We infer that this fault is hidden by the Quaternary deposits (Fig. 3a). Cartographically the Tour back thrust is parallel to the Finhaut back thrust, thus they have possibly been activated at the same time. Le Tour back thrust is seen in the GeoModel, bringing the Posettes Permo-Carboniferous syncline atop the Chamonix Synclinorium (Fig. 4 and Fig. 14a, b, and c).

5 Implications on the structural evolution of the Mont-Blanc and Aiguilles Rouges massifs

5.1 Relative timing of the main structures

After the deposition of Mesozoic and Cenozoic sediments, the first widespread shortening tectonic phase in the area involved thrusting of the Mesozoic/Cenozoic cover towards the west along a relatively flat structure that we term the Helvetic basal thrust (HBT) (HBD of Leloup et al., 2005). That structure was later cut and offset by steeper thrusts on both sides of the Chamonix synclinorium: the Mont-Blanc shear zone on the western edge of the Mont-Blanc (Eltchaninoff, 1982; Butler, 1985; Leloup et al., 2005; Egli & Mancktelow, 2013) and the Le Tour (Leloup et al., 2005) and Finhaut back thrusts along the eastern edge of the Aiguilles Rouges.

The relative chronology of the Pormenaz-Merlet shear zone is difficult to establish. Toward the south, the shear zone appears to be cut by the Le Tour back thrust and/or the Mont-Blanc shear zone as it is not seen on the southern side of the Chamonix valley, but the precise field relationships are obscured by Quaternary deposits (Fig. 3). The shear zone cuts and offset the Crête Blanche klippe that we interpret as part of the HBT (Fig. 9a), but further to the north the shear zone does not significantly offset the HBT (Fig. 3). We interpret this apparent inconsistency as due to a decrease of the Merlet-Pormenaz shear-zone offset toward the north, whilst this point still requires further field investigations. We thus infer that the Merlet-Pormenaz shear zone is younger that the HBT and older that the Mont-Blanc shear zone. It is thus an Alpine structure that has never been described as such.

The Vallorcine fault has a polyphase history and corresponds in fact to several structures active both before and during the Cenozoic, but it appears to not significantly offset the Le Tour back-thrust.

The Gietroz normal fault has a limited extent and offsets (Fig. 12c) which renders its relative timing difficult to determine. The main extension phases in the area (Early Jurassic and Eocene-Oligocene) are antecedent to the Alpine shortening phases, but the fault seems to offset the folds associated with the Finhaut back thrust (Fig. 12c).

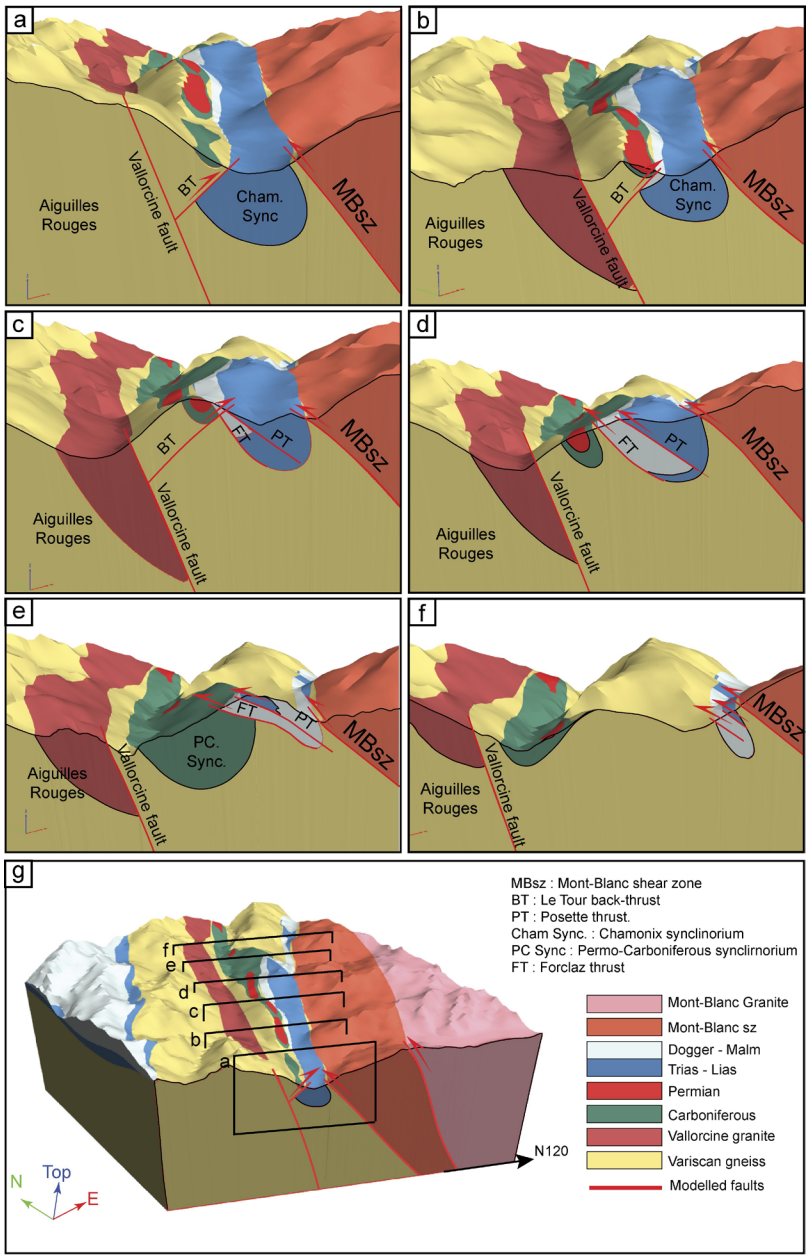

Fig. 14. Cross-sections of the Argentiere 3D GeoModel highlighting the structural continuity of the Chamonix synclinorium. a to f: successive cross-sections from south to north. Note that Finhaut thrust has not been included in this model, and that the precise shape of the Chamonix synclinorium is not constrained at depth.

5.2 Amounts of Cenozoic exhumation

The Cenozoic shortening has led to the exhumation and high altitude of the Aiguilles Rouges and Mont-Blanc ranges. It is now established that the Triassic sandstone basal layer is widely distributed within the western external Alps and can be taken as a reference layer for post-Triassic deformations. That level is found sub-horizontal at about -3000m (a.s.l.) in the Brizon well (46.03617N; 6.441525E [WGS84]), about 30 km north-west of Chamonix (Charollais and Jamet, 1990). Altitude variation of the Triassic sandstone level can thus give a relative uplift with respect to that location. Atop the Aiguilles Rouges, below the Aiguille du Belvédère summit at 2965m (a.s.l.), it is found nearly horizontal (Fig. 8) implying about 6 km of relative uplift of the central Aiguilles Rouges (Fig. S10). Note that the altitude difference could partly result from Mesozoic or Eocene normal faulting. However, the only normal faults that have been described between the Aiguilles Rouges and the Brizon well are Eocene and lead to negligible uplift of the Aiguilles Rouges (Butler et al., 2018).

The corresponding exhumation can also be estimated from the thickness of autochthonous and allochthonous (Helvetic and Penninic nappes) sediments that have been eroded at the top of the ranges. For the Aiguilles Rouges, it amounts to ∼12-15 km depending on the cross-section considered (Escher et al., 1988, 1993; Pfiffner et al., 1993). Temperatures at the top of the basement before exhumation have been estimated at 350 ± 20°C from δ18O (Kirschner et al., 1995) and 325 ± 25°C from RSCM (Girault et al., 2020) below the Morcles Nappe in Switzerland, and 320 ± 25°C from RSCM in the south of the Aiguilles Rouges (Boutoux et al., 2016). This corresponds to a thermal gradient of ∼ 20 − 31°C/km, typical of mountain belts. Note that similar temperatures at the top of the basement in Morcles and the southern Aiguilles Rouges strongly suggest that both locations were buried at the same depth and thus both overlain by the Helvetic and Penninic nappes, confirming our description of the Morcles Nappe at the top of the Aiguilles Rouges.

In the Mont-Blanc, the Triassic sandstones outcrop both in the south (Col du Bonhomme) and the north (Catogne) but not at the top of the range where they have been most likely eroded. Mont-Blanc relative uplift can be estimated with respect to the Brizon well: about 5.6 km in the south (Col du Bonhomme), ≥ 7.8 km near the Mont-Blanc summit, and 5.3 km in the north (Catogne) (Fig. S10). These values are lower bounds as they do not consider the layer tilt. Note that part of this uplift could result from Mesozoic and/or Cenozoic normal faulting. It is now well documented that part of the Mont-Blanc range was eroded during the Pliensbachian yielding to the Grès Singuliers sedimentation and had thus been exhumed before that time (Trumpy, 1971; Eltchaninoff, 1982; Ribes et al., 2020). However, no large normal fault has yet been found between the Mont-Blanc and the Aiguilles Rouges. The highest pressure estimate in the Mont-Blanc for the Cenozoic is 0.5 ± 0.05 GPa and 400 ± 25°C (Rolland et al. (2003), sample MB140, Helbronner area). This corresponds to a depth of 17 to 20 km assuming a rock density of 2.7 and implies an average thermal gradient of 18.5 to 26°C/km. These values imply 2 to 8 km more exhumation in the Mont-Blanc than in the Aiguilles Rouges. Note that this exhumation cannot be due to Mesozoic nor Cenozoic normal faulting. Three temperature estimates from RSCM measurements in the Col du Bonhomme area are between 322±18 and 336±26°C (Dall'Asta et al., 2022), similar to those at the

base of the Morcles nappe thus suggesting a comparable amount of overlying autochthonous, and, allochthonous (Helvetic and Penninic nappes) sediments before the exhumation.

5.3 Constraints on the amount and absolute timing of Cenozoic deformations.

5.3.1 Le Tour and Finhaut back-thrusts

The approximate 6 km of post-Triassic uplift of the Aiguilles Rouges from the Brizon well mostly results from the uplift in the crustal culmination above the Alpine Sole Thrust (Leloup et al., 2005; Bellahsen et al., 2014), including the frontal Aiguilles Rouges thrust (Pfiffner et al., 1997) and the back thrusts (Fig. 1b and Fig. S10). We estimate that ≥1.7 km of this uplift has been accrued on the Vallorcine fault and the back thrusts (Fig. S10). The vertical offset of the Le Tour back trust alone is 935m at the very least (elevation difference between the basement east of the Vallorcine Fault and the Chamonix valley (Fig. S10b). The offset on the Finhaut back thrust is more difficult to evaluate because it is very close to the Vallorcine fault (Fig. 3a).

Cooling histories modeled with the HeFTy software and based on one Apatite Fission Track, the mean of two Zircon U/He, and one Apatite U/He ages from the central part of the Aiguilles Rouges suggest that cooling, and thus exhumation, started at about 18 Ma, and was faster (≥25°C/Ma) from 8 to 4 Ma (Boutoux et al., 2016) (Fig. 15). However, the cooling history is relatively poorly constrained and exhumation could have started between ~ 30 and 16 Ma. All apatite fission tracks ages along a transect (elevations between 1010 and 1350 m asl) perpendicular to the Chamonix valley at the level of the Mont-Blanc tunnel are similar between 3.4 and 4.5 Ma in the Aiguilles Rouges and the Mont-Blanc (Glotzbach et al., 2008). This implies that no significant movement has occurred on the Mont-Blanc shear zone nor the Le Tour back thrust since that time (Leloup et al., 2005; Glotzbach et al., 2008).

The Aiguilles Rouges back thrusts are mostly brittle and offset all the other structures and are thus presumably relatively young. They appear coeval with a WNW-ESE compression phase but are possibly older than the present-day strike-slip regime. Unfortunately, the age of these deformation phases is yet unclear and no geochronological data are available on the back thrusts. Assuming that the back thrusts are linked to the most recent rapid cooling phase would imply that they were active between 8 and ~4 Ma (Fig. 15).

5.3.2 Pormenaz-Merlet shear zone

As discussed above, the shear zone is younger than the HBT but presumably older than the Mont-Blanc shear zone. Vertical offset across the Pormenaz-Merlet shear zone is ≥300m (elevation difference between the basement east of the shear zone and the base of the Pormenaz klippe). The only thermochronology data that can help to constrain the absolute age of the shear zone are samples MBZ10 and MBZ14 (Boutoux et al., 2016) that have similar elevations on both sides of the shear zone and give similar Zircon U/He mean ages: 6.2 ± 0.4 and 6.3 ± 0.4 Ma respectively. This implies that the shear zone offset is antecedent to that age and occurred at temperatures higher

than the Zircon U/He closure temperature (140 − 195°C). Motion on the shear zone contributed to the exhumation of the Aiguilles Rouges and is thus most likely younger than ~ 18 Ma (Fig. 15).

5.3.3 Mont-Blanc shear zone

The overall direction of the Mont-Blanc shear zone is N034° with a N110° direction of thrusting on average. This geometry implies that the Mont-Blanc shear zone has mainly a thrust component (~80%) and a slight dextral component (~20%). The WNW-ESE direction of shortening (~N110° ductile structures) possibly rotated through time towards NNW-SSE (~N155° brittle structures) (Leloup et al., 2005). The vertical offset on the shear zone may be estimated from the offset of the Triassic sandstones across it: ~≥ 1.5 km in the south (Col du Bonhomme), ≥3 km at the level of the Mont Blanc, and ~≥ 1 km in the north (Catogne) (Fig. S10). Pressure-Temperature estimates suggest that the differential exhumation between the Mont-Blanc and the Aiguilles Rouges is 2 to 8 km. Motion on the Mont-Blanc shear zone has increased that difference, while motion on the Le Tour back thrust decreased it.

$^{40}Ar/^{39}Ar$ mica ages have been performed within the Mont-Blanc shear zone, where the mylonitic foliation is underlain by chlorite ± white mica ± biotite. Biotite from sample C6 (Rolland et al., 2008) yields saddle age spectra suggestive of excess argon, with the youngest step at 19.75 ± 0.21 Ma, the inverse isochrone age being 21.8 ± 3 Ma (40/36i = 316.1 ± 4, MSWD= 2.0) (Rolland et al., 2008) (Fig. 15, Table S4). K-Feldspar from nearby sample ME27 yields complex age spectra with a minimum age step at 10.61 ± 0.15 Ma (Leloup et al., 2005). Two duplicates of white micas from sample DE65 located further north along the Angle fault yield raising ages spectra, respectively in the ranges, 14.30-20.41 and 15.13-20.32 Ma, both with a mini plateau at ~18 Ma (Table S4) (Egli et al., 2017). Other $^{40}Ar/^{39}Ar$ ages from undeformed rocks yield constraints on the cooling history. Biotites of sample C8 from the undeformed Mont-Blanc granite yield an inverse isochron age of 16.6 ± 0.7 Ma (Fig. 15, Table S4) that probably reflect the cooling of the hanging wall through 300± 50°C (Leloup et al., 2005). K-feldspar from the same sample yields a minimum age step at 10.98 ± 0.2 Ma which could be interpreted as a maximum age for K-Feldspar recrystallization at about 200°C (Leloup et al., 2005). All these samples do not give clear plateaux and the ages are difficult to interpret probably because the protolith is quite old (≥300 Ma) and the Alpine deformation temperature is below 450°C (Leloup et al., 2005; Rolland et al., 2008). However, all these ages are between ~ 22 and ~ 11 Ma and could correspond to the timing of deformation within the Mont-Blanc shear zone between ~ 400 and ~ 200°C (Fig. 15, Table S4).

White micas from sample S8 along the Vallorcine fault yield two $^{40}Ar/^{39}Ar$ mini-plateau ages at 14.3±0.2 Ma (1σ) and 22.9±0.9 Ma (2σ) (sample S68 of Rolland et al. (2008), Fig. 3a, Fig. 15, Table S4), that have been interpreted to reflect the duration of reverse faulting that would be coeval with the Mont-Blanc shear zone (Rolland et al., 2008). However, the Vallorcine fault has a long and polyphase history and the correspondence of the ages with a given deformation phase is disputable.

Along the nearly horizontal transect (elevations between 1010 and 1350 m asl) perpendicular to the Chamonix valley at the level of the Mont-Blanc tunnel all zircon fission-track ages, are similar between 11.2 and 13.5 Ma within the Mont-Blanc shear zone (2 samples) and the Mont-Blanc granite (3 samples) suggesting that no significant vertical offset occurred across the Mont-Blanc shear zone and the Angle fault since that time (Glotzbach et al., 2011). The absence of Zircon

fission track age in the Aiguilles Rouges, precludes a similar discussion on the Lavancher fault and the Le Tour back-thrust. Pecube model of a set of low-temperature thermochronology ages (Zircon and Apatite fission track and Apatite U/He) of the Mont-Blanc suggests an episodic exhumation with initiation at 22 ± 2 Ma with a rate of 0.8 ± 0.15 km/Ma, that decreases to values of 0.15 ± 0.65 km/Ma at 6 ± 2 Ma, and finally increase up to 2.0 ± 0.6 km/Ma at 1.7 ± 0.8 Ma. (Glotzbach et al., 2011) (Fig. 15). A phase of relatively fast cooling of the Mont-Blanc before ~ 6 Ma followed by a slow cooling phase was also suggested from apatites fission-track and U/He data alone and HeFTy models (Glotzbach et al., 2008). HeFTy models of one Zircon fission track, two Zircon U/He, one Apatite fission track, and one Apatite U/He ages between 2500 and 2600 m of altitude within and in the hanging wall of the Mont-Blanc shear zone indicate a continuous cooling since 18 ± 2 Ma with possibly increased cooling at 18-14 and 8-4 Ma (Boutoux et al., 2016) (Fig. 15). The average model cooling histories of the Mont-Blanc and Aiguilles Rouges converge at about 11 Ma (Boutoux et al., 2016) which could indicate the end of motion along the Mont-Blanc shear zone and Le Tour back thrust. However, if considering the full range of possible models, the cooling histories of the two ranges may have converged between 18 and 6 Ma.

Horizontal clefts with quartz + Chlorite ± fluorite ± adularia crystallizations are found within the Mont-Blanc and to a lesser extent in the Aiguilles Rouges (e.g., Poty & Cathelineau, 1974; Rossi et al., 2005; Rossi & Rolland, 2014). These clefts are compatible with horizontal compression and are generally considered as coeval to the Mont-Blanc shear zone. Adularia from one cleft in the central Mont-Blanc yields $^{40}Ar/^{39}Ar$ isochron ages of 10.6-13.6 Ma (MB03-70, 11.31 ± 0.68 for grain n°1, 12.8 ± 0.78 for grain n°2) (Fig. 15) (Rossi & Rolland, 2014). In the north of the Mont-Blanc, clefts contain quartz + Stilpnomelane + Epidote + Calcite ± Adularia ± Gold, with the Adularia yielding a 9.9 ± 1 Ma $^{40}Ar/^{39}Ar$ isochron age (Marshall, Meisser, & Taylor, 1998) (Fig. 15). Bergemann et al. (2019) applied the U-Th/Pb method on nine clefts containing monazite that yield ages between 12 and 6 Ma that relate three main growth events at 12-11,11-9 and 9-6 Ma. The two veins located in the Aiguilles Rouges are described as vertical and trending N190° and do not show the first growth stage. This was interpreted as evidence that the two last growth phases are linked with right-lateral shear along the NE-SW Rhône-Simplon fault (Bergemann et al., 2019). However, the orientation of these clefts is compatible with left-lateral, not right-lateral shear along a NE-SW fault, making that interpretation dubious.

From all these data the most probable structural scenario is that reverse/right-lateral deformation started in the Mont-Blanc shear zone at 400°C at ~ 22 Ma and lasted until ~ 11 Ma at ~ 200°C. Because rapid cooling of the Mont-Blanc lasted until 6±2 Ma, and crystallization in the horizontal clefts until 6.71±0.23 Ma., thrusting may have continued along the Lavancher fault until 6 ± 2 Ma but was over (as well as the Le Tour back-thrust) at ~ 4 Ma (Fig. 15). Exhumation in the central Mont-Blanc at 0.8 ± 0.15 km/Ma implies 7.2 ± 1.3 km between 20 and 11 Ma and 4 ± 0.5 km between 11 and 6 Ma, corresponding to a total of 9.5-13 km. This is similar to the thickness of possible overlying nappes and compatible with the offset of the Triassic (≥3km in central Mont-Blanc). This is however much lower than the estimate from the petrographic analysis (18.5 ± 1.85 km from sample MB140, Rolland et al. (2003)). The end of motion on the Mont-Blanc shear zone possibly marks the initiation of the present-day strike-slip stress regime.

5.3.4 Helvetic thrusts

Helvetic thrust deformation affects units from the basement to the Eocene sediments. The Eocene sediments are Priabonian (Collet et al., 1952) thus implying a post-34 Ma deformation. Further,

the Taveyannaz volcaniclastic sandstones that were deposited before the nappe stacking and folding contain 32.5 Ma andesitic clasts ($^{40}Ar/^{39}Ar$ on hornblendes), while biostratigraphic correlations suggest sedimentation between 32 and 29 Ma during the Rupelien (Ruffini et al., 1997) implying a post-Oligocene deformation.

No age data have been published on the Morcles nappe in France, but such ages are available from Switzerland. Fine-grained syn-kinematic white micas (2 - 6 µm) from five ductile carbonate mylonites at the base of the Morcles and Doldenhorm nappes in Switzerland yield staircase $^{40}Ar/^{39}Ar$ age spectra with apparent ages between 12 and 76 Ma with 94% of the gas release yielding ages between 32 and 14 Ma (Kirschner et al., 1996). Analysis of a larger set of twenty-five samples from the Helvetic nappes and comparison with Rb/Sr ages confirm that the $^{40}Ar/^{39}Ar$ ages result from variable mixtures of detrital and syntectonic (neoformed) micas, and that ages tend to young from the highest Helvetic thrusts (Mont Gond and Sublage) to the lowest (Diableret and Morcles) (Kirschner et al., 2003). The age spectrum of sample 93-29-A from deformed Eocene sediments at the base of the Morcles Nappe, yields a strong Miocene signal with two pseudo-plateaux at 19 and 21 Ma in the first 83% of gas release (Kirschner et al., 2003) (Fig. 15). The youngest ages (about 14 Ma) come from the base of the Morcles Nappe, at la Batiaz (Fig. 15) but correspond to less than 20% of the gas in a spectrum that does not show any plateau, so their significance is uncertain. These data suggest that the Morcles nappe mostly emplaced at 21-19 Ma. Unfortunately, from the available data, it is unclear if that deformation ended at ~19 Ma or lasted until ~14 Ma.

At la Batiaz, white mica from sample DE79 from the Aiguilles Rouges gneiss with top to the north-west thrusting evidence yield a 20.28 ± 0.21 $^{40}Ar/^{39}Ar$ plateau age (inverse isochrone: 20.18 ± 0.49 Ma) interpreted as related to motion on the Mont-Blanc shear zone (Egli et al., 2017). This interpretation is in the upper range of the ages discussed above for the Mont-Blanc shear zone. However, our structural mapping rather relates deformation at la Batiaz to the HBT, in the direct prolongation of the Forclaz fault, and we rather relate that age with those obtained at the base of the Morcles Nappe (Fig. 15). Closer to the contact with the sedimentary cover, sample S02 showing top to the south-east normal shear criteria, yields a $^{40}Ar/^{39}Ar$ plateau age of 15.9 ± 0.15 (inverse isochrone: 15.07 ± 0.23) that has been interpreted to correspond to the age of updoming of the Aiguilles Rouges postdating the Mont-Blanc shear zone (Egli et al., 2017). This timing is compatible with that of the uplift of Aiguilles Rouges discussed above.

Available geochronological data thus suggest that the Helvetic nappes in Switzerland emplaced since ~32 Ma, with the Morcles nappe mostly around 21-19 Ma but lasting possibly until ~14 Ma

(Fig. 15). In the absence of any absolute age in our study area, we infer that the timing was the same a few km southwest along-strike, but this deserves further study.

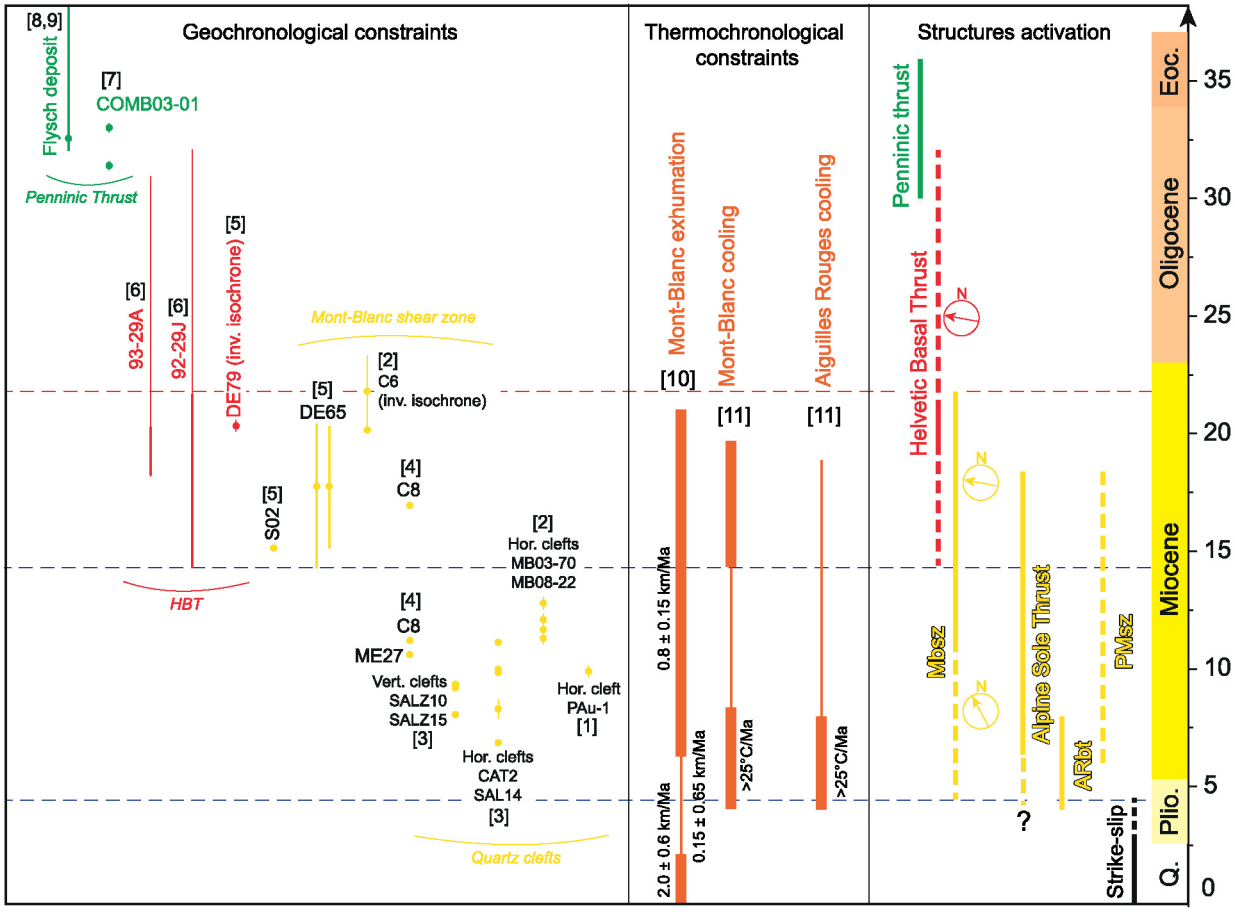

Fig. 15. Time-Deformation constraints on the Cenozoic evolution of The Mont-Blanc and Aiguilles Rouges. Left, geochronological constraints, dots correspond to individual ages and lines to age ranges of individual samples, data listed in Table S4. Center, Thermochronological constraints with exhumation estimate and cooling histories. Bold line indicates fast cooling/rapid exhumation. Right, timing of the main structures, dashed when uncertain. Colors refer to tectonic phases, arrow indicate the thrusting direction (see text for details). References: [1]: Poty et al., (1974). [2]: Rolland et al. (2008). [3]: Bergemann et al., (2019). [4]: Leloup et al. (2005). [5]: Egli et al., (2017). [6]: Kirschner et al., (1996, 2003). [7]: Simon-Labric et al. (2009). [8]: Pfiffner et al., (2002). [9]: Ruffini et al., (1997) ; [10] : Glotzbach et al., (2011). [11]: Boutoux et al., (2016).

6 Implications on the structural evolution of the Alps

6.1 Shortening of the Helvetic nappes and lateral extent of the Helvetic Basal Thrust

The Aiguilles Rouges have been underthrusted below the Penninic nappes along the Penninic thrust until ~30 Ma (Simon-Labric et al., 2009; Pfiffner et al., 2002) (Fig. 15). As discussed above, thrusting at the base of the Helvetic nappes, along the Helvetic Basal Thrust (HBT), lasted until ~19 Ma and possibly until ~14 Ma. Above the HBT, several thrusts sheets are found below the Penninic thrust that has been described in Switzerland and named the Helvetic and Ultrahelvetic nappes (Ramsay, 1981; Escher et al., 1988), and have possibly been activated in sequence from

east to west (top to bottom) (Jeanbourquin, 1994) between ~30 and ~20 Ma (Kirschner et al., 2003).

The present 3D structural study implies that the HBT is a shear zone along which the overlying Morcles nappe was significantly detached from the underlying basement toward the WNW (N110° on average in the Aiguilles Rouges). This follows the interpretation of Paréjas (1925), Collet (1927), and Ramsay (1981) but not that of Escher et al. (1993) and Boutoux et al. (2016), which consider that the Morcles nappe is not significantly detached from the basement and is mostly restricted to Switzerland.

NW-SE shortening of the Urgonian limestone above the HBT can be estimated from the cross-sections of Ferrill and Groshong (1993) and Butler et al., (2018) (Fig. 1a): 4.3 km (22%) and 3.7 km (24.5%) respectively. These are minimum estimates of the total shortening because they do not consider the offset on the HBT which is difficult to constrain as it does not outcrops. From a 3D reconstruction based on the cross-sections of Huggenberger (1985) and Faure (1999), Affolter (2003) calculate a total shortening varying between 13 and 32 km from the NE to the SW of the Aiguilles Rouges (Fig. 1a).

In the ductile folded basement hypothesis (e.g., Escher et al., 1993), the Morcles nappe is expelled from a half-graben with the external Mont-Blanc at its core. The initial length of the cover was at least 21 km while the present-day width of the external Mont-Blanc is only 3 km and it implies more than 86% of shortening of the basement. However, the External Mont-Blanc is not a fold but a reverse shear zone. Moreover, that shear zone is younger than the Morcles Nappe, implying that the nappe roots east of the Mont-Blanc as well as the other Helvetic nappes. In such a case, the amount of internal shortening within the basement is independent of the amount of shortening along and above the HBT which could be quite large.

Southwest of the Mont-Blanc range the sedimentary cover is interpreted as significantly detached from the basement by several authors. In the Mont Joly area (Fig. 1a), three flat thrust sheets have been described within the Mesozoic cover on a ~1500 m thick succession from bottom to top: the Vervex, lower Mont-Joly (or Sangle) and Upper Mont-Joly units (Mennessier et al., 1977; Triboulet, 1980; Epard, 1990). These thrusts are the southward prolongation of the Helvetic nappes (Eltchaninoff, 1982; Epard, 1990), and are overlain by two other thrust sheets: the Roselend and Roselette nappes, both involving the basement (Mennessier et al., 1977; Eltchaninoff, 1982; Butler, 1985). The basal thrust, corresponding to the HBT, prolongs to the north-west, dipping north-west below the Aravis (Triboulet, 1980; Eltchaninoff, 1982; Butler, 1985; Epard, 1990; Bellahsen et al., 2014). The HBT underlies the folded Mesozoic cover and most probably emerges west of the Bornes (Doudoux et al., 1982) between the Brizon (BZN-1) and Faucigny (FAY-1) deep wells (Charollais et al., 1996) (Fig. 1a). That interpretation implies that the whole Aravis, Bornes, Bauges, and Semnoz massif corresponds to a large subalpine klippe above the HBT (Fig. 1). In the Brizon deep well the Tithonian limestones are found five times attesting to strong shortening of the cover (Charollais et Jamet, 1990). Bellahsen et al. (2014) estimate an NW-SE shortening of 17 km within the Bornes, while Affolter (2003) estimates a total thrusting of 30 to 36.5 km for the Helvetic nappes. Further south, Kalifi et al. (2021) propose a similar interpretation for the northern part of Vercors and the eastern part of Chartreuse. These massifs are klippes above a thrust they call Fault Zone 1 (FZ1), with shortening estimates between 14.1 and 5.8 in the north and south of Chartreuse respectively. They further interpret FZ1 to have been active before ~21 Ma has it created a relief

that bounded the Miocene sea to the east (Kalifi et al., 2021, 2022). We propose that the FZ1 of Kalifi et al., (2022) corresponds to the southern prolongation of the HBT that extend from the Morcles Nappe to the northern Vercors.

6.2 Late reverse faults at the boundary of the external ranges

The subalpine klippe is bounded to the east by the external crystalline ranges of external Belledonne and the Aiguilles Rouges which are large basement windows (Fig. 1a). Most authors consider that the Jura and subalpine folds formed above thrusts that root below (west of) the external ranges (e.g., Burkhard & Sommaruga, 1998; Deville & Chauvière, 2000; Bellahsen et al., 2014). However, as described above, the Helvetic basal décollement lies on top of the Aiguilles Rouges external crystalline range, thus implying that it roots above (east of) these ranges: in the Chamonix Synclinorium and the synclinal médian (Fig. 1) (e.g., Eltchaninoff, 1982; Leloup et al., 2005). Further, as discussed above, the HBT roots east of the Mont-Blanc and has been cut and offset by later steep reverse faults including the Mont-Blanc shear zone.

Exhumation of the Mont-Blanc started at ∼22 Ma in the hanging wall of the Mont-Blanc shear zone and lasted until at least ∼11 Ma, very probably until 6 Ma, while motion on the HBT was active at 21-19 Ma and possibly until ~14 Ma. The Mont-Blanc shear zone thus appears to be partly coeval with the HBT that it offsets for a time range between 3 and 8 Ma depending on the timing of the end of motion on the HBT (19 or 14 Ma) (Fig. 15). A simple interpretation is that during this time range the Mont-Blanc shear zone was an imbricate thrust in the footwall of the HBT, before breaching out at ∼19 or 14 Ma and starting to offset the HBT (Fig. 16).

Exhumation of the Aiguilles Rouges above the Alpine sole thrust started at ∼18 Ma (Fig. 15), inducing the bending of the HBT that was possibly still active during ∼5 Ma. The period from ∼22 to ∼19 or 14 Ma thus corresponds to a major transition from the rooting of the main active thrusts from above (east) the external crystalline massifs in the Mont-Blanc area (HBT) to thrusts rooted below (west) of the external crystalline massifs (Alpine sole thrust).

Further south in Chartreuse, the molasse depocenter migrated at ∼18 Ma toward the west from the footwall of the HBT to the footwall of the Voreppe thrust rooting below Belledonne (Kalifi et al., 2021). This timing is coeval with the onset of rapid exhumation of the Belledonne external crystalline massif and is interpreted as the switch from distributed to localized (shear zones) deformation (Girault et al., 2022). However, that timing could as well mark a major transition from rooting of the thrusts east (above) to the west (below) of the external crystalline massifs as in the Aiguilles Rouges – Mont-Blanc, and we propose below a conceptual model for the external crystalline massifs Alpine deformation, based on our observations in the Aiguilles Rouges and Mont-Blanc massifs.

6.3 A conceptual model for Alpine External Crystalline Massifs deformation

We suggest that three major thrust systems with large horizontal displacement (so-called thin-skin tectonics) succeeded in the western Alps from the east (internal) to the west (external): the Penninic, Helvetic, and Basal thrust systems. In this interpretation, the Helvetic deformations are not limited to a buckle folding but are linked to a major thrust system more than 50 km long across-

strike that absorbed between 13 and 36 km kilometers of ENE-WSW shortening: the Helvetic thrust system, with the Helvetic Basal Thrust at its base.

These thrusts induced large-scale folding of the Helvetic units with fold axis perpendicular to the thrust motion in the upper part of the thrust sheet, and sheath folds in the basal décollement level. Note that such sheath folds can barely be explained in a para-autochthonous hypothesis. That thrust system roots southeast (above) of the Mont-Blanc and Belledonne, close to, and possibly within the Penninic thrust. The thrust system is composed of ramps usually located in the less deformable units (i.e., basement, Urgonian and Thithonian limestone), and long flats located in the less competent layers (i.e., Triassic siltites and dolostones, Liassic marls). The main flat appears to be in the Triassic a few meters above the basement and has induced a large décollement of the cover with respect to the basement. Starting from a horizontal geometry would imply that no basement slice could be found along with the thrust within sedimentary rocks unless the thrust does cut down-section within the basement before climbing up section, the so-called plucked basement slice (Platt, 1984), which seems unlikely. However, as the basement/cover interface had more likely a roughed geometry in part because of preexisting normal faults (either Jurassic or Eocene), the local cutoff of that interface, for example at the tip of tilted blocks, can explain how basement pieces can be found within the sedimentary series (Fig. 16e).

Helvetic thrusting lasted from ~30 Ma to ~14 Ma. During a first stage (~30 to ~22 Ma) the HBT is rooted southeast of the Mont-Blanc (Fig. 16a). To the west, the HBT thrust system bounded the Miocene Sea and was coeval with the sedimentation of the Lower Freshwater molasse in the Swiss molasse basin (Garefalakis & Schlunegger, 2019) and the initial deposits of the Miocene molasse in the Rhodano–Provencal molasse basin (Kalifi et al., 2021, 2022). In a second stage (~22 to ~18 Ma) a duplex formed (Fig. 16b). The Mont-Blanc was the central bloc of that duplex bounded to the northwest by the Mont-Blanc shear zone, and to the southeast by a ramp along the HBT. At ~18 Ma, the main locus of deformation migrated towards the west and the Alpine Sole thrust initiated rooting west (below) the Aiguilles Rouges inducing uplift of the Aiguilles Rouges, while the HBT was still active (Fig. 16c). This transition period ended at ~14 Ma when the HBT ended, but several steep faults initiated in the Alpine Sole Thrust hanging wall (Fig. 16d). Some of the HBT ramps eventually became breach thrusts that cut up-section across their previous flat (Platt, 1984). This was the case for the Mont-Blanc shear zone that was active together with the HBT between ~22 and 14 Ma, before offsetting that structure between 14 and ~6 Ma. The activation of such breach thrust is coeval with that of the back-thrusts and the formation of horizontal clefts and would correspond to the transition of thin-skin to thick-skin tectonics in the Mont-Blanc, while thin-skin tectonics takes place in the Jura. Note that this model does not imply any major strike-

slip motion along the Chamonix Synclinorium, nor the synclinal median in Belledonne before ~6 Ma.

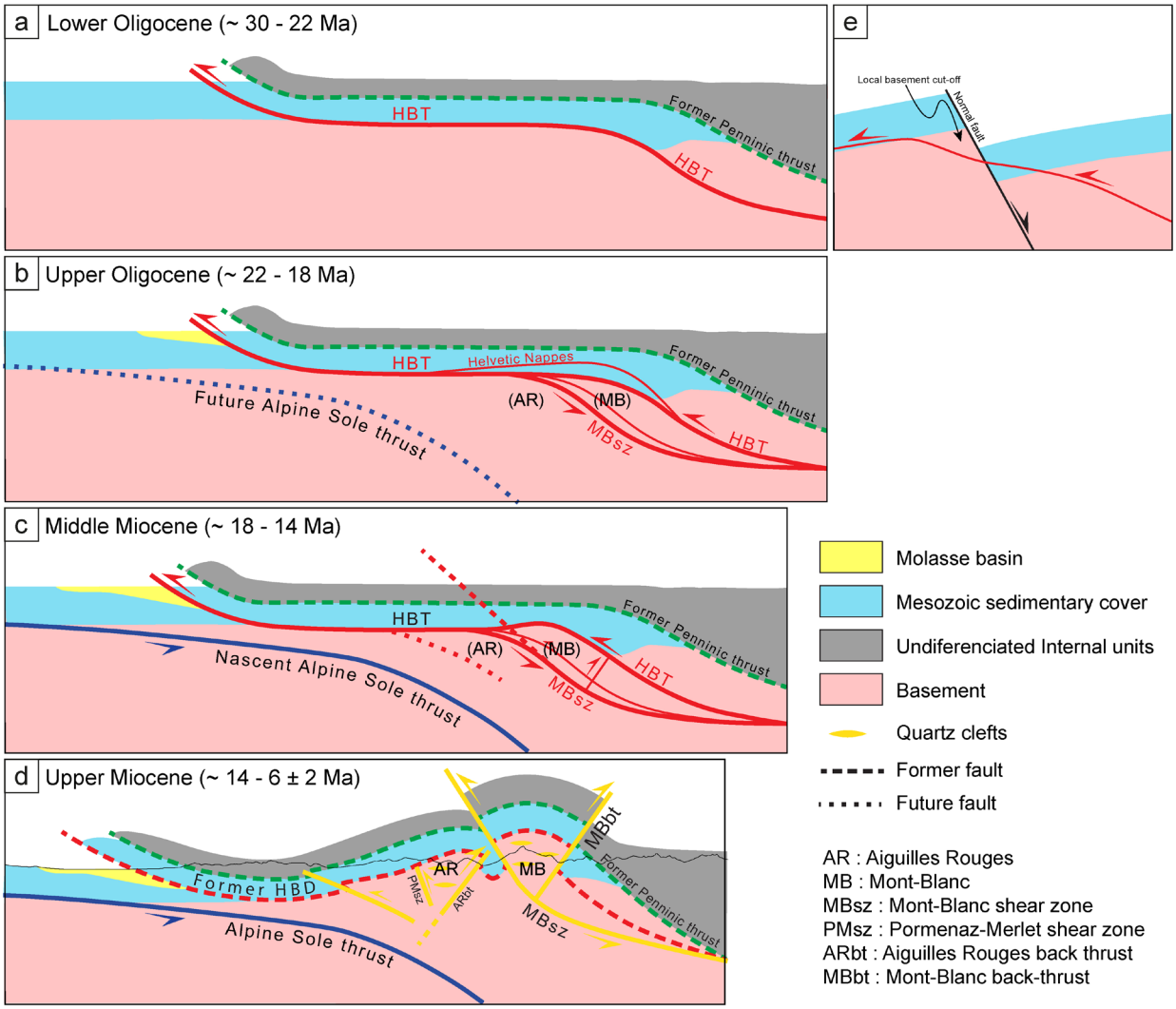

Fig. 16. A conceptual model for western Alps External Crystalline massifs deformation. a) Lower Oligocene (30-22 Ma) stage of Helvetic nappe stacking (thin shin). Helvetic Basal Décollement at the base of the Helvetic nappes taking root southeast (above) of the Mont-Blanc. b) Upper Oligocene (22-18 Ma) stage of further Helvetic nappe stacking with duplexing. The external crystalline massifs are structured in duplexes between two branches of the HBT where the deformation is more (Mont-Blanc) or less (Aar, Belledonne) localized. c) Middle Miocene (18-14 Ma) transition stage. The HBT is bent at the top of the duplex where back-thrusting takes place. Initiation of the Alpine Sole thrust induces Aiguilles Rouges exhumation. d) Upper Miocene (14-6 Ma) stage of breach thrust and steep faults (thick skin), the main stage of the external crystalline massifs exhumation above the Alpine Sole thrust that roots northwest (below) the external crystalline massifs. The Mont-Blanc shear zone becomes a breach thrust through the former HBT coevally with back-thrusting of the Mont-Blanc and Aiguilles Rouges. Horizontal quartz clefts open within the external crystalline massifs. Note that the Alpine sole thrust induces thin skin tectonics in the Jura at the same time. e) Sketch of a possible configuration with a roughed geometry of the cover/basement interface leading to the incorporation of basement pieces within the sedimentary series at the base of the thrust.

6.4 Implications on the Alpine orogenic wedge.

Mountain belts are often described as orogenic wedges with the internal part of the belt consisting of a structural culmination formed by basal accretion of crystalline thrust sheets, and an external part of imbricated thrusts formed by frontal accretion of sedimentary units (Pfiffner, 2017, for a review). In the case of the external Alps, the External Crystalline Massifs have been interpreted as such a culmination (e.g., Lacassin et al., 1990; Pfiffner et al., 1997; Menard & Thouvenot, 1987). Analog and numerical experiments have emphasized the importance of décollement layers, erosion, and sedimentation in the formation of such orogenic wedges and their influence on the deformation style. In analog sandbox experiments, a geometry similar to the external alps has been obtained with an antiformal culmination refolding previous flat thrust sheets (e.g., Konstantinovskaya & Malavieille, 2005; Bonnet et al., 2007). In that case, the culmination is achieved by basal accretion of basement slices in a duplex, and back thrusting in the internal part (Bonnet et al., 2007). The same kind of geometry is obtained in visco-elastoplastic numerical models when two flat decollement levels are present with the upper one weaker than the basal one (Dal Zilio et al., 2020). In some of these cases, the uplift of the antiformal culmination is achieved not by basal accretion but by out-of-sequence breach thrusting at the front of the culmination and back thrusting at the back (Model M5, Dal Zilio et al., 2020). In every case, the vertical growth of the culmination is enhanced by strong erosion. Basic features of our conceptual model, such as the up doming and breach thrusting of a previously flat décollement, are obtained in some of these wedge models. However, these models correspond to a brittle wedge over a rigid basement as rheology is independent of temperature, and one can question their applicability to the Mont-Blanc where the Miocene temperature may have reached 400°C (Poty et al., 1974; Poty and Cathelinau., 1974; Rolland et al., 2003). Numerical thermo-mechanical simulations with visco-elastoplastic rheology have been designed to discuss the mechanical parameters that control the deformation style (thin-skin versus thick-skin) during nappe formation (Spitz et al. 2020; Bauville and Schmalholz, 2015; Kiss et al., 2020). In these simulations in the absence of any softening mechanism, strain localization occurs along weak layers and is thus mainly controlled by the viscosity contrast between the basement (high viscosity) and the cover (low viscosity), and the initial geometry of that boundary. Flat low viscosity layers (i.e., evaporite layer) promote large horizontal thrust nappe transport, while steep boundaries (i.e. inherited normal fault) promote folding of the basement and sediments (Spitz et al. 2020; Bauville and Schmalholz, 2015; Kiss et al., 2020). These models suggest that for a basement with high viscosity ($\geq 10^{23}$ Pa.s) and in the absence of any localization mechanism, shortening of a previous graben can yield folding of the basement and squeeze out of the sediments with a geometry comparable to the basement fold nappe proposed for the Morcles Nappe by Escher et al. (1988) (Fig. 2a); while in the absence of graben thrust nappe with large horizontal transport such as the Wildhorn and Glarus nappes develop. In our study area, there is no clear evidence for a Mesozoic normal fault, no evidence of basement folding, and clear evidence for décollement of the cover with respect to the basement along the HBT, and the situation is thus comparable to that of the Glarus, but with a later deformation, phase inducing thrusting of the basement in the internal part of the system (Fig. 2b). The presence of basement pieces inside the HBT shear zone (Fig. 6) suggests that, even in the absence of a deep

basin, the basement/cover interface had a roughed geometry, and basement highs have been cut off (Fig. 16e).

7 Conclusions

A décollement thrust is evidenced at the bottom of the Helvetic nappes (named the Helvetic Basal Thrust or HBT). The HBT was a major thrust system active mostly between ~30 and ~14 Ma, in an ~N110° direction, with a total shortening between 13 and 36 km. An HBT flat is located within the Triassic a few meters above the basement and another within the Liassic shales. The HBT is an apparent normal fault on the NW flank of the Aiguilles Rouges, but this is because it has been tilted during the later uplift of the Aiguilles Rouges above the more external Alpine Sole Thrust. The HBT extends below the Haut-Giffre and most probably emerges west of the Prealps klippe during the Miocene, the HBT was cut by several steep reverse faults: in the Aiguilles Rouges the Merlet-Pormenaz shear zone, the Le Tour and Finhaut back thrust, and the Mont-Blanc shear zone in the Mont-Blanc. The HBT was uplifted and folded above the basement culminations of the external crystalline massifs, and it is these late faults that mostly shape the present-day external crystalline massifs map geometry. These late deformations obscured the HBT continuity and precluded its recognition as a major structure even if it was previously described at several localities. The HBT roots in the Chamonix synclinorium, but its internal roots have in fact to be found on the eastern side (above) of the Mont-Blanc because of the late offset by the breach faults, and back thrusts.

We propose a tectonic scenario where the Mont-Blanc shear zone acted as a ramp of the HBT between ~22 and 14 Ma, before becoming a breach thrust between 14 and 6 Ma. The period between ~22 and 14 Ma was a transition of the major thrust system between the HBT rooting southeast (above) of the external crystalline massifs to the Alpine Sole thrust rooting northwest (below) of the external crystalline massifs. Before ~6 Ma, there is no evidence of large strike-slip motion along the Chamonix synclinorium, thus no direct connection through the Rhône fault between exhumation in the Mont-Blanc and the footwall of the Simplon normal fault.

The main structural characteristics of the Mont-Blanc area can most probably be extrapolated in the southwest, with the external Belledonne, Synclinal Median, Internal Belledonne being an equivalent of the Aiguilles Rouges, the Chamonix Synclinorium, and the Mont-Blanc respectively. We suggest that the Helvetic nappes above the HBT extend in the Chablais, the Bornes, eastern Chartreuse, and northeast Vercors defining a large klippe that roots east (above) Belledonne. After ~18 Ma a major transition occurred within the Alpine sole thrust rooting west (below) the external crystalline massifs, and steep reverse faults shaping the Belledonne geometry.

This re-discovery of a major thrust system has several implications: the first one is that three major thrust systems, not only two, have shaped the external western Alps: the Penninic, Helvetic, and Alpine Sole thrust systems. These thrust systems have propagated in sequence from the internal (east) part to the external one (west). Because the Helvetic phase has been overlooked, shortening in the external Alps has been underestimated. The second implication is that the exhumation of the external ranges of the western Alps was mostly controlled by steep reverse faults, including back thrusting and limited folding above the more external thrust system since ~18 Ma. At that time, thick-skin deformation in the more internal part of the belt was coeval with thin-skin deformation in the external part.

Data availability

GeoModeller software used in this research is available for download at https:// www.intrepid-geophysics.com/product/geomodeller/ with a valid commercial or research Licence. 3D Geological models are provided in GeoModeller native format (.xml). The models are also provided in a 3D portable document format (.pdf) that can be opened with free Acrobat Reader software. See data repository.

Samples are identified with a persistent identifier of the International Geo Sample Number (IGSN:https://www.igsn.org/): these numbers are indicated in the Samples.csv table in the data repository.

Stereographic plots were performed using the Stereonet v.11 programs of Allmendinger et al. (2011) and Cardozo and Allmendinger (2013), freely available at https://www.rickallmendinger.net/stereonet.

3D photogrammetric digital elevation model (DEM) of the Aiguille du Belvédère is built from 260 shots with a spatial resolution of about 6 cm, acquired by drone, assembled with Agistoft Metashape 1.7.3 software. The model is visible online with annotations and detailed images in the Sketchfab platform at the following link: https://skfb.ly/o9Wsw. The high-resolution source of the model is retrievable in the data repository.

All data used in this publication: location of observations, measurements, samples, GeoModels source format, and 3D photogrammetric models are stored in a repository with the following link: https://data.mendeley.com/datasets/snx9zkrvts/1

Acknowledgments

This study was partly supported by INSU-CNRS through the “SYSTER-FEI-UMR5276-Dotation Performance 2022” and the RGF “Alpes et bassins périphériques” from the French Geological Survey. It forms part of the Ph.D. project of Antoine Mercier at Université Claude Bernard Lyon 1, supported by the French Ministry of Research and Higher Education. The authors thank B. Boulicaut and J. Jacquod from the Emosson SA company for providing the geological sections along the water penstock pipes. We also thank Clémentine Fellah, Cyril Langlois, and Thierry Douillard from the INSA Lyon laboratory that performed the EBSD experiment for the quartz LPO analysis. Finally, we thank the conservatory of natural areas (ASTER), for authorizing the drone surveying (n°DDT-2020-1166) above the Aiguille du Belvedere in the Aiguilles Rouges massif, and especially the guard Laurent Delomez for coming us in the field. A. Pfiffner and an anonymous reviewer are thanked for reviews that enriched and helped to clarify the manuscript.

References

Affolter, T. (2003). Étude des déformations et restauration 3D d'un bassin de front de chaîne : l'exemple du Jura et des massifs subalpins français, (Doctoral dissertation). Université Joseph-Fourier Grenoble I.

Affolter, T., 2004. Map view retrodeformation of an arcuate fold-and-thrust belt: the Jura case. J. Geophys. Res. 109 (B3). doi:10.1029/2002jb002270.

Affolter, T., Faure, J.-L., Gratier, J.-P., Colletta, B., 2008. Kinematic models of deformation at the front of the Alps: new data from map-view restoration. Swiss J. Geosci. 101 (2), 289–303. doi:10.1007/s00015-008-1263-3.

Allmendinger, R.W., Cardozo, N., Fisher, D.M., 2011. Structural Geology Algorithms: Vectors and Tensors. Cambridge University Press.

Amberger, G.F. (1959). L' autochtone de la partie Nord-Ouest du massif des Aiguilles Rouges: Haute-Savoie et Valais (Doctoral dissertation). University of Geneva.

Argand, E., 1916. Sur l'arc des Alpes occidentales. Eclogae Geol. Helv. 14, 145–192.

Ayrton, S., 1972. Sur la prolongation de la nappe de Morcles en France. Eclogae Geol. Helv.. doi:10.5169/SEALS-164096.Ayrton, S. (1980). La géologie de la zone Martigny Chamonix (versant suisse) et l'origine de la nappe de Morcles (un exemple de subduction continentale). *Eclogae Geolicae Helvetiae*, 73 (1), 137-172. Retrieved from https://hal-insu.archives-ouvertes.fr/insu-00925393

Ayrton, S., Barféty, J., Bellière, J., Gubler, Y., & Jemelin, L. (1987). Carte géologique de la France, feuille de Chamonix (Sheet 680, scale 1:50,000). French geological survey: Bureau de Recherches Géologiques et Minières.

Badoux, H. (1972). Tectonique de la nappe de Morcles entre Rhône et Lizerne. Mat. Carte géol. Suisse. (143).

Bauville, A., & Schmalholz, S.M. (2015). Transition from thin-to thick-skinned tectonics and consequences for nappe formation: Numerical simulations and applications to the Helvetic nappe system, Switzerland. Tectonophysics, 665, 101-117. Doi : 10.1016/j.tecto.2015.09.030.

Bellahsen, N., Mouthereau, F., Boutoux, A., Bellanger, M., Lacombe, O., Jolivet, L., & Rolland, Y. (2014). Collision kinematics in the western external Alps. *Tectonics*, 33 (6), 1055-1088. doi:10.1002/2013tc003453

Bellière, J. (1956). Caractère de la déformation Alpine dans les schistes cristallins du massif du Mont-Blanc. *Bulletin de la Société Géologique de France*, VI , 691-6988.

Belliere, J. (1988). On the age of mylonites within the Mont Blanc massif. *Geodinamin. Acta*. 2.1 13-16.

Bergemann, C. A., Gnos, E., Whitehouse, M. J., 2019. Insights into the tectonic history of the Western Alps through dating of fissure monazite in the Mont Blanc and Aiguilles Rouges Massifs. Tectonophysics 750, 203-212.

Berthé, D., Choukroune, P., & Gapais, D. (1979). Orientations préférentielles du quartz et orthogneissification progressive en régime cisaillant : l'exemple du cisaillement sud-armoricain. *Bulletin de Minéralogie*, 102 (2-3), 265-272.

Bertrand, M. (1881). Failles de la lisière du Jura entre Besançon et Salins. *Bulletin de la Société Géologique de Franc*e, 3(10), 114-126.

Bonnet, C., Malavieille, J., & Mosar, J. (2007). Interactions between tectonics, erosion, and sedimentation during the recent evolution of the Alpine orogen: Analogue modeling insights. Tectonics, 26(6). Doi : 10.1029/2006TC002048.

Bousquet, R., Engi, M., Gosso, G., Oberhänsli, R., Berger, A., Spalla, M. I., & Goffé, B. (2004). Explanatory notes to the map: metamorphic structure of the Alps transition from the Western to the Central Alps. Mitteilungen Der *Österreichischen Mineralogischen Gesellschaft* , 134 (1), 279-298.

Boutoux, A., Bellahsen, N., Nanni, U., Pik, R., Verlaguet, A., Rolland, Y., & Lacombe, O. (2016). Thermal and structural evolution of the external Western Alps: Insights from (U–Th–Sm)/He thermochronology and RSCM thermometry in the Aiguilles Rouges/Mont Blanc massifs. Tectonophysics, 683 , 109-123. doi:10.1016/j.tecto.2016.06.010

Burkhard, M., Sommaruga, A., 1998. Evolution of the western Swiss Molasse basin: structural relations with the Alps and the Jura belt. Geol. Soc. Lond., Spec. Publ. 134 (1), 279–298. doi:10.1144/gsl.sp.1998.134.01.13.

Bussy, F., & Von Raumer, J. (1993). U–Pb dating of Palaeozoic events in the Mont-Blanc crystalline massif, Western Alps. Terra Nova, 5(1), 56-57.

Bussy, F., Hernandez, J., & Von Raumer, J. (2000). Bimodal magmatism as a consequence of the post-collisional readjustment of the thickened Variscan continental lithosphere (Aiguilles Rouges-Mont Blanc Massifs, Western Alps). *Earth and Environmental Science Transactions of the Royal Society of Edinburgh*, 91 (1-2), 221-233. doi:10.1017/s0263593300007392

Butler, R. W. (1985). The restoration of thrust systems and displacement continuity around the Mont Blanc massif, NW external Alpine thrust belt. *Journal of Structural Geology* , 7(5), 569-582. doi:10.1016/0191-8141(85)90029-x

Butler, R. W., Bond, C. E., Cooper, M. A., & Watkins, H. (2018). Interpreting structural geometry in fold-thrust belts: Why style matters. *Journal of Structural Geology*, 114 , 251-273. doi:10.1016/j.jsg.2018.06.019

Calcagno, P., Chilès, J., Courrioux, G., & Guillen, A. (2008). Geological modelling from field data and geological knowledge. *Physics of the Earth and Planetary Interiors*, 171 (1-4), 147-157. doi:10.1016/j.pepi.2008.06.013

Campani, M., Herman, F., & Mancktelow, N. (2010). Two-and three-dimensional thermal modeling of a low-angle detachment: Exhumation history of the Simplon Fault Zone, central Alps. *Journal of Geophysical Research*: Solid Earth, 115(B10). doi:10.1029/2009JB007036

Capuzzo, N., & Bussy, F. (2000). High-precision dating and origin of synsedimentary volcanism in the Late Carboniferous Salvan-Dorénaz basin (Aiguilles-Rouges Massif, Western Alps). *Schweizerische mineralogische und petrographische Mitteilungen*, 80 , 147-167. doi:10.5169/SEALS-60958

Capuzzo, N., Handler, R., Neubauer, F., & Wetzel, A. (2003). Post-collisional rapid exhumation and erosion during continental sedimentation: the example of the late Variscan Salvan-Dorénaz basin (Western Alps). *International Journal of Earth Sciences*, 92 (3), 364-379. doi:10.1007/s00531-003-0332-0

Capuzzo, N., & Wetzel, A. (2004). Facies and basin architecture of the Late Carboniferous Salvan-Dorénaz continental basin (Western Alps, Switzerland/France). *Sedimentology* , 51 (4), 675-697. doi:10.1111/j.1365-3091.2004.00642.x

Cardozo, N., & Allmendinger, R. W. (2013). Spherical projections with OSXStereonet. *Computers & Geosciences,* 51 , 193-205. doi:https://doi.org/10.1016/j.cageo.2012.07.021

Ceriani, S., Fügenschuh, B., & Schmid, S. M. (2001). Multi-stage thrusting at the ”Penninic Front” in the Western Alps between Mont Blanc and Pelvoux massifs. *International Journal of Earth Sciences* , 90 (3), 685-702. doi:10.1007/s005310000188

Charollais, J., and Jamet, M. (1990). Principaux résultats géologiques du forage Brizon 1 (BZN1) Haute-Savoie, France. *Mémoires de la Société géologique de France* (1833), 156, 185-202.

Charollais, J., Davaud, E., & Jamet, M. (1996). Evolution of the southeastern Jura plateform-margin between the upper Jurassic and the Oligocene: new data from three oil wells. *Géologie de la France*, 1 (3), 25-42.

Cobbold, P. R., & Quinquis, H. (1980). Development of sheath folds in shear regimes. *Journal of structural geology*, 2(1-2), 119-126.

Collet, L. W. (1927). The Structure of the Alps. Edward Arnold, London.

Collet, L. W., Oulianoff, N., & Reinhard, M. (1952). Carte géologique Suisse : feuille de Finhaut n°525 (scale 1 :25,000). Commission géologique Suisse.

Collet, L. W., & Paréjas, E. (1920). The Structure of the Alps. doi:10.5169/SEALS-742613

Corbin, P., & Oulianoff, N. (1928). carte géologique du mont-blanc : feuille des tines (scale 1:20,000). *Institut de Géologie et de Paléontologie*. Retrieved from https://hal-insu.archives-ouvertes.fr/insu-01026264

Dall'Asta, N., Hoareau, G., Manatschal, G., Centrella, S., Denèle, Y., Ribes, C., & Kalifi, A. (2022). Structural and petrological characteristics of a Jurassic detachment fault from the Mont-Blanc massif (Col du Bonhomme area, France). Journal of Structural Geology, 159, 104593. Doi: 10.1016/j.jsg.2022.104593

Dal Zilio, L., Ruh, J., & Avouac, J.-P. (2020). Structural evolution of orogenic wedges: Interplay between erosion and weak décollements. *Tectonics*, 39 (10), e2020TC006210. doi:https://doi.org/10.1029/2020TC006210

Deville, E., & Chauvière, A. (2000). Thrust tectonics at the front of the western Alps: constraints provided by the processing of seismic reflection data along the Chambéry transect. *Comptes Rendus de l'Académie des Sciences Series IIA Earth and Planetary Science*, 331 (11), 725-732. doi:10.1016/s1251-8050(00)01463-4

Dobmeier, C., & Von Raumer, J. (1995). Significance of Latest-Variscan and Alpine Deformation For the Evolution of Montagne de Pormenaz (SouthWestern Aiguilles-Rouges massif, Western Alps. *Eclogae Geologicae Helvetiae*, 88 (2), 267-279.

Doudoux, B., de Lepinay, B. M., & Tardy, M. (1982). Une interprétation nouvelle de la structure des massifs subalpins savoyards (Alpes occidentales): nappes de charriage oligocènes et déformations superposées. *Comptes Rendus de l'Académie des Sciences de Paris*, II (64), 63-68.

Duparc, L., Lugeon, M., Michel-Lévy, A., & Mrazec, L. (1966). Carte géologique de la France, feuille de Vallorcine Mont-Blanc (Sheet 160, scale 1:80,000). French geological survey: Bureau de Recherches Géologiques et Minières.

Egli, D., & Mancktelow, N. (2013). The structural history of the Mont Blanc massif with regard to models for its recent exhumation. *Swiss Journal of Geosciences*, 106 (3), 469-489. doi:10.1007/s00015-013-0153-5

Egli, D., Mancktelow, N., & Spikings, R. (2017). Constraints from $^{40}Ar/^{39}Ar$ geochronology on the timing of Alpine shear zones in the Mont-Blanc Aiguilles Rouges region of the European Alps. *Tectonics*, 36 (4), 730-748. doi:https://doi.org/10.1002/2016TC004450.

Eltchaninoff, C. (1982). Etude géologique entre Belledonne et Mont Blanc: la terminaison septentrionale du massif de Belledonne et les terrains de son enveloppe Alpes françaises.

Bulletin de la Société Géologique de France, S7-XXIV (4), 817-830. doi:10.2113/gssgfbull.S7-XXIV.4.817

Epard, J. L. (1986). Le contact entre le socle du Mont-Blanc et la zone de Chamonix: implications tectoniques. *Bulletin de la société Vaudoise des sciences naturelles*, 288 , 225-245.

Epard, J. L. (1990). La nappe de Morcles au sud-ouest du Mont-Blanc (Doctoral dissertation, Université de Lausanne). Retrieved from https://tel.archives-ouvertes.fr/ tel-00923347 (Mémoires de Géologie (Lausanne) No. 8, 1990)

Escher, A., Masson, H., & Steck, A. (1988). Coupes géologiques des Alpes occidentales Suisses. Mémoires des laboratoires de géologie, minéralogie, géophysique et du musée géologique de l'Université de Lausanne, 2.

Escher, A., Masson, H., & Steck, A. (1993). *Nappe geometry in the western swiss Alps*. Journal of Structural Geology, 15 (3-5), 501-509. doi:10.1016/0191-8141(93)90144-y

Faure, J. L., Colletta, B., Deville, E., & Lecomte, J. C. (1999). Méthodologie d'équilibrage de coupes structurales en zones compressives: la coupe de la vallée de l'Arve et la coupe du massif des Bornes (profil Ecors Alp1 et Alp2). (Tech. Rep.). Etude FSH. (139 pages, 102 Fig. s). Rapport IFP 45584.

Ferrill, D. A., & Groshong Jr, R. H. (1993). Kinematic model for the curvature of the northern Subalpine Chain, France. Journal of structural Geology, 15(3-5), 523-541. Doi: 10.1016/0191-8141(93)90146-2.

Fréchet, J., Thouvenot, F., Frogneux, M., Deichmann, N., & Cara, M. (2011). The Mw 4.5 Vallorcine (French Alps) earthquake of 8 September 2005 and its complex aftershock sequence. *Journal of Seismology*, 15(1), 43-58. Doi: 10.1007/s10950-010-9205-8

Gapais, D., & Barbarin, B. (1986). Quartz fabric transition in a cooling syntectonic granite (Hermitage Massif, France). *Tectonophysics*, 125 (4), 357-370. doi:https://doi.org/10.1016/0040-1951(86)90171-X

Garefalakis, P., & Schlunegger, F. (2019). Tectonic processes, variations in sediment flux, and eustatic sea level recorded by the 20 myr old burdigalian transgression in the swiss molasse basin. *Solid Earth*, 10 (6), 2045–2072. Retrieved from https://doi.org/10.5194/se-10-2045-2019 doi:10.5194/se-10-2045-2019

Genier, F., Bussy, F., Epard, J.-L., & Baumgartner, L. (2008). Water-assisted migmatization of metagraywackes in a Variscan shear zone, Aiguilles-Rouges massif, western Alps. *Lithos*, 102 (3-4), 575-597. doi:10.1016/j.lithos.2007.07.024

Girault, J. B., Bellahsen, N., Bernet, M., Pik, R., Loget, N., Lasseur, E., Sonnet, M. (2022). Exhumation of the Western Alpine collisional wedge: New thermochronological data. *Tectonophysics*, 822 , 229155. doi:https://doi.org/10.1016/j.tecto.2021.229155

Girault, J. B., Bellahsen, N., Boutoux, A., Rosenberg, C. L., Nanni, U., Verlaguet, A., & Beyssac, O. (2020). The 3D Thermal Structure of the Helvetic Nappes of the European Alps: Implications for Collisional Processes. *Tectonics*, 39 (3), e2018TC005334. e2018TC005334 2018TC005334). doi:https://doi.org/10.1029/2018TC005334

Glotzbach, C., Reinecker, J., Danisik, M., Rahn, M., Frisch, W., & Spiegel, C. (2008). Neogene exhumation history of the Mont Blanc massif, western Alps. *Tectonics*, 27 (4). doi:https://doi.org/10.1029/2008TC002257

Glotzbach, C., van der Beek, P., & Spiegel, C. (2011). Episodic exhumation and relief growth in the Mont Blanc massif, Western Alps from numerical modelling of thermochronology data. *Earth and Planetary Science Letters*, 304 (3-4), 417-430. doi:10.1016/j.epsl.2011.02.020

Gourlay, P., & Ricou, L. (1983). Dextral strike-slip tectonics along the Chamonix suture zone (French and swiss Alps). *Comptes rendus de l'académie des sciences*, 296.

Hanmer, S., & Passchier, C. (1991). Shear-sense indicators: a review. *Geological Survey of Canada*, 130 (3). doi:10.1017/s0016756800020112

Hielscher, R., & Schaeben, H. (2008). A novel pole Fig. inversion method: specification of the MTEX algorithm. *Journal of Applied Crystallography*, 41 (6), 1024-1037. doi:10.1107/s0021889808030112

Homewood, P. (1983). Palaeogeography of Alpine flysch. *Palaeogeography, Palaeoclimatology, Palaeoecology* , 44 (3-4), 169-184. doi:10.1016/0031-0182(83)90101-3

Hubbard, M., & Mancktelow, N. S. (1992). Lateral displacement during Neogene convergence in the western and central Alps. *Geology* , 20 (10), 943-946. doi:10.1130/ 0091-613(1992)020⟨0943:LDDNCI⟩2.3.CO;2

Huggenberger, P. (1985). Faltenmodelle und verformungsverteilung in deckenstrukturen am beispiel der morcles-decke (helvetikum der westschweiz) (Doctoral dissertation). doi:10.3929/ETHZ-A-000365939

Jeanbourquin, P. (1994). Early deformation of Ultrahelvetic mélanges in the Helvetic nappes (Western Swiss Alps). *Journal of Structural Geology*, *16*(10), 1367-1383.

Kalifi, A., Leloup, P. H., Sorrel, P., Galy, A., Demory, F., Spina, V., . Rubino, J.-L. (2021). Chronology of thrust propagation from an updated tectono-sedimentary framework of the Miocene molasse (western Alps). *Solid Earth*, 12 (12), 2735-2771. doi:10.5194/se-12-2735-2021

Kalifi, A., Sorrel, P., Leloup, P.-H., Galy, A., Spina, V., Huet, B., J.-L., Rubino, (2022). Tectonic control on the palaeogeographical evolution of the miocene seaway along the western Alpine foreland basin. *Geological Society, London, Special Publications* , SP523–2021–78. doi:10.1144/sp523-2021-78

Kerrich, R., Allison, I., Barnett, R. L., Moss, S., & Starkey, J. (1980). Microstructural and chemical transformations accompanying deformation of granite in a shear zone at Mieville, Switzerland, with implications for stress corrosion cracking and superplastic flow. *Contributions to Mineralogy and Petrology*, 73(3), 221-242. doi:10.1007/bf00381442

Kirschner, D. L., Cosca, M. A., Masson, H., & Hunziker, J. C. (1996, 08). Staircase $^{40}Ar/^{39}Ar$ spectra of fine-grained white mica: Timing and duration of deformation and empirical constraints on argon diffusion. *Geology*, 24 (8), 747-750. doi:10.1130/ 0091-13(1996)024⟨0747:SAASOF⟩2.3.CO;2

Kirschner, D. L., Masson, H., & Cosca, M. A. (2003, July). An $^{40}Ar/^{39}Ar$, and stable isotope study of micas in low-grade fold-and-thrust belt: an example from the Swiss Helvetic Alps. *Contributions to Mineralogy and Petrology*, 145(4), 460-480. doi:10.1007/s00410-003-0461-2.

Kirschner, D. L., Sharp, Z. D., & Masson, H. (1995). Oxygen isotope thermometry of quartz-calcite veins: Unraveling the thermal-tectonic history of the subgreenschist facies Morcles nappe (Swiss Alps). *Geological Society of America Bulleti*n, 107(10), 1145-1156. doi:10.1130/0016-7606(1995)107⟨1145:OITOQC⟩2.3.CO;2.

Kiss, D., Duretz, T., & Schmalholz, S. M. (2020). Tectonic inheritance controls nappe detachment, transport and stacking in the Helvetic nappe system, Switzerland: insights from thermomechanical simulations. *Solid Earth*, 11(2), 287-305. Doi: 10.5194/se-11-287-2020.

Konstantinovskaya, E., & Malavieille, J. (2005). Accretionary orogens: Erosion and exhumation. *Geotectonics*, 39 (1), 69-86.

Lacassin, R. (1988). Large-scale foliation boudinage in gneisses. *Journal of Structural Geology* , 10 (6), 643-647. doi:10.1016/0191-8141(88)90030-2

Lacassin, R., & Mattauer, M. (1985). Kilometre-scale sheath fold at Mattmark and implications for transport direction in the Alps. *Nature*, 315(6022), 739-742. doi:10.1038/315739a0

Lacassin, R., Tapponnier, R., & Bourjot, L. (1990). Culminations anticlinales d'échelle crustale et imbrication de la lithosphère dans les Alpes, apports du profil ECORSCROP. Comptes rendus de l'Académie des sciences. Série 2, *Mécanique, Physique, Chimie, Sciences de l'univers, Sciences de la Terre*, 310 (6), 807-814.

Lajaunie, C., Courrioux, G., & Manuel, L. (1997). Foliation fields and 3D cartography in geology: Principles of a method based on potential interpolation. Mathematical Geology , 29 (4), 571-584. doi:10.1007/bf02775087

Leloup, P. H., Arnaud, N., Sobel, E. R., & Lacassin, R. (2005). Alpine thermal and structural evolution of the highest external crystalline massif: The Mont Blanc. *Tectonics*, 24(4). doi:10.1029/2004tc001676

Lemoine, M., & Tricart, P. (1986). Les Schistes lustrés piémontais des Alpes occidentales: approche stratigraphique, structurale et sédimentologique. *Eclogae Geologicae Helvetiae*, 79 (2), 271-294.

Marshall, D., Meisser, N., Taylor, R. P., 1998. Fluid inclusion, stable isotope and Ar-Ar evidence for the age and origin of gold-bearing quartz veins at Mont Chemin, Switzerland. Mineralogy and Petrology 62 (3), 147–165.

Menard, G., & Thouvenot, F. (1987). Coupes équilibrées crustales : méthodologie et application aux Alpes occidentales. *Geodinamica Acta*, 1(1), 35-45. doi:10.1080/09853111.1987.11105123.

Mennessier, G., Carme, F., Belliere, J., Dhellemes, R., Antoine, P., Dabrowski, H., & Bordet, C. (1977). Carte géologique de la France, feuille de Saint-Gervais-les-Bains (Sheet 703, scale 1:50,000). French geological survey: Bureau de Recherches Géologiques et Minières.

Mosar, J. (1989). Deformation interne dans les Prealpes medianes (Suisse). *Eclogae Geologicae Helvetiae*, 82(3), 765-793.

Pairis, B., Pairis, J. L., & Porthault, B. (1973). Présence de Crétacé supérieur reposant sur le socle dans le massif des Aiguilles Rouges, Alpes de Haute Savoie. Comptes rendus de l'Académie des Sciences de Paris , 276 , 1131-1134.

Pairis, J. L., Pairis, B., Bellière, J., Rosset, J., Détraz, H., Muller, A., .& Uselle, J. P. (1992). Carte géologique de la france, feuille de Cluses, (sheet 679, scale 1:50,000). French geological survey: Bureau de Recherches Géologiques et Minières.

Paréjas, E. (1922). Géologie de la zone de Chamonix comprise entre le Mont-Blanc et les Aiguilles rouges. Mémoires de la Société de Physique et d'Histoire naturelle de Genève, 39 (7), 374-442.

Paréjas, E. (1925). La tectonique du Mont Joly (Haute-Savoie). *Eclogae Geologicae Helvetiae*, 19(2), 420-503. doi:10.5169/SEALS-158423

Passchier, C., & Trouw, R. (2005). Foliations, Lineation and Lattice Preferred Orientation. In *Microtectonics* (p. 67-109). Springer Berlin Heidelberg.

Pfiffner, O. A. (1993). The structure of the Helvetic nappes and its relation to the mechanical stratigraphy. *Journal of Structural Geology*, 15 (3-5), 511-521. doi:10.1016/0191-8141(93)90145-z.

Pfiffner, O. A., Lehner, P., Heitzmann, P., Mueller, S., & Steck, A. (1997). Deep structure of the Swiss Alps: results of NRP 20. Birkhäuser.

Pfiffner, O. A., Schlunegger, F., & Buiter, S. J. H. (2002). The Swiss Alps and their peripheral foreland basin: Stratigraphic response to deep crustal processes. *Tectonics*, 21(2), 3-16. doi:10.1029/2000tc900039.

Pfiffner, O. A., Burkhard, M., Hänni, R., Kammer, A., Kligfield, R., Mancktelow, N. S., Menkveld, J. W., Ramsay, J. G., Schmid, S. M. & Zurbriggen, R. (2010): Structural Map of the Helvetic Zone of the Swiss Alps, including Vorarlberg (Austria) and Haute Savoie (France), 1: 100 000. *Geological Special Map* 128.

Pfiffner, O. A. (2014). *Geology of the Alps* (2nd edition, translated from German.). Wiley-Blackwell.

Pfiffner, O. A. (2017). Thick-skinned and thin-skinned tectonics : a global perspective. Geosciences, 7(3), 71. Doi : 10.3390/geosciences7030071.

Plancherel, R., P. Broquet and C. Caron, Carte géol France (1/50 000) feuille de Samoëns-Pas-de-Morgins (655), Orléans, 1998

Platt, J. (1984). Balanced cross-sections and their implications for the deep structure of the northwest Alps: discussion. *Journal of Structural Geology*, 6 (5), 603-606. doi:https://doi.org/10.1016/0191-8141(84)90072-5

Poty, B., & Cathelineau, M. (1974). La formation des cristaux dans les fentes alpines du massif du Mont-Blanc. *Le Règne Minéral*, 5, 19-21.

Poty, B., Stadler, H. A., & Weisbord, A. M. (1974). Fluid inclusions studies in quartz from fissures of western and central Alps. *Schweizerische Mineralogische und Petrographische Mitteilungen*, 54, 717-752.

Quinquis, H., Audren, C., Brun, J. P., & Cobbold, P. R. (1978). Intense progressive shear in Ile de Groix blueschists and compatibility with subduction or obduction. *Nature*, 273 (5657), 43-45. doi:10.1038/273043a0.

Ramsay, J. G. (1981). Tectonics of the Helvetic Nappes. *Geological Society*, London, Special Publications, 9 (1), 293-309. doi:10.1144/gsl.sp.1981.009.01.26 Wallis).

Reinhard, M., Preiswerk, H., 1927. Über Granitmylonite im Aiguilles-Rouges-Massiv (westliches Wallis). Buchdruckerei Emil Birkhäuser.

Ribes, C., Ghienne, J.-F., Manatschal, G., Dall'Asta, N., Stockli, D. F., Galster, F., & Karner, G. D. (2020). The Grès Singuliers of the Mont Blanc region (France and Switzerland):s tratigraphic response to rifting and crustal necking in the Alpine Tethys. *International Journal of Earth Sciences,* 109(7), 2325-2352. doi:10.1007/s00531-020-01902-z.

Rolland, Y., Cox, S., Boullier, A. M., Pennacchioni, G., & Mancktelow, N. (2003). Rare earth and trace element mobility in mid-crustal shear zones: insights from the mont blanc massif (western alps). *Earth and Planetary Science Letters*, 214(1-2), 203-219. doi:10.1016/s0012-821x(03)00372-8.

Rolland, Y., Rossi, M., Cox, S. F., Corsini, M., Mancktelow, N., Pennacchioni, G., & Boullier, A. M. (2008). $^{40}Ar/^{39}Ar$ dating of synkinematic white mica: insights from fluid-rock reaction in low-grade shear zones (mont blanc massif) and constraints on timing of deformation in the NW external alps. *Geological Society*, London, Special Publications, 299(1), 293-315. doi:10.1144/sp299.18

Rossi, M., Rolland, Y., 2014. Stable isotope and Ar/Ar evidence of prolonged multiscale fluid flow during exhumation of orogenic crust: example from the Mont Blanc and Aar Massifs (NW Alps). Tectonics 33 (9), 1681–1709. doi:10.1002/2013TC003438.

Rossi, M., Rolland, Y., Vidal, O., & Cox, S. F. (2005). Geochemical variations and element transfer during shear-zone development and related episyenites at middle crust depths:

insights from the Mont Blanc granite (French - Italian Alps). *Geological Society of London, Special Publications*, 245(1), 373-396. doi:10.1144/GSL.SP.2005.245.01.18.

Ruffini, R., Polino, R., Callegari, E., Hunziker, J., & Pfeifer, H. (1997). Volcanic clast-rich turbidites of the Taveyanne sandstones from the Thônes syncline (Savoie, France): Records for a Tertiary postcollisional volcanism. *Schweizerische mineralogische und petrographische Mitteilungen*, 77(2), 161-174.

Seward, D., & Mancktelow, N. S. (1994). Neogene kinematics of the central and western Alps: Evidence from fission-track dating. *Geology*, 22(9), 803-806. doi:10.1130/ 0091-7613(1994)022⟨0803:NKOTCA⟩2.3.CO;2

Simonetti, M., Carosi, R., Montomoli, C., Cottle, J. M., & Law, R. D. (2020). Transpressive deformation in the southern european variscan belt: New insights from the aiguilles rouges massif (western alps). *Tectonics*, 39(6). doi:10.1029/2020tc006153.

Simon-Labric, T., Rolland, Y., Dumont, T., Heymes, T., Authemayou, C., Corsini, M., & Fornari, M. (2009). $^{40}Ar/^{39}Ar$ dating of Penninic Front tectonic displacement (Western Alps) during the Lower Oligocene (31–34 Ma). *Terra Nova*, 21(2), 127-136. doi:https://doi.org/10.1111/j.1365-3121.2009.00865.x.

Spitz, R., Bauville, A., Epard, J. L., Kaus, B. J., Popov, A. A., & Schmalholz, S. M. (2020). Control of 3-D tectonic inheritance on fold-and-thrust belts: insights from 3-D numerical models and application to the Helvetic nappe system. Solid Earth, 11(3), 999-1026. Doi: 10.5194/se-11-999-2020.

Steck, A., & Vocat, D. (1973). Zur mineralogie der granitmylonite von miéville, aiguilles rouges massiv. Schweizerische Mineralogische und Petrographische Mitteilungen, 54 , 474-477.

Steyrer, H. P., & Sturm, R. (2002). Stability of zircon in a low-grade ultramylonite and its utility for chemical mass balancing: the shear zone at miéville, switzerland. *Chemical Geology*, 187(1-2), 1-19. doi:10.1016/s0009-2541(02)00010-4.

Triboulet, S. (1980). Etude geologique entre Belledonne et Mont Blanc : la terminaison septentrionale du massif de Belledonne et les terrains de son enveloppe Alpes françaises (Doctoral dissertation, Université Pierre et Marie Curie Paris VI). Retrieved from https://tel.archives-ouvertes.fr/tel-00616709.

Trumpy, R. (1971). Sur le jurassique de la zone helvétique en suisse. *Annales of the Geological Institute of Hungary,* 54(2), 370-382.

Vanardois, J., Roger, F., Trap, P., Goncalves, P., Lanari, P., Paquette, J.-L., .& Barou, F. (2022). Exhumation of deep continental crust in a transpressive regime: The example of variscan eclogites from the aiguilles-rouges massif (western alps). *Journal of Metamorphic Geology*. doi:10.1111/jmg.12659.

Von Raumer, J., & Bussy, F. (2004). Mont blanc and aiguilles rouges geology of their polymetamorphic basement (external massifs, westerns alps, france-switzerland). Mémoires de Géologie (Lausanne), 42, 1-210.

Supporting Information

Contents of this file

- Tables S1 to S4.
- Figures S1 to S10.

Introduction

The supplements provide the location of the outcrops discussed in the publication (Table S1), the average measures reported in the stereographic plots from the figure 3a (Table S2), technical information about the EBSD analysis (Table S3), details about the datations from the bibliography cited in the publication (Table S4), the figure 3a without stereo-plots and surcharge (Figure S1), stereo plots from figure 3a with all the data used for calculating average plane and lineation (Figure S2), complementary field pictures (Figure S3 to S8), the image at microscale of the sample ARe096 from the Gietroz normal fault (Figure S9) and the sections used for the estimation of exhumation (Figure S10).

Table S1. Locations of outcrops used in the study.

Location ID	Studied Sites	Decimal Longitude	Decimal Latitude	Elevation in Meters	Verbatim Locality
AR0025	FF1	6.950569	46.02661	1965	Col des Posettes, Vallorcine, France
AR0027	FF1	6.953102	46.02507	2008	Col des Posettes, Chamonix-Mont-Blanc, France
AR0139	HGT6	6.874016	45.98791	2955	Aiguilles Rouges, Aiguille du Belvedere, Chamonix-Mont-Blanc, France
AR0141	HGT6	6.873149	45.987858	2966	Aiguilles Rouges, Aiguille du Belvedere, Chamonix-Mont-Blanc, France
AR0152	TB1	6.883872	45.94979	1287	Aiguilles Rouges, Les Praz, Chamonix-Mont-Blanc, France
AR0162		6.87577	46.019135	2630	Mont-Oreb, Aiguilles Rouges, Vallon de Berard, Vallorcine, France
AR0178	HGT2	6.861869	46.01774	2532	Mont-Buet, Aiguilles Rouges, Vallon de Berard, Vallorcine, France
AR0184		6.857506	46.01343	2454	Mont-Buet, Aiguilles Rouges, Vallon de Berard, Vallorcine, France
AR0184b		6.857152	46.013	2450	Mont-Buet, Aiguilles Rouges, Vallon de Berard, Vallorcine, France
AR0190	FF3	6.999964	46.05488	1490	Forclaz pass, Valais, Switzerland
AR0271	FF2	6.97485	46.04682	2040	Carraye, Les Tseppes, Valais, Switzerland
AR0358	FB1	6.973778	46.08449	1360	Aiguilles Rouges, Finhaut, Valais, Switzerland
AR0359	FB1	6.976246	46.085842	1332	Aiguilles Rouges, Finhaut, Valais, Switzerland
AR0370b		6.96539	46.06789	1070	Aiguilles Rouges, Finhaut, Valais, Switzerland
AR0391	TB2	6.93418	46.000328	1517	Montroc, Chamonix-Mont-Blanc, France
AR0392	TB2	6.934502	46.000233	1509	Montroc, Chamonix-Mont-Blanc, France
AR0393	TB2	6.935156	46.000435	1488	Montroc, Chamonix-Mont-Blanc, France
AR0394	TB2	6.934862	46.000626	1488	Montroc, Chamonix-Mont-Blanc, France
AR0395	TB2	6.935742	46.000843	1500	Montroc, Chamonix-Mont-Blanc, France
AR0396	TB2	6.936321	46.001965	1525	Montroc, Chamonix-Mont-Blanc, France
AR0411	TB1	6.889766	45.95017	1153	Aiguilles Rouges, Les Praz, Chamonix-Mont-Blanc, France
AR0447	PMsz2	6.791885	45.95824	2059	Crete Blanche, Pormenaz, Servoz, France
AR0453	PMsz2	6.79339	45.95871	2076	Crete Blanche, Pormenaz, Servoz, France
AR0454	PMsz2	6.793369	45.958714	2082	Crete Blanche, Pormenaz, Servoz, France
AR0455	PMsz2	6.793432	45.958782	2082	Crete Blanche, Pormenaz, Servoz, France
AR0482	PMsz1	6.806119	45.90461	1365	Le Coupeau, Les Houches, France
AR0483	PMsz1	6.80579	45.904827	1346	Le Coupeau, Les Houches, France
AR0484	PMsz1	6.805527	45.9048	1347	Le Coupeau, Les Houches, France
AR0485	PMsz1	6.805086	45.90484	1337	Le Coupeau, Les Houches, France
AR0486	PMsz1	6.804257	45.90493	1326	Le Coupeau, Les Houches, France
AR0765	FB2	6.917144	45.9997	1733	Les Cheserys, Aiguilles Rouges, Chamonix-Mont-Blanc, France
AR0779	FB2	6.918403	46.00137	1688	Les Cheserys, Aiguilles Rouges, Chamonix-Mont-Blanc, France
AR0874	FB3	6.922863	46.07913	1986	Eastern side of Emosson lake, Valais, Switzerland
AR0875	FB3	6.9227004	46.08043	1976	Eastern side of Emosson lake, Valais, Switzerland
AR0892	HBT4	6.906337	46.09824	1986	North of Emosson lake, Valais, Switzerland
AR0894	FB3	6.922009	46.083485	1971	Aiguilles Rouges, Eastern side of Emosson lake, Valais, Switerland
AR0895	FB3	6.924889	46.07647	1996	Aiguilles Rouges, Eastern side of Emosson lake, Valais, Switerland
AR0896	FB3	6.924889	46.07618	1994	Aiguilles Rouges, Eastern side of Emosson lake, Valais, Switerland
AR0897	FB3	6.916172	46.075157	1997	Aiguilles Rouges, Eastern side of Emosson lake, Valais, Switerland
AR0903		6.928097	46.099403	2269	Col de Barberine, Valais, Switzerland
AR0909		6.92832	46.09988	2283	Col de Barberine, Valais, Switzerland
AR0905	HBT1	6.928226	46.09963	2280	Col de Barberine, Valais, Switzerland
AR0906	HBT1	6.928317	46.099693	2279	Col de Barberine, Valais, Switzerland
AR0907	HBT1	6.928324	46.099777	2280	Col de Barberine, Valais, Switzerland
AR0912	HBT1	6.928404	46.100166	2298	Col de Barberine, Valais, Switzerland
AR0914	HBT1	6.928567	46.100517	2314	Col de Barberine, Valais, Switzerland
AR0915	HBT1	6.92848	46.10068	2342	Col de Barberine, Valais, Switzerland
AR0916	HBT1	6.928534	46.1008	2346	Col de Barberine, Valais, Switzerland
AR0917	HBT1	6.928748	46.100895	2355	Col de Barberine, Valais, Switzerland
AR0919	PMsz3	6.796878	45.95758	2189	Pointe Noire de Pormenaz, Servoz, France
AR1451		6.837431	46.0711	1003	Haut-Giffre, Nant des Pères, Sixt-Fer-a-Cheval, France
AR1470		6.8435555	46.072613	1056	Haut-Giffre, Nant des Pères, Sixt-Fer-a-Cheval, France
AR1472	HGT5	6.813543	45.977247	2159	Moede d'Anterne, Passy, France
AR1925	HGT3	6.813335	45.977212	2170	Moede d'Anterne, Passy, France
AR1926	HGT3	6.81643	45.979589	2179	Moede d'Anterne, Passy, France

Table S2. Measures plotted in the stereographic diagrams in figure 3. HGT: Haut-Giffre Thrust; TB: Tour Back Thrust; PMsz: Pormenaz-Merlet shear zone; FB: Finhaut back thrust; FF: Forclaz fault.

Site	Mean Fault Plane Strike ; Dip ; Quadrant	Mean Lineation Trend/Plunge
HGT1	N019 ; 23°W	285/25
HGT2	N020 ; 33°W	280/32
HGT3	N045 ; 13°W	288/05
HGT5	N038 ; 32°E	-
HGT6	N058 ; 09°NW	288/05
TB1	N179 ; 50°W	309/39
TB2	N003 ; 39°W	303/31
PMsz1	N157 ; 34°E	96/55
PMsz2	N006 ; 72° SE	105/80
PMsz3	N055 ; 22° SE	96/55
FB1	N013 ; 43°W	297/42
FB2	N019 ; 75°W	285/75
FB3	N015 ;67°W	304/62
FF1	N031 ; 62°E	95/60
FF2	N008 ; 28°E	133/24
FF3	N030 ; 77°E	186/61

Table S3. Summarizing measurement conditions, details of used instruments, and sample preparation during Electron BackScattered Diffraction (EBSD) analysis.

Instrument	FIB Zeiss NVision 40
Location	INSA Lyon
Working conditions	Acceleration voltage 340 kV Acquisition speed 10 Hz Exposure time 20 ms
Acquisition software	Oxford Instruments Channel 5.0
Sample ID	ARe42
Sample preparation	Polished carbon-coated (5 microns) thin section (30 um)
Image resolution	385x292 px
Mean indexing	72.5%
Optical step size	6um
Field width	2
Field height	1.74 um
Number of data points	111 650

Table S4. Details on datations samples from figure 15.

Sample	Latitude	Longitude	Location	Tectonic Unit	Mineral	Plateaux Ages (Ma, 2σ)	Inv. Isochrone Age (Ma, 2σ)	Age Range (Ma)
	Decimal (EPSG:4326)							
C6[1]	45.89639	6.87835	Plan de l'Aiguille	MBsz	Biotite	19.75 ± 0.21	21.8 ± 3	
S68[1]	46.05072	6.94603	Vallorcine	VMsz	Phengite	14.3 ± 0.2 & 22.9 ± 0.9	14.5 ± 0.3 & 23.4 ± 0.4	
ME27[2]	45.89951	6.88742	Plan de l'Aiguille	MBsz	K-Feldspar	10.61 ± 0.15 (min age)		
C8[2]	45.89534	6.89365	Plan de l'Aiguille	MBsz	Biotite	16.6 ± 0.7		
C8[2]	45.89534	6.89365	Plan de l'Aiguille	MBsz	K-Feldspar	10.98 ± 0.2 (min age)		
DE65[3]	46.06699	7.07607	Angle Fault	MBsz	White mica			14.30 - 20.41
DE79[3]	46.10759	7.06844	La Bâtiaz	HBT	White mica	20.28 ± 0.21	20.18 ± 0.49	
S02[3]	46.10666	7.06827	Sur le Sex	HBT	White mica	15.09 ± 0.15	15.07± 0.23	
93-29-A[4]	46.17236	7.12788	Morcles	HBT	2-6 µm mica	~19 & 21		
92-29-J[4]	46.10615	7.06903	Morcles	HBT	2-6 µm mica			13.6 - 22.7

[1] Rolland et al., 2008
[2] Leloup et al., 2005
[3] Egli et al., 2017
[4] Kirschner et al., 2003

MBsz : Mont-Blanc shear zone
VMsz : Vallorcine Miéville shear zone
HBT : Helvetic Basal Thrust

Figure S1. Same as figure 3a without stereo plots and surcharge.

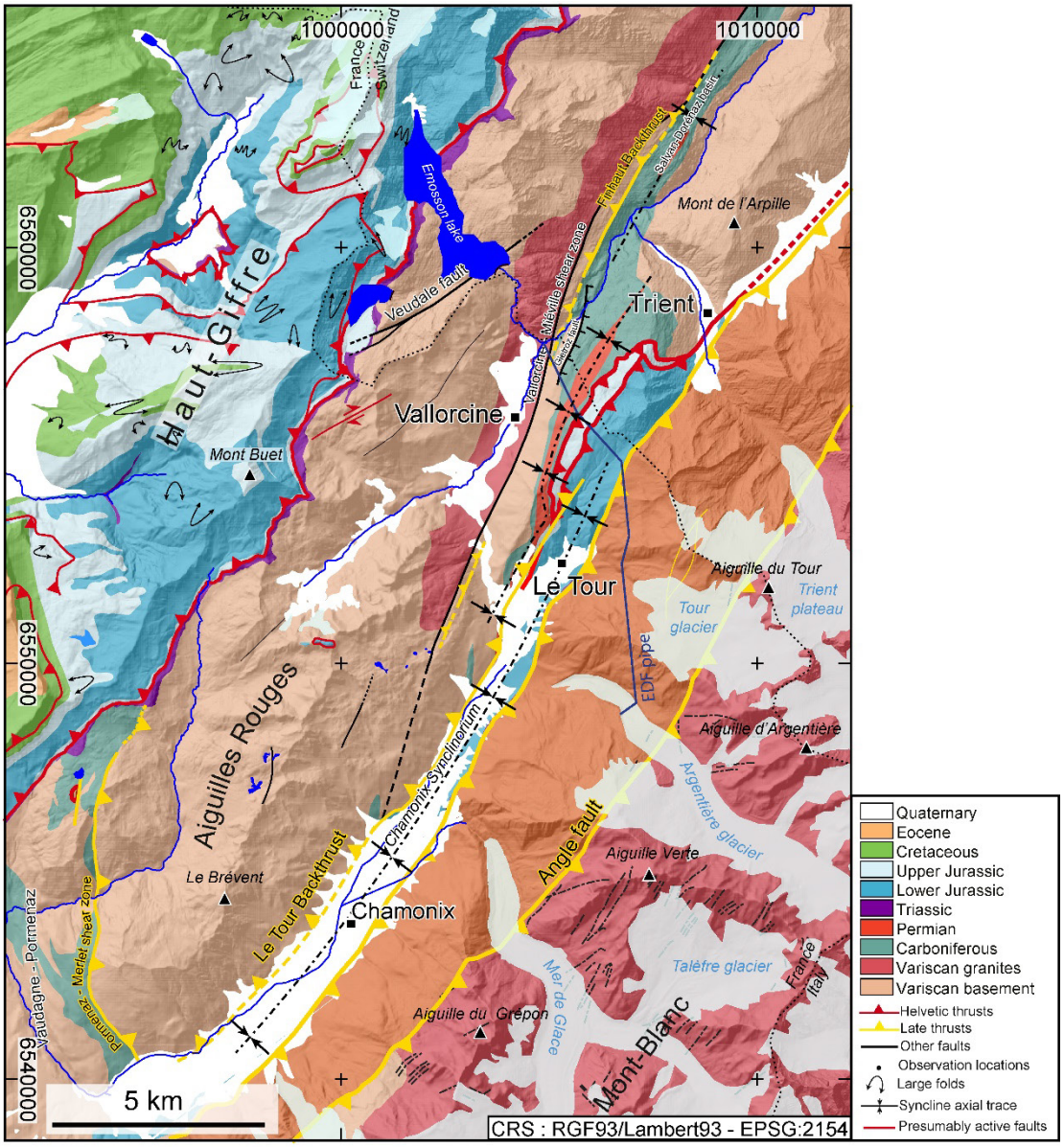

Figure S2. All data used for the calculation of the mean plane and mean lineation in the stereo plots used in figure 3a. Stereoplots are in lower hemisphere, equal area, north up.

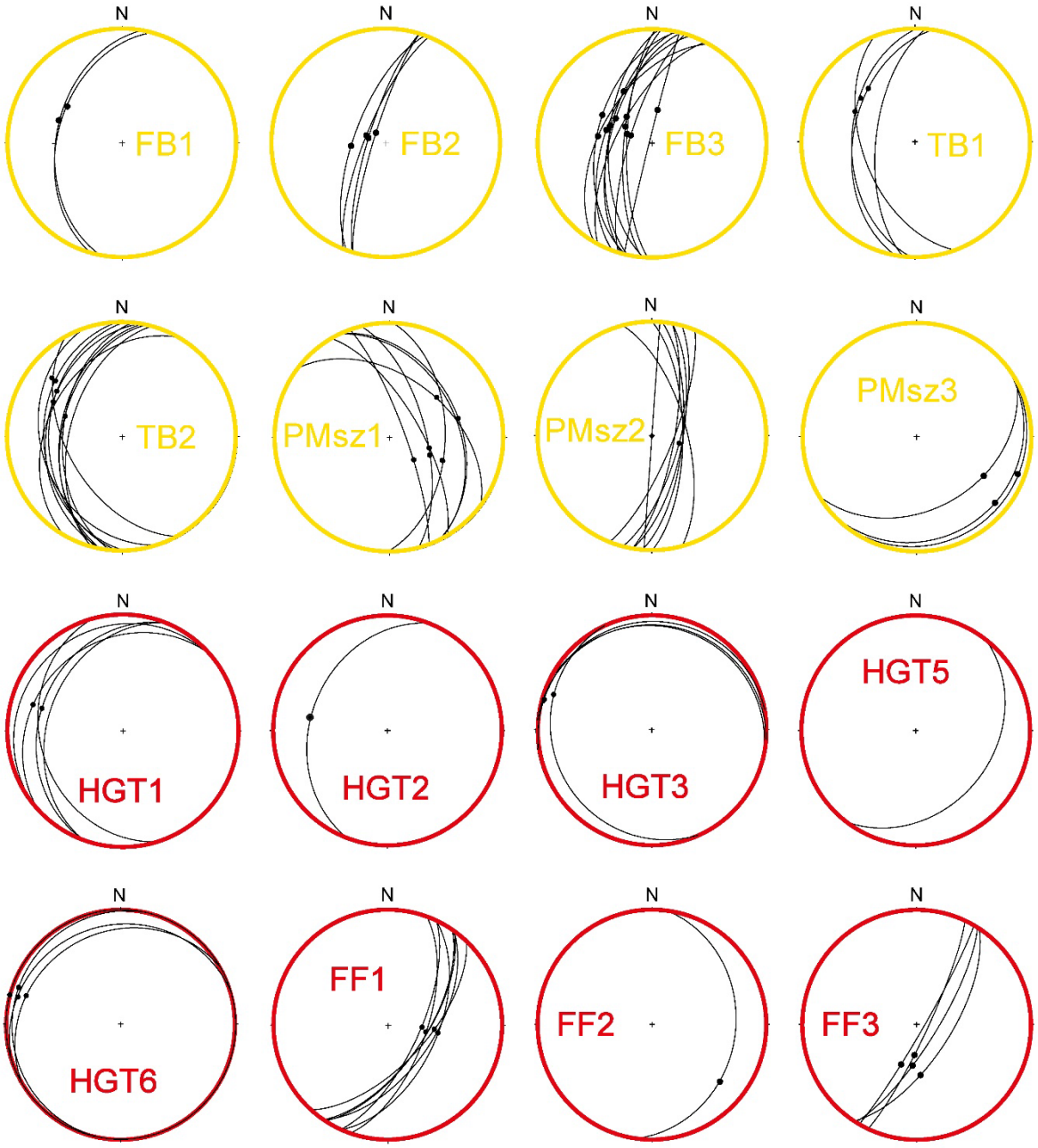

FB : Finhaut back thrust
HGT : Haut-Giffre Thrust
FF : Forclaz fault
PMsz : Pormenaz-Merlet shear zone

: Shear or fault plane
• : Lineation

Figure S3. Undeformed Triassic: a) Basal Triassic unconformity with stratigraphic and angular unconformity above Variscan gneiss that show a steep foliation (bottom of the Haut-Giffre); b) red and green siltites showing ripple marks (Barberine pass area).

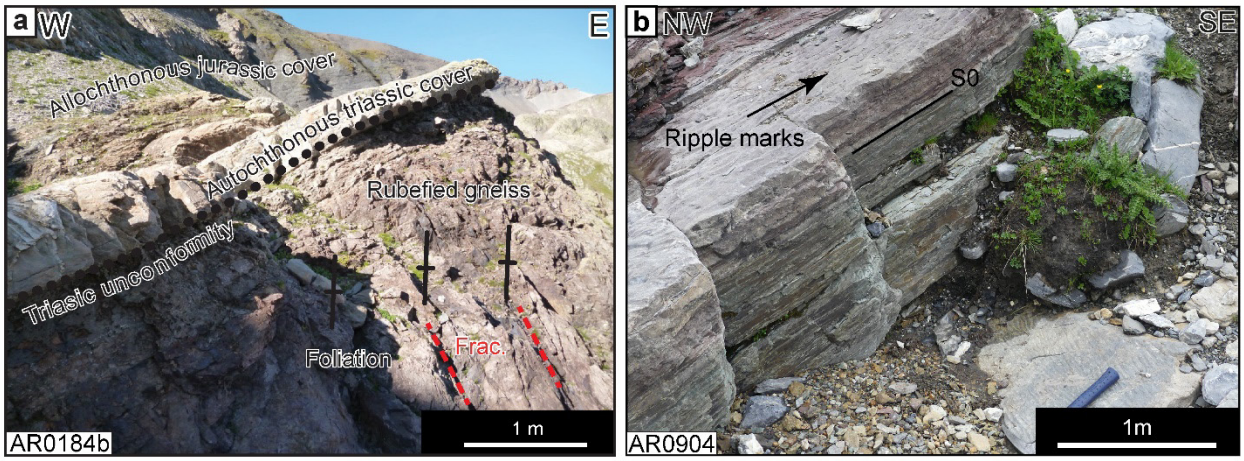

Figure S4. (a) Site HGT2 Stretching lineation trending N280°, compatible with a displacement towards the WNW inside the shear zone at the bottom of the Mesozoic sedimentary serie. (b) Triassic sandstone layer affected by an isoclinal fold with the fold axis trending N279°. This fold is a sheath fold that has highly curvilinear axes, with the axis parallel to the direction of transport. Such folds occur in shear zones with a high simple shear rate (γ ≥10) (Cobbold and Quinquis, 1980; Quinquis et al., 1978, Lacassin & Mattaeuer, 1985).

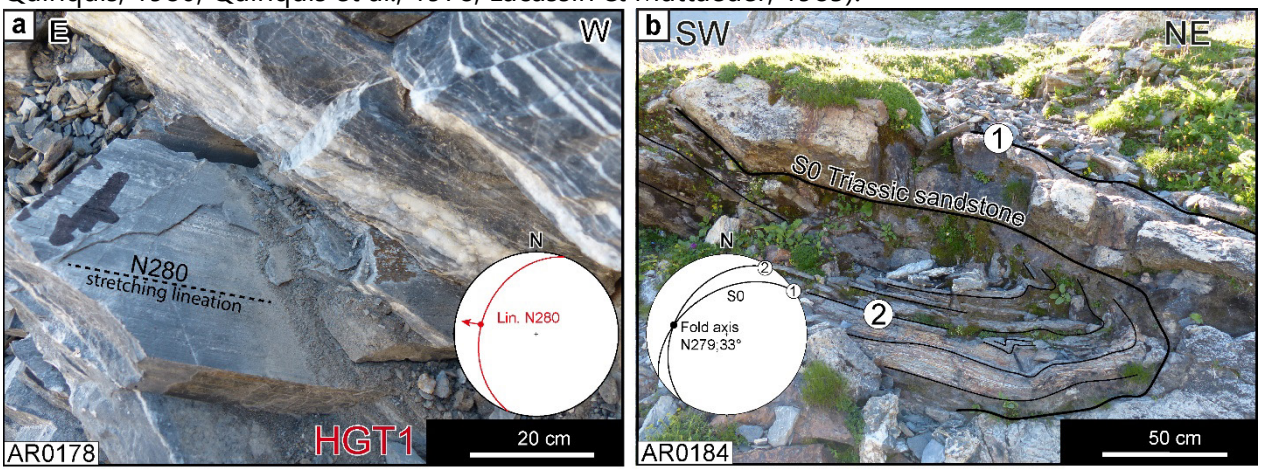

Figure S5. Site HGT3 (Souay area): a) white limestones that are mylonitized and metamorphosed into marbles. They bear a well-visible stretching lineation, trending N288°. The limestones are also asymmetrically folded with axis trending N032° and shear planes cross cutting the axial plane. The lineation, shear plane, and asymmetry of the fold suggest a direction of shear towards the WNW.

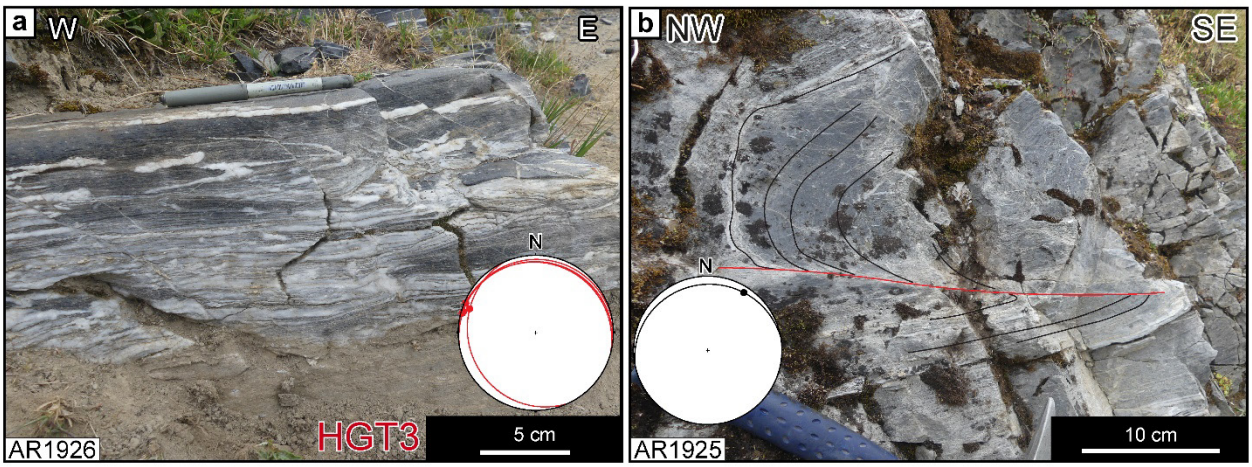

Figure S6. Site HGT5 (Sixt window): a) Horizontal basal Triassic unconformity above chloritoschist basement.; b) Thrust fault into the Jurassic limestones above the Triassic serie. The shear sense is towards the NW.

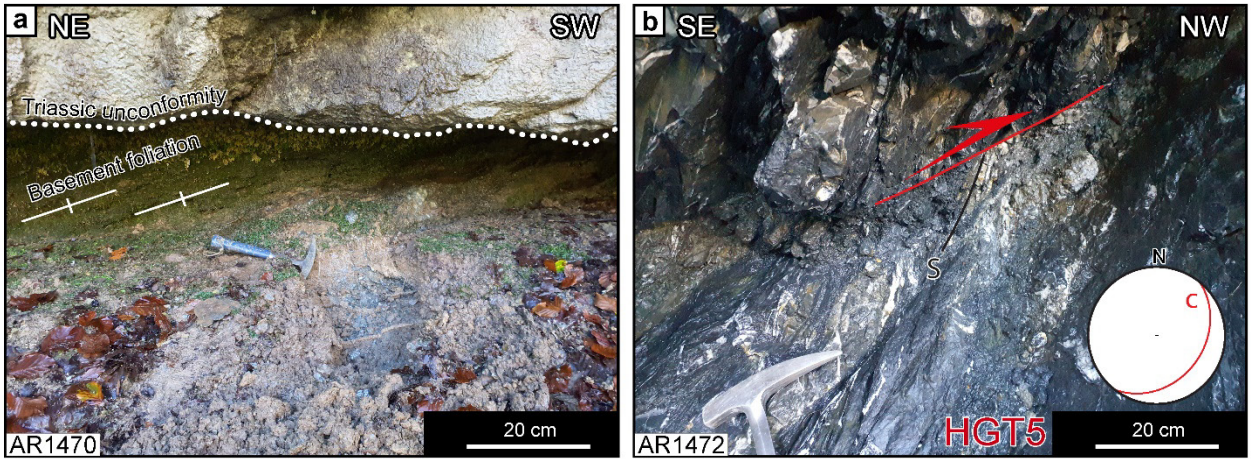

Figure S7. Site HGT6 (Aiguille du Belvedère): a) Stretching lineation trending N285°, affecting the black slates atop the summit; b) Sheared and stretched dolomites above the Triassic unconformity. The stretching lineation trends N130°.

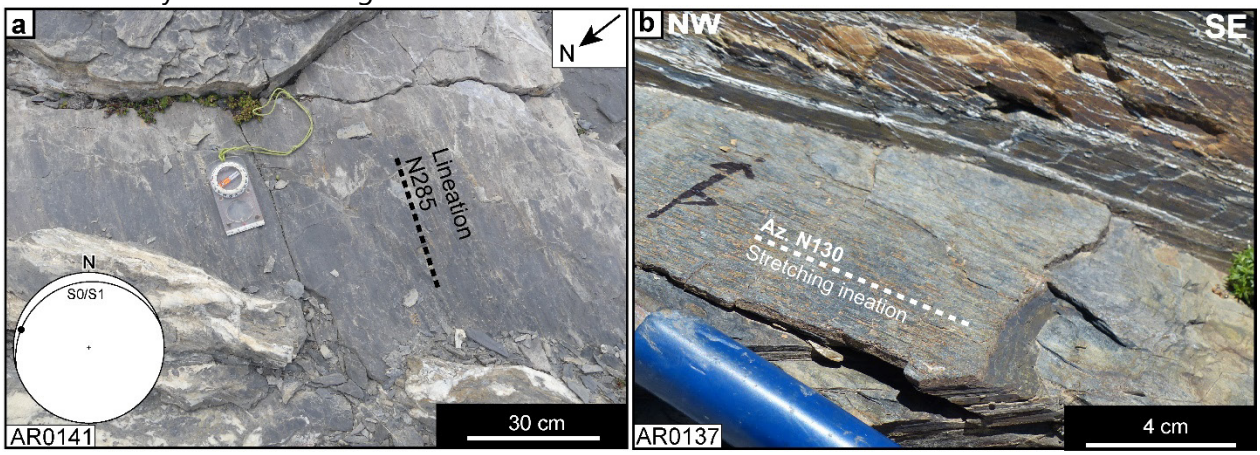

Figure S8. a) Steep thrust affects the limestones, and initial foliation is cross cut by steep faults (station AR453). b) Flat reverse fault associated with the Pormenaz-Merlet shear zone with a striation trending N120°, indicating top to the northwest.

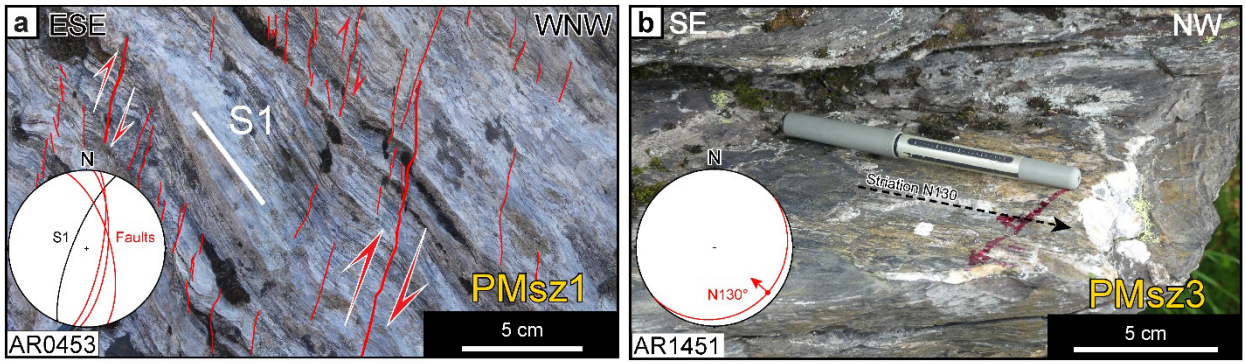

Figure S9. Thin section of sample ARe096, (station AR0370b) from the Gietroz fault (Cf. Figure 10 and 3a). The sample is a pseudotachylite with quartz and micas, the C/S relation is interpreted as normal sens of shear (SE down).

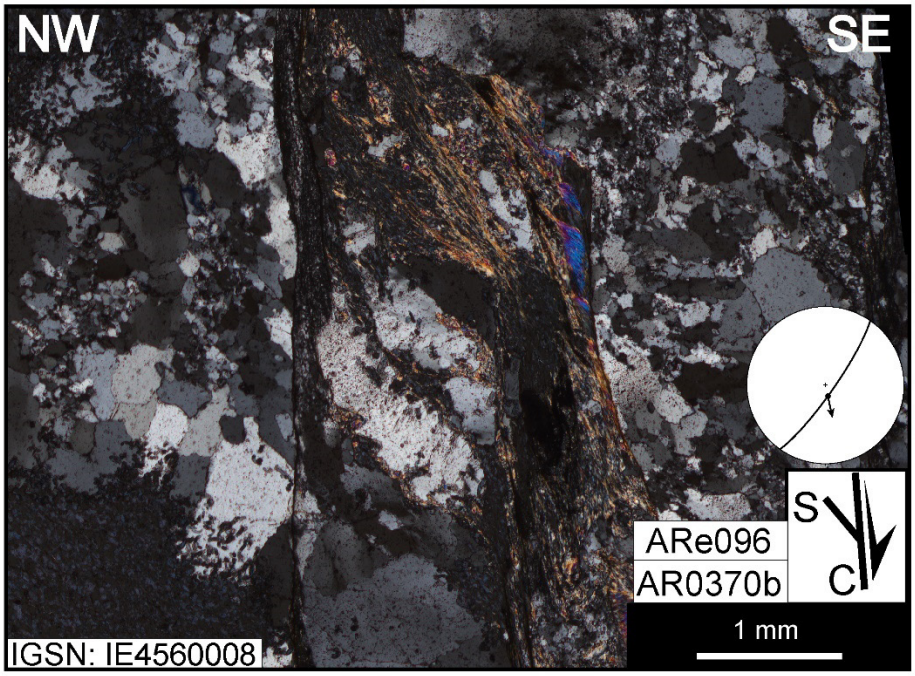

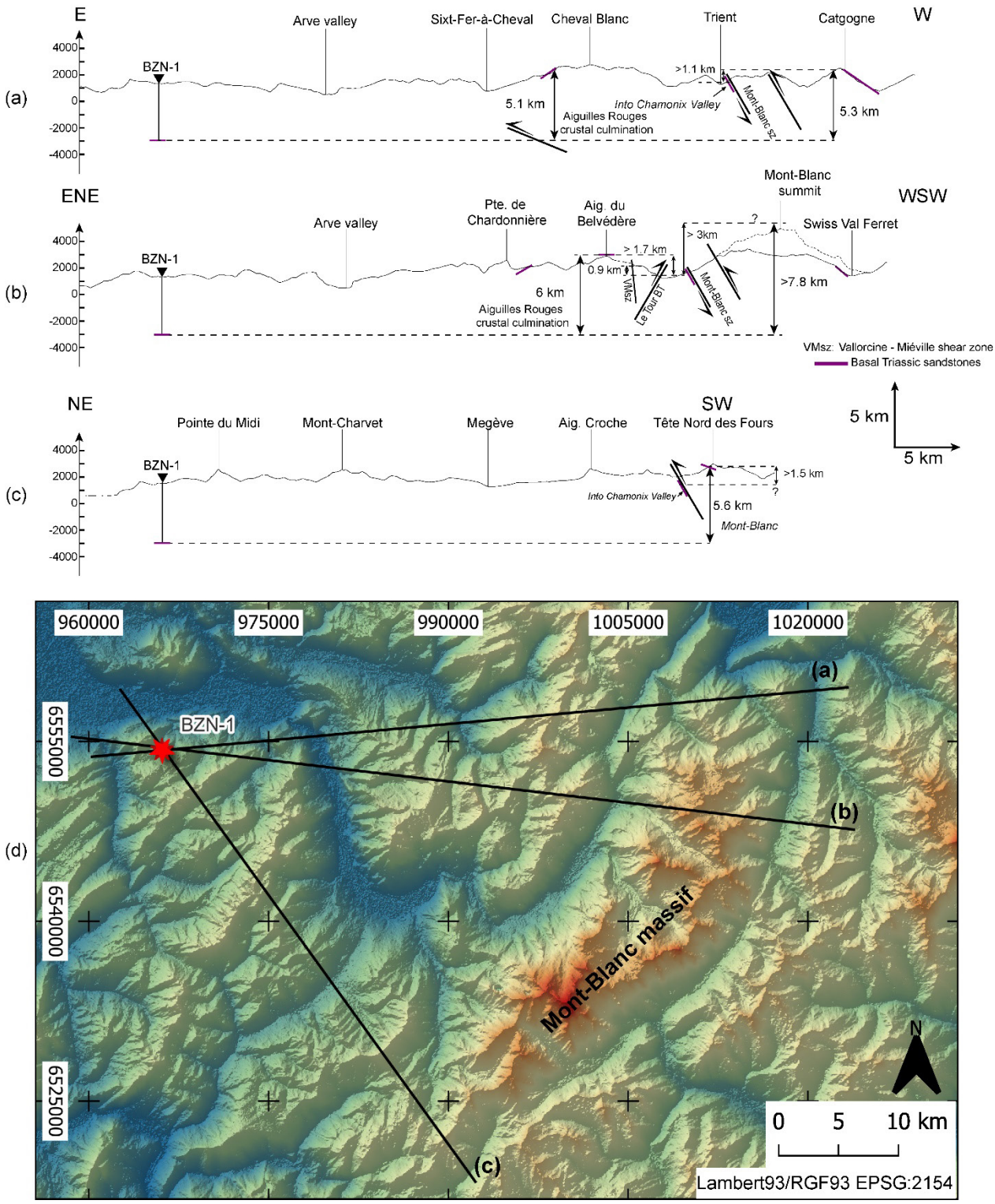

Figure S10. Sections highlighting the Triassic unconformity in order to estimate the amount of exhumation between the massifs: (a) Section through Chablais, Haut-Giffre, Aiguiles Rouges and northern Mont-Blanc massif (Catogne); (b) Section through Désert de Platé, Aiguille du

Belvédère and Mont-Blanc massif (Âmone); (c) Section through Aravis, Mont-Joly, Col du Bonhomme and southern Mont-Blanc massif (Tête Nord des Fours).